Faculty of Aerospace Engineering

Solar Powered Amphibious Unmanned Aerial Vehicle (UAV)

Final Report

Design and Synthesis Exercise (DSE) 2012/2013 - Group 4

Authors:

R. Augustinus
C. Çakıroğlu
J. Chang
M.A. Estrada
J.J. van Gorcum
B. Groenenboom
M.J. Koot
A.E. Naruta
H.H. Ubbens
M.E. Wassenaar

Tutor:
Dr. M.J. Martinez

Coaches:
Dr.ir. E. van Kampen
Dr. U.L. Lafont

Preface

The beautiful island of Curaçao is a holiday destination for thousands of people. The Caribbean island with its colourful houses, its characteristic marine life and its gentle inhabitants is facing a problem though; it is located in a region notorious for its drug trafficking routes, the so-called Caribbean Corridor. Currently the region is being monitored by the Dutch Caribbean Coastguard (DCCG). Performing their work, they combine aerial and naval fleets. In addition to drug traffic prevention they also perform Search and Rescue (SAR) operations, fishery control and environmental monitoring tasks.

The work presented in this report was done as part of the 2012 DSE. The aim of this exercise is to design a solar powered UAV for the purpose of aiding current DCCG surveillance operations. This document expands upon the work presented in the project baseline and mid-term report by documenting the final design of this UAV, also the process leading to this design will be in this report. The project was conducted by a group of ten students under the supervision of tutor Marcias Martinez, who acts as a client, and two coaches: Erik-Jan van Kampen and Ugo Lafont.

January 29th, 2013

Contents

Page

Preface ii

Nomenclature vii

Summary x

1 Introduction 1

Part I: Systems Engineering 3

2 Project organisation 4
2.1 Gantt chart 4
2.2 Human resource budgeting 7

3 Market analysis 8
3.1 Current coastguard operations 8
3.2 Comparable UAVs in mission 9
3.3 SWOT analysis 11
3.4 Customers 12

4 Mission 13
4.1 Mission outline 13
4.1.1 Basic operations 13
4.1.2 Operational scenarios 14
4.1.3 Other considerations 14
4.2 Functional flow diagram 15
4.3 Functional breakdown 15

Part II: Conceptual Design 18

5 Preliminary concept evaluation 19

6 Concepts 20
6.1 Blimp concept 20
6.2 Concept 2: Fixed wing 21
6.3 Concept 3: Dynastat 22

7 Trade-off 23
7.1 Trade-off method organisation 23
7.2 Trade-off summary table 24

Part III: Detailed Design 25

8 Contingency management 26

9 Configuration selection 27
9.1 Wing configuration . . . 27
9.2 Floater configuration . . . 28
9.3 Motor configuration determination . . . 29

10 Mass and power budgets 30

11 Environment 32
11.1 Weather conditions . . . 32
11.1.1 Sea state code . . . 32
11.1.2 Curaçao weather conditions . . . 33
11.2 Waves . . . 34
11.3 Coatings . . . 35
11.4 Surroundings . . . 35

12 Aerodynamics and flight dynamics 38
12.1 Airfoil selection . . . 38
12.1.1 Wing airfoil . . . 38
12.1.2 Vertical tail airfoil . . . 39
12.2 Wing and tail lay-out . . . 40
12.2.1 Wing and tail lay-out . . . 40
12.2.2 Stability analysis . . . 41
12.2.3 Tail layout & static lateral stability . . . 43
12.2.4 Drag estimation . . . 44
12.2.5 Dynamic stability . . . 45
12.3 Control surfaces . . . 47
12.3.1 Placement . . . 47
12.3.2 Roll control . . . 48
12.3.3 Pitch control . . . 50
12.3.4 Yaw control . . . 52
12.3.5 Integration . . . 53
12.4 Conclusion . . . 53

13 Maritime 55
13.1 Hull parameters . . . 55
13.2 Take-off . . . 57
13.3 Landing . . . 59
13.3.1 Landing behaviour . . . 59
13.3.2 Impact . . . 59
13.4 Stability . . . 61
13.4.1 Longitudinal stability . . . 61
13.4.2 Transverse stability . . . 62
13.5 Floaters . . . 64
13.5.1 Floater design . . . 64
13.5.2 Floater impact . . . 66
13.6 Maritime conclusion . . . 67

14 Operations **68**
14.1 On-board communication system . . . 68
14.1.1 Operating environment . . . 68
14.1.2 Autopilot . . . 69
14.1.3 Other components of on-board communication system . . . 71
14.1.4 Other considerations . . . 72
14.2 Ground control system . . . 73
14.2.1 Hardware . . . 74
14.2.2 Software . . . 74
14.3 Imaging system . . . 75
14.4 Communication system test . . . 77
14.5 Flight cycle . . . 79
14.5.1 Pre-flight operations . . . 79
14.5.2 Flight operations . . . 79
14.6 Conclusion . . . 80

15 Propulsion and power **81**
15.1 Motor and propeller selection . . . 81
15.1.1 Motor selection . . . 81
15.1.2 Propeller selection . . . 82
15.2 Motor controller . . . 85
15.3 Battery sizing and selection . . . 86
15.4 Solar panel design . . . 87
15.4.1 Available solar energy . . . 87
15.4.2 Solar panel sizing . . . 88
15.4.3 Effect of water on solar panel performance . . . 91
15.5 Electrical power conversion . . . 91
15.6 Electrical Block Diagram . . . 91
15.7 Conclusion . . . 93

16 Structures, materials and maintenance **95**
16.1 Load cases . . . 96
16.2 Structural analysis methodology . . . 96
16.2.1 Abaqus analysis . . . 97
16.2.2 MATLAB numerical model . . . 97
16.3 Structures and parts . . . 99
16.3.1 Wing structure . . . 99
16.3.2 Wing mounting . . . 101
16.3.3 Hatch . . . 102
16.3.4 Motor mount . . . 102
16.3.5 Analysis of the hull . . . 103
16.3.6 Floaters . . . 104
16.3.7 Camera mount and dome . . . 104
16.4 Materials . . . 105
16.4.1 Material selection . . . 105
16.4.2 Fatigue properties . . . 106
16.4.3 Corrosion properties . . . 107
16.5 Maintenance . . . 107
16.5.1 Modularity and parts replacement . . . 107
16.5.2 Inspection . . . 108

17 Final design **111**
17.1 Layout . . . 111
17.2 Costs . . . 112
17.2.1 Cost breakdown . . . 112
17.2.2 Return on investments . . . 112
17.3 Requirement compliance . . . 113
17.4 RAMS characteristics . . . 114
17.5 Production plan . . . 115
17.5.1 Hull . . . 116
17.5.2 Wings . . . 116
17.5.3 Floaters . . . 116
17.5.4 Motor mount . . . 116
17.5.5 Assembly . . . 117
17.6 Material characteristics . . . 117

18 Sustainable development strategy **119**

19 Technical risk assessment **121**
19.1 List of risks . . . 121
19.2 Risk mapping . . . 124

20 Post Project Development **125**
20.1 Project design and development logic . . . 125
20.2 Project Gantt chart . . . 125

21 Conclusion **128**

22 Recommendations **129**
22.1 Aerodynamics . . . 129
22.2 Maritime . . . 129
22.3 Structures and maintenance . . . 130
22.4 Propulsion and power . . . 130
22.5 Operation . . . 131

Bibliography **132**

A UAV requirements **137**

B Deliverable item list **139**

Nomenclature

List of Symbols

$\bar{V}$	Volume coefficient	-
β	Deadrise angle	$^\circ$
β	Panel slope	$^\circ$
β	Sideslip angle	$^\circ$
Δ	Weight	lbs
δ	Control surface deflection	$^\circ$
δ	Declination angle	$^\circ$
Γ	Dihedral angle	$^\circ$
γ	Surface azimuth angle	$^\circ$
Λ	Wing sweep	$^\circ$
λ	Vertical direction	m
λ	Wetted length to beam ratio	-
μ	Friction coefficient	-
∇	Water displacement	m^3
ν	Kinematic viscosity	ft^2/s
ω	Argument of perigee	$^\circ$
ϕ	Geographic latitude	$^\circ$
ϕ	Roll angle	$^\circ$
ρ	Density	kg/m^3
σ	Normal stress	N/m^2
τ	Control surface efficiency parameter	[-]
τ	Shear stress	N/m^2
τ	Trim angle	$^\circ$
θ_i	Angle of incidence	$^\circ$
AR	Aspect Ratio	-
b	Wingspan	m
b	wingspan	m
b_h	Beam	m
C	Channel capacity	Hz
c	chord	m
C_f	Friction coefficient	[-]
C_L	Lift coefficient	-
C_V	Velocity coefficient	[-]
D	Drag	N
d	Diameter	m
E	Energy	Wh
E	Young's modulus	MPa
F	Force	N
g	Gravitational acceleration	m/s^2
G_{AR}	Receiving Antenna Gain	dB

G_{FS}	Free space loss	dB
H	Flight Height	m
I	Moment of inertia	m^4
J	Advance ratio	-
K	Beam coefficient	-
K_D	Derivative gain	-
K_I	Integrational gain	-
K_P	Proportional gain	-
L	Lift	N
m	Mass	kg
N	Noise power	dB
N	Normal force	N
N	Safety factor	-
n	revolutions per second	1/s
P	Motor shaft power	W
P	Radiated power	dB
p	Pressure	Pa
p	Roll rate	rad/s
P_{RX}	Received signal power	dB
q	Shear flow	N/m
R	Data-Rate	bps
r	Yaw rate	rad/s
R_{atm}	Function of roughness and stability in the atmosphere	-
Re	Reynolds number	[-]
rpm	rotations per minute	1/min
S	Wing area	m^2
SNR	Signal to Noise Ratio	-
T	Thrust force	N
T	Torque	Nm
t	Time	s
u	Wind speed	m/s
V	Velocity	m/s
V	Volume	m^3
V_0	Vertical velocity	m/s
W	Weight	N
x	Longitudinal direction	m
y	Lateral direction	m
z	Vertical direction	m

Abbreviations

AES	Advanced Encryption Standard
BEC	Battery Eliminator Circuit
BLOS	Beyond Line Of Sight
c.b.	Centre of buoyancy
c.g.	Centre of gravity
CCI	Command and Control Interface
CFD	Computational Fluid Dynamics
COTS	Commercial off-the-shelf
CS-VLA	Certification Specification for Very Light Aircraft
DCCG	Dutch Caribbean Coastguard
DLI	Data Link Interface
DSE	Design and Synthesis Exercise

EASA	European Avation Safety Agency
EDA	European Defence Agency
EO	Electric Optic
ESC	Electronic Speed Controller
ESS	Electronics Support Structure
FC	Fibre Composites
FDM	Frequency Division Multiplexing
FEA	Finite Element Analysis
GCS	Ground Control Station
HF	High Frequency
HMNLS	Her Netherlands Majesties Ship
IR	Infrared
ISM	Industrial, Scientific, Medical
LCG	Longitudinal position of the Centre of Gravity
LOS	Line Of Sight
MAC	Mean Aerodynamic Chord
mc	Metacentre
MNS	Mission Need Statement
MPPT	Maximum Power Point Tracker
NATO	North Atlantic Treaty Organization
PD&D	Project Design & Development
PFD	Primary Flight Diagram
PID	Proportional, Integral, Derivative
PMI	Polymethacrylimide
POS	Project Objective Statement
PPM	Pulse-Position Modulation
PV	Photovoltaics
RAMS	Reliability, Availability, Maintainability and Safety
RF	Radio Frequency
RHIB	Rigid-Hulled Inflatable Boat
RoC	Rate of Climb
SAR	Search and Rescue
SIGAT	Study on the Insertion of unmanned aircraft systems in the General Air Traffic
STANAG	Standardization Agreement
UAV	Unmanned Aerial Vehicle
VCG	Vertical position of the Centre of Gravity
VHF	Very High Frequency
WMO	World Meteorological Organisation

Summary

This is a report on the design of a solar powered amphibious UAV for surveillance missions in the territorial sea around Curaçao. The eventual design will be manufacturable in quantities of around 200. When built, they will provide full coverage of the territorial sea and when a suspicious object is spotted, images are sent to a ground control station. In this stage of the design process a detailed concept has been developed. This report presents the rationale and design decisions that have led to the detailed concept of the UAV over the course of ten weeks. The final design is called the 'Dragonfly'.

In the preliminary design stages of the project, a set of three concepts has been selected for evaluation. These are a blimp, a conventional fixed wing and a hybrid lighter-than-air lifting wing body, referred to as the dynastat. It is found that the conventional fixed wing is the best candidate for the surveillance mission, largely on account of the other concepts' impractical size. Also, the fixed wing aircraft is able to fly faster and it covers more area per day. The fixed wing concept is then further developed and the final wing configuration is a tandem wing, as depicted on the cover of this report. A tandem wing is chosen because of its smaller wingspan and a higher efficiency compared to a conventional configuration.

This report presents a design for an amphibious solar powered UAV, with characteristic parameters as listed in Table 1. It is able to take-off and land from water. Surveillance is performed using a commercial off-the-shelf pan-tilt camera and the autopilot is based on the open-source Paparazzi software running on a Lisa/M 2.0 board. The Dragonfly is powered by two in-line Plettenberg Orbit 15/14 motors, consuming a total of 166 W in cruise. Power is delivered by lithium-polymer batteries which are in turn charged by a solar cell area of 0.6 m^2. Communication is done with a modem operating in the 900 MHz band and surveillance data can be transferred via a 1 Mbit/s data-link. Manual take-off and landing via radio control are possible within a range of 2-3 km. The structure mainly consists of epoxy resin glass fibre composites in the hull and hybrid glass- and high modulus carbon fibre composites in the wings and tail. Foam cores are used in the laminate to add stiffness. The Dragonfly presented in this report is to be further developed into a real product.

Table 1: Characteristic parameters of the amphibious UAV

Span	2.55 m
Length	2.25 m
Mass	8.75 kg
Battery capacity	433 Wh
Cruise altitude	2000 m
Cruise speed	22 m/s
Daytime endurance	1.8 hrs
Nighttime endurance	1 hr
Cost	€32717

With one Dragonfly, a total area of 718 km^2 can be covered per day.

Chapter 1

Introduction

The island of Curaçao brings thoughts of sandy beaches, blue sea and weather to spend a holiday in. Being an island, Curaçao is rich in this coastal blue paradise, which brings along the responsibility of monitoring the sea around the island for immigration, illegal trade and environmental hazards[1]. The Dutch Caribbean Coastguard (DCCG) is tasked with these duties, which may be performed more efficiently by deploying a fleet of UAVs in the territorial sea around Curaçao.

This report contains all progress made concerning the design of the UAV. The design is defined by the following Project Objective Statement (POS) and Mission Need Statement (MNS).

POS: *Design an autonomous amphibious solar powered UAV with a production run of about 200 units, whose purpose is to reduce surveillance costs on the coastal area of Curaçao. This should be done with 10 students within 10 weeks.*

MNS: *To conduct an economically and ecologically competitive autonomous maritime surveillance operation in the coastal area of Curaçao.*

These statements, together with a set of client-imposed top-level requirements, form the basis of the design process. The top-level requirements are:

- Upper weight limit of 35 kg
- Maximum air speed of at least 15 m/s
- Rate if climb of 10m/s for at least 5 seconds
- Minimum flight endurance of 1 hour
- Endurance at maximum thrust larger than 10 minutes
- Propulsion must be electric
- Minimum production series of 200 units
- Take-off and landing from water with waves no greater than 2.5 meters or World Meteorological Organization (WMO) sea state 4

This report consists of three parts. Part I will deal with the systems engineering, part II deals with the the conceptual design and finally part III deals with the detailed design.

In Part I, first, the project organisation for the entire project will be explained in Chapter 2, it will also include the Gantt chart. After that the market analysis in Chapter 3 will explain the current operation of the DCCG, other existing comparable systems, a strengths, weaknesses, opportunities and threats analysis of the UAV and finally some other possible costumers for the UAV. Chapter 4 will show the mission outline, the functional flow diagram and the functional breakdown.

Part II deals with the conceptual design of the UAV. The three concepts are described in Chapter 6. In Chapter 7 the trade-off is done between the three concepts. The methodology, criteria and weight factors and the conclusion are described here.

Part III deals with the final design. First, Chapter 8 describes all the projects' contingencies and in Chapter 9 the process concerning the selection of the final concepts' configuration is shown. Chapter 10 deals with the budget breakdowns. In Chapter 11 the weather conditions, the sea conditions and the consequences these have for the coatings are described. Then the interaction between the UAV and the wildlife are described. Chapter 12 deals with the description of the aerodynamic and flight dynamic design process and the final lay-out. Also described are the control surfaces Chapter 13 deals with the maritime design decisions, the influence the landing and taking off on water, has on the hull and stability. Chapter 14 explains the communication, the ground control system, imaging and flight control systems. Chapter 15 describes the power and propulsion systems. This includes the propeller and motor selection, the motor controller, the battery sizing and selection and the solar panel design. Also show in this chapter are the electrical power conversion and the electrical block diagram. Chapter 16 explains the production, material and structures. It starts off with the different load cases, then the structural analysis methodology is explained. This leads to the structure & parts and the material selection. Finally the maintenance is explained in this chapter. The final design is fully described in Chapter 17. This includes the configuration and lay-out, the costs, a design analysis, a manufacturing and assembly plan. A performance analysis and different characteristics of the airplane. In Chapter 18 the sustainable development strategy is described. Chapter 19 deals with technical risks and what consequences they have for the final design. Chapter 20.1 tells about the further steps to be taken to get from this final design to a working (prototype) UAV and in Chapter 21 the conclusion is given. In Chapter 22 the recommendations are listed for future work. Finally, in B all the deliverables are listed in a table which states where the deliverables can be found.

Part I
Systems Engineering

Chapter 2

Project organisation

The project organisation consists of a comparison between the original and final Gantt chart in Section 2.1 and a Human Resource budgeting in Section 2.2.

2.1 Gantt chart

Project management requires a full overview of the work progress. To achieve such an overview, a Gantt chart is created. A Gantt chart is a tool used for managing project planning. In order to understand a Gantt chart, first the data required for the chart is discussed. Tasks and subtasks are defined and for every task the amount of work hours, people needed, start date and finish date are required. Finally, predecessors are included. By defining predecessors, the order in which tasks can be performed will be displayed correctly. Also, this order defines the critical path.

With all the information entered correctly, Microsoft Project provides a Gantt chart, which is used as a tool to control and observe the planning and progression throughout the complete project. Therefore the Gantt chart is updated every time a task is finished. To update this, the activity logbook is used, in which the duration of each task take is recorded.

In the end of the project the original Gantt chart is transformed into the final Gantt chart where all the hours and tasks are updated. This updated final Gantt chart can be found in Figure 2.1.

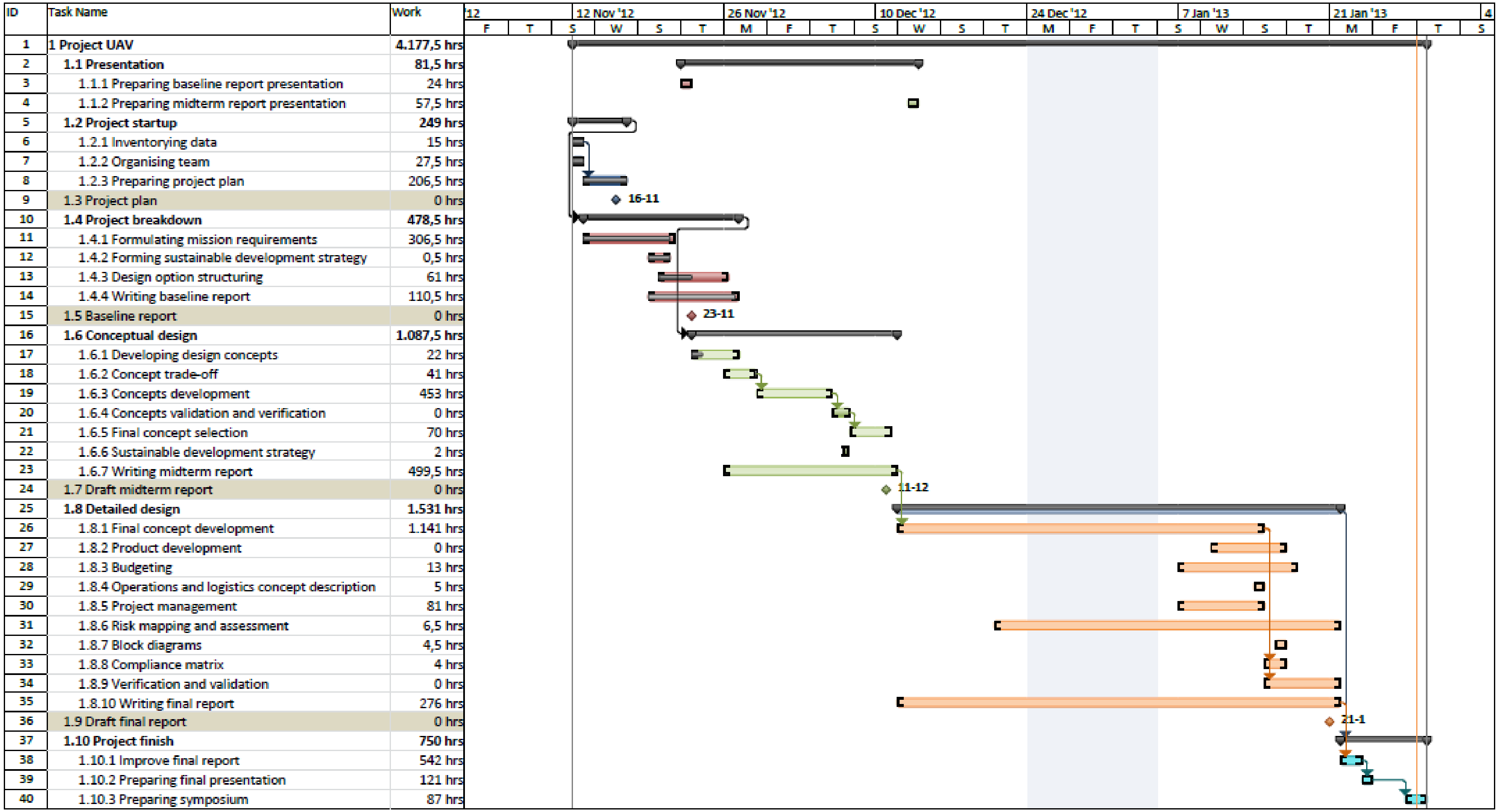

Figure 2.1: The final Gantt chart

When this final Gantt chart is compared to the original Gantt chart, a comparison can be made with the estimated amount of hours needed and the amount of hours that were actually used. This table can be seen in Table 2.1.

Table 2.1: Hours per task

Task	Assigned hours	Actual hours
1.1.1 Preparing BR presentation	8	24
1.1.2 Preparing MTR presentation	80	57.5
1.2.1 Inventorying data	20	15
1.2.2 Organising team	5	27.5
1.2.3 Preparing project plan	142.5	206.5
1.4.1 Formulating mission requirements	246	306.5
1.4.2 Sustainable development strategy	4	0.5
1.4.3 Design option structuring	110	61
1.4.4 Writing baseline report	85	110.5
1.6.1 Developing concepts	56	22
1.6.2 Concept trade-off	120	41
1.6.3 Concepts development	272	453
1.6.4 Concepts validation and verification	140	0
1.6.5 Final concept selection	90	70
1.6.6 Sustainable development strategy	4	2
1.6.7 Writing midterm report	124	499.5
1.8.1 Final concept development	600	1141
1.8.2 Product development	140	0
1.8.3 Budgeting	32	13
1.8.4 Operations and logistics concept description	8	5
1.8.5 Project management	26	81
1.8.6 Risk mapping and assessment	16	6.5
1.8.7 Block diagrams	8	4.5
1.8.8 Compliance matrix	6	4
1.8.9 Verification and validation	220	0
1.8.10 Writing final report	200	276
1.10.1 Improve final report	160	542
1.10.2 Preparing final presentation	80	121
1.10.3 Preparing symposium	160	87
Meetings and presentations	250	329
Total hours	3412.5	4506.5

It can be noted that the amount of hours in the Gantt chart does not match the total amount of hours in Table 2.1 Meetings and presentations were originally not in the Gantt chart, so for the first half of the project these hours are not included.

When these hours are compared, it can be seen that more hours were performed during the project than was originally assigned for. An extra 32% was required to finalise the project. These extra hours are mainly due to writing of the report. As can be seen in Table 2.1 an extra amount of 45% of the assigned time was needed to write the project plan. Further, the baseline report and the midterm report needed extra amounts of time of 30% and 303% respectively. Finally, the final report required 818 hours, which is an overshoot of 127%.

Further, the amount of hours spent for the validation and verification of the design and the product development are given as zero. This is due to the logging of the hours, the hours spend validating, verifying and developing the product were actually logged in the (final) concept development.

Now that all the tasks and their corresponding hours are known, the hours spent by each group member can be computed. This is done in Section 2.2.

2.2 Human resource budgeting

Using the updated Gantt chart, the human resource budget can be updated. The distribution of human resources can be visualised as the hours spent by each team member per week. These hours per person are given in Table 2.2.

Table 2.2: Amount of hours spent by each group member per week

Group member	Wk 1-5	Wk 6	Wk 7	Wk 8	Wk 9	Wk 10	Total hours
R. Augustinus	205	39	47.5	60.5	57	27.5	436.5
J. Chang	204.5 (1)	39	45.5	45.5	53	24.5	412
J.J. van Gorcum	217	31.5 (3)	49.5	58.5	65.5	28	450
M.J. Koot	214	39	51	65.5	61	27.5	458
H.H. Ubbens	221	39	47	64	62	29	462
C. Çakiroglu	206.5	38.5	45	48	54	26.5	418.5
M.A. Estrada	194 (2)	41.5	46.5	60	59.5	26	427.5
B. Groenenboom	199	39.5	51	53	70	30.5	443
A.E. Naruta	249.5	39.5	67.5	78.5	54.5	31	520.5
M.E. Wassenaar	224.5	40.5	57	59.5	68 (4)	29	478.5
Total hours	2135	387	507.5	593	604.5	279.5	4506.5

[1] One day of absence due to personal matters.
[2] Two days of absence due to illness.
[3] One day of absence due to holiday.
[4] One day of absence due to tutor training.

Table 2.2 shows the work performed per week, where a week is defined from Monday to Sunday. A regular work week contains of five eight-hour work days which add up to a total of 40 hours per week.

As can be seen in Table 2.2 the total hours spent in the first five weeks added up to an average of 42.7 hours per week per person.

When the design process arrived at the sixth week, the team started with the the final design. As can be seen, this first week for the final design, week six, was a normal work week.

When the seventh week started, it became clear that a lot of work still had to be performed. This can be traced back to the amount of hours spent in weeks seven, eight and nine. The design had to be finalised and a very detailed concept was expected. Therefore the work performed in weeks seven, eight and nine contain 27%, 48% and 51% of overtime hours respectively.

Week 10 has the least amount of hours spent, due to only three working days and the Design Synthesis Exercise Symposium on Thursday the 31^{st} of January.

To conclude, 132% of the assigned time was required to finish the project and to present the final design.

Chapter 3

Market analysis

When designing a product, understanding the market for this product is vital. First the specific market of this mission, namely that of the DCCG, is analysed. Then, UAVs at the current market are compared. Following that; a SWOT diagram that sums up the strengths, weaknesses and opportunities of the product and the mission and possible threats to the product and mission for further analysis. Finally some other different costumers are considered.

3.1 Current coastguard operations

Besides the different possible customers, the to be designed UAV will be designed for the field of maritime security with the DCCG as a possible client. They define their objective as 'Providing maritime law enforcement (surveillance and detection) as well as maritime security within the area of responsibility as defined in the provisional regulation of the DCCG'[2]. Their tasks include tracking and prevention of drug and weapon trade, illegal immigration, illegal fishing and environmental pollution. In their work they cooperate with police, customs and other authorities. The DCCG exists as a joint effort between the governments of Curacao, Aruba, Sint Maarten and Caribbean Netherlands. Their area of operations is shown in Figure 3.1.

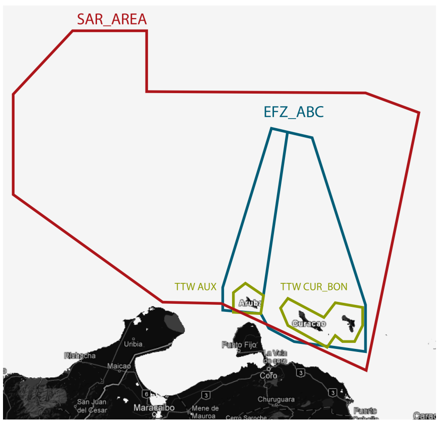

Figure 3.1: DCCG area of operation [3]

As can be seen from Figure 3.1, the DCCG performs Search And Rescue (SAR) initiatives in the SAR-AREA. The other areas in Figure 3.1 are the Exclusive Fishery Zone (EFZ) and the Territorial Waters (TTW) of the different Caribbean islands. Currently DCCG employs a number of assets to complete the tasks described. Their fleet is listed as follows:

The flagships of the DCCG are three coastguard cutters complete with a Rigid-Hulled Inflatable Boat (RHIB).[1] These ships (the Panter, the Jaguar and the Poema) are about 41 meters long and host a crew of 11. They fulfil various roles, each in their assigned sector (Aruba, Curaçao or Sint-Maarten). Each cutter is deployed for about 120 days per year. These ships are equipped with radar equipment, ION scanners (a scanner used in drug searches), a fixed machine gun and a movable fire extinguisher. Furthermore, these ships are in possession of imaging equipment which is used to collect evidence material if necessary.

In addition, the DCCG operates 12 Super RHIBs, six light RHIBs, a single station ship (Her Netherlands Majesties Ship) for their naval fleet. The aerial fleet consists of two Augusta Westland AW-139 helicopters, a Lynx helicopter and two Dash-8 type (MPA-D8) planes.

Table 3.1: DCCG asset use based on press-releases (Oct 2011 - Oct 2012)

	Incidents			
	Drug smuggling	Illegal migration	SAR	Various
Cutter	1	-	4	-
Super RHIB	6	3	10	4
RHIB	-	-	3	-
Dash-8	-	-	6	-
AS355	-	-	2	1
Lynx heli	-	-	1	-
Station Ship	1	1	1	-
Alouette III	1	-	1	-
Not specified	5	5	-	2

The majority of tasks that DCCG performs could be classified as either SAR type operations or prevention of drug smuggling and illegal migration. DCCG aerial fleet is used extensively for SAR tasks, while the detection and interception of violating vessels is generally done by the fleet of Super RHIBs. Based on press-releases alone, it is evident that aerial surveillance is not used as extensively for spotting violating vessels and its use is mostly confined to SAR type of missions. However, the mission that this UAV is designed for will be initially for the TTW of Curaçao. So, in order to ease the surveillance and detection of vessels, the UAVs can be alternatives for part of the DCCG fleet. With the main mission discussed, now comparable UAVs can be considered.

3.2 Comparable UAVs in mission

It is important to know the alternatives for UAVs and relate them to the current market. Though effort is made to find comparable surveillance UAVs executing a similar mission, no currently existing amphibious solar-powered UAVs were found. There are some UAVs that are solar-powered or amphibious or conduct a very similar mission and have approximately the same weight as the requirement for this UAV. These UAVs range from amphibious petrol engine UAV to High Altitude Long Endurance (HALE) UAV and electrical rotary observation platforms. These reference UAVs are list in Table 3.2 and elaborated and related to the designed UAV afterwards.

Warrior (Aero-Marine) – Gull 24 One of the comparable UAVs is the Gull 24, manufactured by Warrior (Aero-Marine) Ltd.[4] The Gull 24 is a small amphibious UAV with technologies that enable the UAV to meet navy and coastguard demands. By using a wave-piercing hull the Gull 24 can operate in Seastate 3 conditions. The advantage of this configuration is that the Gull can take-off and land on water and it uses waves as a ramp to get airborne during take-off.

Table 3.2: Comparable reference UAV data

Name	m [kg]	Payload [kg]	b [m]	Endurance [h]	Power Source [-]
Gull 24	18	6	2.7	6.8	Petrol Engine
Zephyr	53	2.5	22.5	336	Solar
Fury 1500	136	34	3.7	16	Petrol Engine
SR 100	16	2.5	N/A	0.67	Battery
Scaneagle	18	6	3.1	18	Battery
RQ-15 Neptune	36	9	2.13	4	Petrol Engine

Because the Gull 24 is an amphibious UAV, it can serve as an example to the UAV to be designed. However, the Gull is not solar powered and not autonomous. The key specifications that makes the UAV interesting for the UAV design are the size and its ability to take-off, land and float on water.

QinetiQ – Zephyr The Zephyr by QinetiQ is a HALE solar-powered UAV. It is designed to remain airborne for three months and has demonstrated that it is capable of flying for 14 days straight.[5] Its sole power source are the solar panels which cover the entire wing. These panels charge the batteries to power it throughout the night.

The relevance of this aircraft to our UAV is the long endurance and the fact that the Zephyr is fully solar powered and is perform for observation missions.

Rotomotion – SR100 The SR100, built by Rotomotion is an unmanned helicopter -with a gross take-off weight of 16 kilogram- can handle a payload of 9 kilogram. It can be used as a motion-controlled audio/video turret and its flight is fully autonomous. The optional electric motor version is considered. The helicopters rotor is belt driven and it has a telemetry system with a range of 800 meters.[6] The SR100 can be considered as a well-built alternative for fixed wing aircraft and has good audio/video recording possibilities.

Lockheed Martin – Fury 1500 The Fury 1500 is an unmanned aircraft made by Chandler/May (recently bought by Lockheed Martin) and is a UAV that carries out intelligence, surveillance, reconnaissance and electronic warfare missions for the US Armed Forces.[7]

The aircraft has a blended wing design and a three bladed rotor at the rear section. Its propulsion system consists of a heavy fuel engine which uses JP-8 as fuel. It can be controlled manually from its portable ground control system or through a fully automated flight using SharkFin software, which carries out navigation control, video display and payload control missions. The UAV is launched with a pneumatic launcher so a runway is not needed.

It could serve as an example for the UAV to be designed in terms of its endurance, size and implementation of commercial-off-the-shelf (COTS) components.

Boeing/Insitu – ScanEagle The ScanEagle is a mini combat surveillance UAV developed by Insitu and Boeing at the Phantom Works facility. The missions the ScanEagle can perform are surveillance missions, escort operations, sea-lane and convoy protection and high-speed wireless voice, video and data communications.[8] The UAV is composed of five major modules: nose, fuselage, avionics, wings and the propulsion system. All these systems are infield-replaceable, which is a major advantage during missions.

In the design process of the proposed UAV, the ScanEagle can serve as an example regarding its size and its comparable missions. Simplicity and ease of maintenance are convenient for an UAV as well, and should therefore be bearing in mind.

DRS – RQ-15 Neptune The DRS – RQ 15 Neptune is an amphibious reconnaissance UAV, it is designed by DRS for the US Navy. The Neptune has electro-optical and infra-red sensors on-board. The Neptune is powered by a petrol engine. The Neptune can land and take-off from water, or be launched by a catapult and land on a skid.[9]

The Neptune is comparable to our UAV because it is of roughly the same size, has the same kind of mission (albeit with a longer endurance) and is able to float on water.

This data can be used in the design process, which also includes the analysis of the strengths and weaknesses. With this it is possible to formulate requirements and a mission outline.

3.3 SWOT analysis

With the use of the reference aircraft, a SWOT analysis can be performed. The SWOT analysis states the strengths, weaknesses, opportunities and threats of the mission in a clear overview. The strengths and weaknesses are of internal origin, while the opportunities and threats are of external origin. These "SWOT" are determined on different areas with no priorities and no weight. To evaluate the opportunities and threats it is important to give them a weight factor. This allows to evaluate these threats and opportunities with respect to each other. The same can be done by assigning priorities to the SWOT. Priorities are assigned to each of the points. In Table 3.3 the SWOTs are listed from highest priority to lowest, from top to bottom, respectively. However, achieving an optimal result remains an iterative process. [10]

Table 3.3: SWOT diagram

	Advantages	Disadvantages
Internal effects	**Strengths** 1. Requires minimal human interference and interaction 2. Many UAVs 3. Amphibious 4. Solar power (no need to refuel) 5. Possibility to fly high and be barely visible	**Weaknesses** 1. Solar power (no recharging at night) 2. If technical difficulties occur, UAV has to be picked up 3. You have to trust on computers that don't have human instinct 4. Limited endurance
External effects	**Opportunities** 1. Reduce drug trafficking 2. Possibility for technical breakthroughs 3. Save costs 4. Government support 5. Increase of demand for aircraft operations	**Threats** 1. Collisions 2. When floating weak against environment 3. Lack of experience in the field 4. Certification issues

In Table 3.3 the most important strength of a UAV system is that it requires minimal human interaction. This gives the opportunity to reduce the cost. As many UAVs are used, the coverage area increases. This results in a more extensive monitoring of the desired area. This can reduce the illegal drug trafficking and immigration, the most important opportunities for this mission. Another strength that is mentioned in the table is that the UAV is amphibious, this means that the UAV can remain away from the coast and therefore improve the coverage of the area. This again leads towards the opportunity of reducing drug trafficking. With this UAV the possibility emerges that it can fly at a high altitude which makes it harder to be detected. The final major strength of the UAV is that it is solar-powered. This means that it can remain at sea for extended periods of time and that it is sustainable. The fact that governments are interested in sustainable solutions, gives the opportunity to have their support for this project.

The main weakness of the UAV is that it cannot generate power during night time and reduced power during clouded weather, so it has no continuous power input. This results in a longer period for which it might be idle and therefore be more exposed to environmental conditions. Another weakness of this operation occurs in the case of technical difficulties. When this happens, the UAV will have to be retrieved for repair. When they need to be retrieved by the DCCG, they might be exposed to the environment for an extended period of time, which poses a potential threat. The problem with autonomous systems is the reliability and obstacle avoidance. This weakness can create the threat of collisions, which has to be avoided at all costs. The final weakness is limited endurance. This increases the chances of collisions due to the fact that the UAVs will move between cruise height and sea level more frequently and thus exposes them to each other and to other moving objects.

3.4 Customers

In the field of surveillance, there are many applications for UAVs. Different customers use UAVs in a variety of ways. Compared to manned aircraft they are relatively cheap, easy to work with, barely need humans for interaction and can be used in dangerous situations without having human lives at risk. Several applications of UAV surveillance are:

- **Law enforcement**: Many different types of police forces will have use for a surveying UAV. For example, an UAV could take over the task of helicopters that chase criminal suspects on the run. Border control can also be an area that would value the use of UAVs, to be able to easily track activity around the borders.[11] Lastly, the coast guard can use UAVs to survey all maritime activity in territorial waters under their jurisdiction. For the example of Curaçao, they can be used to track illegal drug trafficking and immigration.
- **Military**: In general, UAVs are very useful in the military. Examples of tasks they can do are weapon delivery, communication in war zones and even deception. A good example of what a surveillance UAV can do for the military is reconnaissance in and around war zones, sometimes in combination with stealth equipment for covert operations. [12]
- **Environmental**: Environmental control is another one of the fields UAVs could be used in. An example of this is wildlife protection organisations, who can track and follow wildlife activity in areas of interest or perform environmental monitoring tasks. [13]
- **Civil**: In civil operations, there are also a number of uses for UAVs. Dangerous areas or 'risk' areas for natural disasters can be monitored, warning the public of upcoming earthquakes, tsunamis, etc.[14] Another use would be to search an area for survivors of natural disasters, making search and rescue operations a lot more efficient.
- **Security**: Although there is some overlap to this category with both police and military, security is also one of the uses for UAVs. They could be used privately for surveillance of large areas, to check for intruders or for example look for poachers in wildlife reserves.

All these potential customers have different uses for UAVs, but every customer uses it for surveillance. The main customer for this market is the DCCG, which can be categorised as a costumer in law enforcement.

Chapter 4

Mission

4.1 Mission outline

Taking into consideration the market analysis in Chapter 3, the UAV to be designed is intended to survey the coastal area of Curaçao. It has to comply with a list of top level requirements set by the client. These requirements partly determine the mission profile of the UAV. Moreover, the mission profile is a function of current coastguard operations in the region. In order to develop a feasible mission solution, this situation is assessed based on: current assets, practices and objectives of the client (DCCG). All have been treated as part of the market analysis, which allows proposal of some possible improvements.

Market analysis shows the Dutch Caribbean Coast Guard (DCCG) performs a wide variety of tasks in the Caribbean region. In doing so, they employ a fleet of both marine and aerial vehicles. However, this fleet is insufficient for providing 24 hour visual surveillance of the area under their control. This could be greatly improved by employing a number of small UAVs to survey the area. These UAVs can be used to identify suspected vessels. For instance, they could be used to detect smaller vessels such as a yola boat.

These small boats are often used to transport illegal migrants and drugs. They are hard to detect using radar alone. In SAR missions, multiple UAVs could assist in surveying large areas. Overall, maintaining a fleet of small semi-expendable UAVs would allow to improve efficiency of the DCCG aerial fleet, by allocating some of the tasks that are currently performed to these portable platforms instead. Moreover, the drones are capable of complementing the DCCG marine fleet, which currently lacks means to survey the shallow water areas such as internal waters and bays [15].

Basic operations the UAV will have to perform are evaluated in Section 4.1.1. In Section 4.1.2 the different types of possible UAV missions are stated. Finally, Section 14.1.4 addresses some last mission considerations.

4.1.1 Basic operations

The main mission objective for the UAV to be designed is to provide aerial surveillance in the Caribbean region. It is required to be equipped with earth observation sensors, including night vision capabilities. Also it is required to feed the data in real time while operating beyond line of sight (BLOS). In the development of such a vehicle, priority is given to make the UAV fully autonomous. The UAV should be simple in operation and maintenance, which would make it versatile in deployment and operation. Moreover, the UAV is expected to operate autonomously for at least a week before returning to base for inspection. The aircraft is expected to be developed using Commercial Off-The-Shelf (COTS) components and to be able to work based on open-source technology. It also has to integrate with the current DCCG fleet and ground operation stations.

Each mission deployment of the to be designed UAV can be split up into launch, operational and retrieval phases. The UAV must be able to take-off from water and land on it. During its operational phase it is required to perform surveillance sweeps while staying airborne for at least an hour. The UAV should be able to do this with a maximum speed of at least 15 m/s. It is expected to be able to recharge its on-board batteries with an array of solar cells. While airborne, the aircraft must collect data from its sensors while transmitting imaging and video data and its location to the operator. During flight it must be capable of way-point navigation, autonomous object tracking and in-flight route mapping. These features are typical for surveillance UAVs currently available on the market. Modularity of payload would be advantageous because it would allow the UAV to be more flexible in the tasks it carries out.

The end-user must receive a processed, usable video feed. A typical sensor for such a UAV vehicle is a type of Earth Observation/Infrared (EO/IR) gimbal. It also needs to have a positioning system implemented, so the operator is able to pinpoint its location; and a communication system to transmit data to the operator, receive commands and broadcast its location, even in case of minor malfunctions. The system must include a Ground Control Station (GCS) for the operator.

The mission planning and control has to be done by the UAV operator with help of GCS tools. The interface and capabilities of GCS should be accessible and useful with minimal amount of prior training. This would reduce the overall life cycle costs of the system. The UAV avionics must be capable of navigating and maintaining flight with minimal input from the end user. The same principle accounts for payload operations. This, however, puts some strain on aircraft power consumption. Fully automated flight requires increased processing power to be available on board. The complexity of such a system means increased development costs. Additionally, it affects the reliability of the UAV: the flight control system must be able to adapt to a wide variety of weather patterns and contingencies.

4.1.2 Operational scenarios

With the main required capabilities of the UAV outlined in the previous section, typical operational scenarios can be described. Some possible scenarios include surveillance operations and patrol.

In patrol missions, multiple drones are distributed to cover an area of interest. The drones would stay at their assigned positions for several days, performing regular patrol sweeps over the assigned territory. Additionally, they would be available for immediate deployment upon call from the ground station or a nearby coastguard vessel. In that case, an airborne drone would travel to the area of interest, inspect it and then return to its assigned post. Such a mission would require the drones to be available continuously; the operator must be able to pinpoint the location of each drone at any given moment and communicate commands if necessary. Optionally, live video data would be transmitted to GCS. Continuous video transmission would require a lot of power, so it would improve efficiency of the system if it is able to decide when live video data is needed. In this case a high level of autonomy is required. It would improve overall efficiency of the system if drone software would be able to detect and distinguish vessels or heat signatures and notify the operator. Patrol missions would require communication beyond line of sight. This could be achieved by using a satellite link, a network of re-translators or a direct link in the range of High Frequency (HF), or Very High Frequency (VHF) bands.

In surveillance missions multiple drones are deployed. Once in position, they perform a pattern sweep in the area of interest. Drones would either employ a creep, sector, track line or parallel type of pattern, depending on the circumstances. When they sweep the area, they would communicate live video data to the operator. The flight patterns for this type of missions must be pre-programmed and adjustable so that the drones could be employed in a wide variety of situations. These drones would complement the current DCCG aerial fleet, allowing to survey large areas with increased efficiency.

4.1.3 Other considerations

A high degree of automation significantly reduces complexity of operation. However, all drones must be regularly inspected and maintained. Drones assigned to patrol tasks are expected to return to base every week. This has an effect on mission planning and overall logistics of the operation.

The basic operation layout of the drone fleet organisation could be split in multiple sectors: A team of operators coordinating the drone assignments and monitoring their status. A technical maintenance team which would inspect and maintain the drone fleet. And a deployment team, which would be responsible for drone deployments and possible retrieval of malfunctioning units. All these aspects should be developed in more detail in later stages of the design process.

4.2 Functional flow diagram

This section elaborates on the basic functions of the UAV. Therefore, the functions described in this chapter are elementary. First of all, the main functions are determined, such as preflight actions, flying and taking off. In order to complete these functions, a sequence of corresponding actions must be carried out. These actions involve the UAV and/or ground personnel and their equipment. For example, the UAV will have to be able to turn on the cameras, survey and communicate to the ground during the flight phase. The sequence in which the basic functions are displayed, will be commonly chronologically performed. However, since the flight endurance is much shorter than the time interval between two maintenance sessions, the missions will involve the UAV operating several take-off and landing loops before returning to base. In the diagram this is represented by the arrow after the second flight session going back to landing on water, as well as the arrow from the maintenance session back to initial take-off. Many other basic functions and corresponding actions are explicitly shown in Figure 4.1.

4.3 Functional breakdown

After the FFD has been established the functional breakdown can be performed. The functional breakdown diagram, which can be seen in Figure 4.2, represents the basic UAV functions required to perform its mission. As illustrated in Figure 4.1, all basic functions can be easily collected. The functional breakdown diagram elaborates the function flow diagram and adds a division of the functions. These functions are then subdivided into sub-functions required to perform respective mission aspects as displayed in Figure 4.1. The functional breakdown can be visualised in Figure 4.2

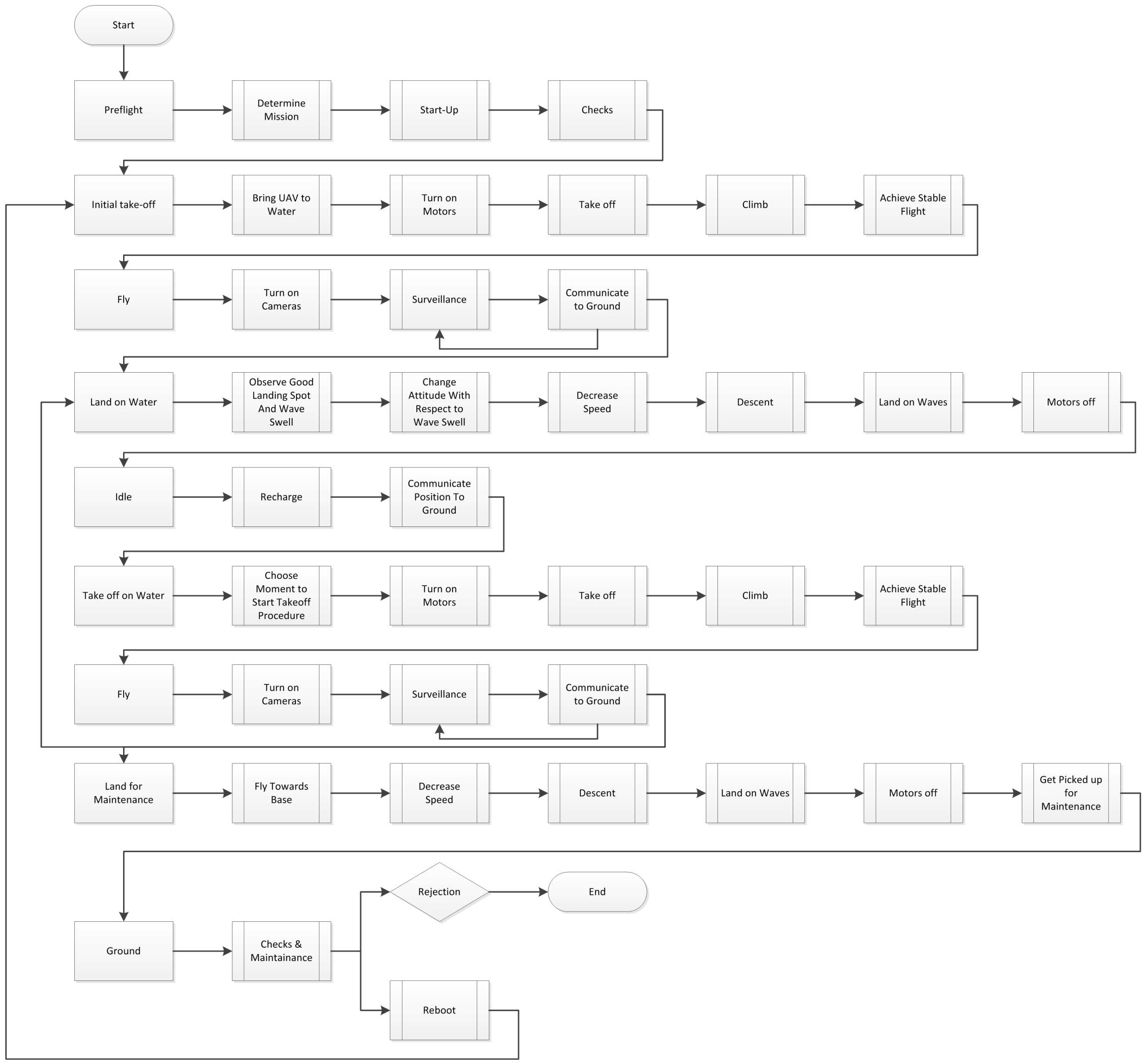

Figure 4.1: The functional flow diagram

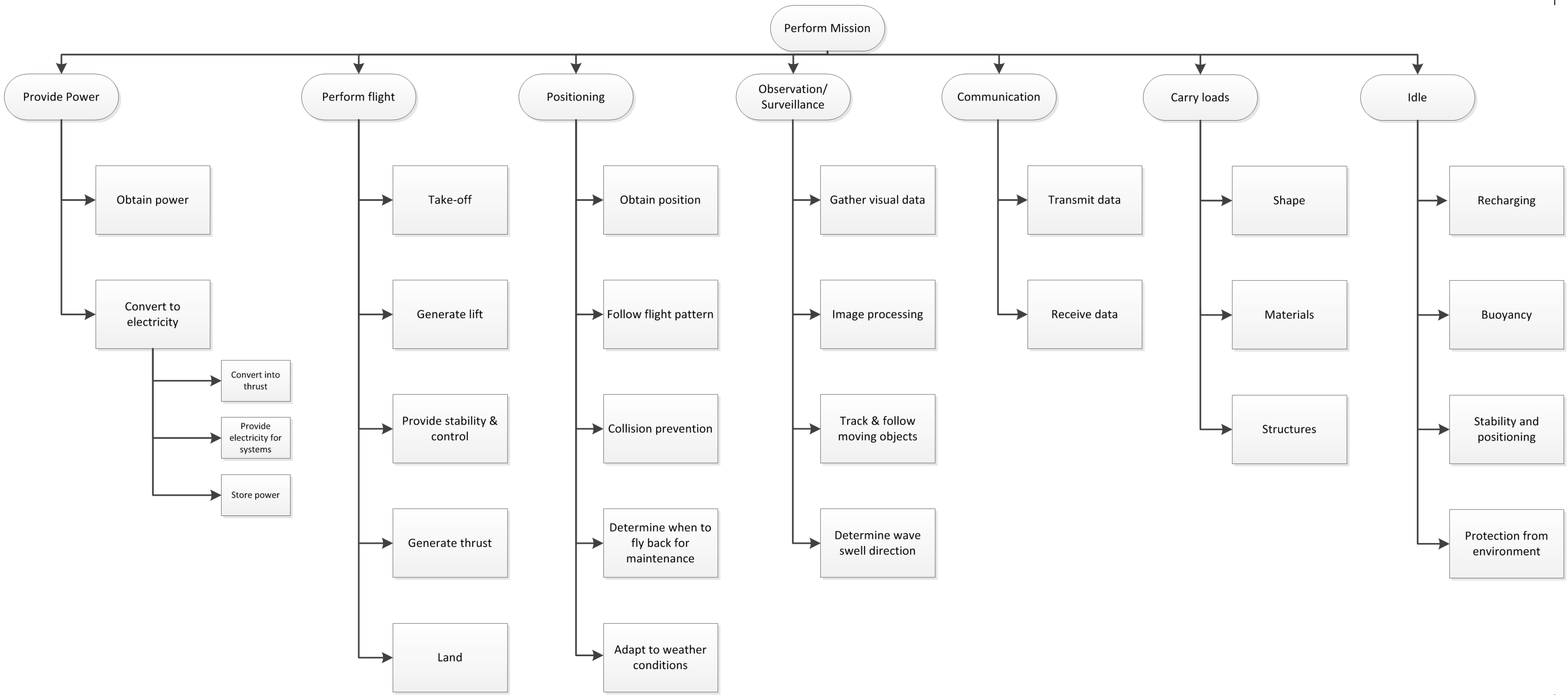

Figure 4.2: Functional breakdown structure

Part II
Conceptual Design

Chapter 5

Preliminary concept evaluation

This chapter explains the first concept selection. From 43 generated concepts, three concepts are selected for further evaluation.

Preliminary concept evaluation
43 concepts generated by the members of the design team. In order to select concepts that will be researched in more detail, trade-off criteria for the current selection of concepts are set up. The concepts are then graded based on the evaluation criteria. The grades range between one and five, where five is the best score and one is the worst score.

The emphasis of the trade-off lies on endurance and production, since these are imposed by the client as primary design goals. In addition, four other criteria are set: technical feasibility, complexity (which includes production), recharging potential and seaborne stability. These criteria are elaborated below. First, the primary criteria are presented:

- Technical feasibility: How designable is this concept? Is it based on proven concepts?
- Complexity: To what extent can the design be completed with COTS parts?
- Endurance: In the conceptual phase this is represented by the qualitative question: how energy-efficient can this design potentially perform its tasks?

These first three factors are weighted heavier than the rest; the primary trade-off criteria are given a weight of 1.5, the secondary criteria receive a weight of 1. The secondary trade-off criteria are:

- Recharging potential: How many PV cells can be fitted on the design?
- Seaborne stability: How well will this design remain stable in the sea, during the idle phase, take-off and landing?

The actual trade-off consists of individually grading each concept on the criteria presented above. Team member grades are averaged to produce a feasible weighted list of the 43 concepts. A check for grading differences between team members is done and large discrepancies are discussed. The selected concepts are listed below:

Conventional fixed wing: The design of this concept is of a conventional lay-out. The lift is generated using a wing and stability will (most likely) be provided using a tail.

Blimp: The focus of this concept is on generating lift using the lighter-than-air principle. This way the UAV is able to hover at a single spot.

Lifting body dynastat: This concept is a hybrid between a fixed wing and a blimp. It generates both dynamic lift by being wing-shaped and buoyant lift by being filled with a lighter-than-air gas such as helium or hydrogen.

Chapter 6

Concepts

In this section the results of the concept evaluation are briefly described. First the blimp is evaluated, then the fixed wing concept and finally the dynastat concept is elaborated.

6.1 Blimp concept

The blimp concept is a lighter than air vehicle and obtains its lift from the use of lighter than air gasses, its appearance can be seen in figure 6.1.

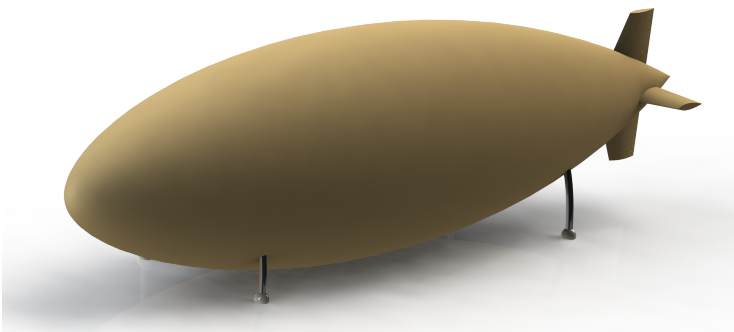

Figure 6.1: Rendering of the blimp

Aerodynamics: The lift of a blimp is obtained form the use of Helium, the volume of Helium required for lift off of the blimp determines the balloon size, the shape of the balloon is determined for aerodynamic drag reduction. The balloon therefore has a length of 12 meters and has the shape of an symmetric airfoil turned around it chord.

Control and Stability: The Control of the blimp is performed with rudders, elevators ballonets and thrust vectoring for the control. Ballonets are balloons within the Helium balloon which can store normal air inside them, in this way the attitude of the blimp can be controlled. The stability will be achieved by a low centre of gravity due to the payload which is mounted at the bottom, also the ballonets can be used to actively control the stability of the blimp.

Power and Propulsion: The power required by the blimp will be obtained from thin film solar cells which cover the entire top side of the blimp, these solar cells would generate enough power for continues flight, this is easily achievable due to the large size of the blimp. The batteries are sized for the maximum speed requirement due to the high drag of this UAV at higher speed conditions. Therefore the blimp can fly for 1.5 hours continuously in night conditions. The electronic motors required are also sized for the maximum speed conditions, since the rate of climb is obtained through buoyancy only. The total motor power required for the blimp would be 2.5 kW.

Weight estimation: The main contribution to the weight of the blimp is the Envelope with a weight of 29 kg, the Helium which weighs 8.6 Kg and the batteries which will weigh 3.4 kg, the total weight of the Blimp is estimated at 44 kg.

Manufacturing and maintenance: The operation costs are considered to be low for the blimp design, and maintenance cost equate to a small airplane. The specialities in the manufacturing of the blimp are its envelope and a non rigid supporting structure. The envelope should be made of a combinations of materials which together give low permeability and high strength, synthetics like polyester and polyurethane can be used for this purpose. The non rigid structures consist of strings which bring the envelope under tension, which should be installed very precisely.

Maritime: The blimp will not have a take off run since vertical lift of is possible, therefore only floaters need to be considered for stability when on water. 4 ball shaped floaters will be used which in total will have an emerged area of 2.44×10^{-3} m^3

6.2 Concept 2: Fixed wing

This section presents the results of the evaluation of the fixed wing concept. Analysis is based on the areas of aerodynamic performance, stability, maritime performance, battery & motor sizing and solar panel sizing. In addition, weight is estimated and manufacturing & maintenance are considered.

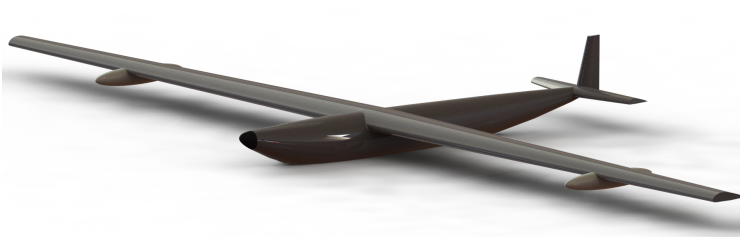

Figure 6.2: Rendering of the fixed wing

Weight estimation: From reference data of 12 reference aircraft, a total mass of 31 kg is estimated for the fixed wing. Payload typically takes up around 20%. 30% is assumed to be needed for batteries.

Power and propulsion: Sizing the propulsion system for the climb requirement, motor power needed is found to be 4.7 kW. A battery capacity of 1376 kWh is needed to fulfil the endurance requirement. A wing area of 1.88 m^2 can be filled with PV cells, delivering a total of 375 W of recharge power.

Control and Stability: For control of the fixed wing a canard and conventional configuration are considered. A conventional layout provides stability more readily, but is less efficient than a canard due to the horizontal tail producing downwards lift.

Manufacturing and maintenance The manufacturing of a UAV fixed wing is comparable to the manufacturing of a small airplane. This is due to the fact that it has the same configuration and materials as a small airplane. Compared to the other UAV concepts, a lot of experience and possibilities are already present; this reduces the costs.

Maritime For the fixed wing, a catamaran- and trimaran type floater configuration is looked into. Trimaran set-up is found the result in a lower wetted area (1.27 m^2), which is preferred for take-off drag.

6.3 Concept 3: Dynastat

This section presents the results of the evaluation of the dynastat. Analysis is based on the areas of aerodynamic performance, stability, maritime performance, battery & motor sizing and solar panel sizing. In addition, weight is estimated and manufacturing & maintenance are considered.

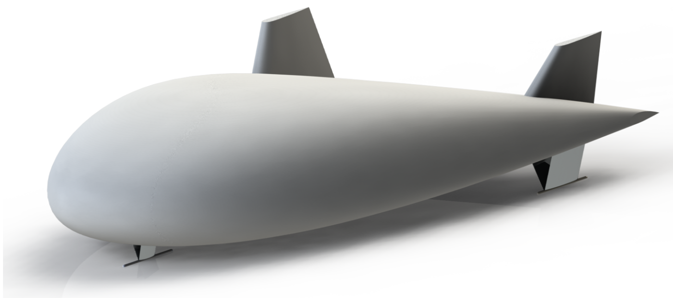

Figure 6.3: Rendering of the dynastat

Aerodynamic performance: The dynastat produces lift from its airfoil shape and from static buoyant lift. The body is a NACA 4424 airfoil with a wing surface S of 12 m^2. Drag is calculated from zero lift and induced drag, to be 58.2 N at a cruise speed of 10 m/s.

The dynastat is controlled via two rudders and two elevons near the rear of the plane. By absence of a tailplane, stability is a challenge. Placement of the c.g. will thus be sensitive.

Propulsion and power: Motor output power required for cruise is found to be 950 W. At maximum thrust, defined by the climb requirement, this increases to 2.99 kW. For a 1.2 hour cruise the total energy needed is found to be 920 Wh. Lithium polymer batteries are used for energy storage, amounting to an estimated battery life of 11.4 kg.

To recharge the batteries, monocrystalline silicon solar panels are selected with an efficiency of 20%. A PV area of 9.15 m^2 is needed to recharge within 1 hour.

Weight estimation: The dynastat envelope is assumed to weigh 0.35 kg/m^2[16]. With a payload mass of 1.5 kg and 2.9 kg of PV cells, the total weight is estimated at 29.6 kg.

Manufacturing and maintenance The dynastat mainly consists of a polymer laminate envelope with an aluminium frame. Maintenance costs for airships are similar to those of a small airplane [16]. Maintenance costs will be higher for the dynastat than for the blimp, due tot the rigid structure.

Maritime The dynastat is stabilisedon the water by three floaters. These can be relatively small, as the dynastat weight is partially supported by the lighter-than-air gas.

Chapter 7

Trade-off

With the three concepts developed in more detail, it is possible to compare the performance of the concepts in different parts of the mission. Based on these performance differences the best option for this mission will be determined. The exhaustive trade-off can be found in [17]

7.1 Trade-off method organisation

To get towards a good concept, first a good trade-off method has to established. For this final concept trade-off a weighted trade-off is chosen. The weights are allocated to each of the trade-off criteria; the most important criteria having the highest weight. The fixed wing concept is chosen as a reference: the dynastat and the blimp are graded from 0 to 6 for every criterion, relative to the fixed wing concept. If the blimp or dynastat are in a criteria equal to the fixed wing concept, a score of 3 will be given. If it is worse, a lower score is allocated to that concept, if it is better a higher score will be given. Quantifiable criteria are graded with a precision of half points and the non-quantifiable criteria with whole integers. In the end everything is multiplied with the weight factor and summed up. The concept with the highest total grade will be considered the best concept for this mission.
The ability to take-off and land on water and the endurance of one hour, are established as a go or no-go requirement. This means that if meeting this requirement is not feasible for a concept, the concept can immediately be discarded as a failure. Because these concepts are only graded as go or no-go, they are not listed in the summary table.

The other criteria are sorted by importance and given their relevance towards each other, the weights of each criteria can also be seen in Table 7.2

During the development of the trade-off most of these criteria are quantified with values. These quantifiable trade-off criteria are graded via these values, which can be found in Table 7.1.

Table 7.1: The quantifiable criteria and their values for each concept

Trade-off criteria	Fixed wing	Dynastat	Blimp
Area coverage per day[km^2]	390	316	146
Uptime[% per day]	23	38	28
Endurance [hr]	1.7	1.8	1.46
Maximum speed [m/s]	78	22	10
Rate of climb [m/s]	10	10	5.2
Endurance at maximum thrust [min]	20	16.8	12
Mass [kg]	31	30	44
Manoeuvrability - 300m [s]	4.9	13	32

The rest of the criteria are not quantifiable for this trade-off, the grading for this was done by the entire design group. The arguments were given for each criteria; grading is done based on these arguments.

7.2 Trade-off summary table

With the quantifiable criteria elaborated the final summary table is made, which can be found in Table 7.2. In this table the grades are given to the concepts. The colour scale is made by using red, yellow and green, where red is the worst and green is the best. The total score of the concepts is shown at the bottom of the table.

Table 7.2: The trade-off summary table

Trade-off criteria	Weight factor	Fixed wing	Dynastat	Blimp
Area coverage per day	4	3	2.5	1
Uptime	3	3	5	3.5
Manufacturing complexity	2	3	2	3
Technical feasibility	2	3	1	2
Airborne stability	1.7	3	2	3
Seaborne stability	1.7	3	1	0
Maximum speed	1.7	3	2	0
Rate of climb	1.7	3	3	1.5
Manoeuvrability	1.2	3	1.5	0.5
Mass	1.2	3	3	2
Environmental impact	1.1	3	3	2
Recoverability	1	3	2	2
Total	22.3	66.9	55.3	37.35

From Table 7.2 it is concluded that the fixed wing is the best concept for the surveillance mission.In the coming chapters this final concept will be further detailed into a complete and final design.

Part III
Detailed Design

Chapter 8

Contingency management

Until the UAV is really built and operative, uncertainties in the design will remain. To take this uncertainty into account contingency management is performed. In contingency management, safety factors are added or subtracted from the required values in order to account for inherent deviation from target parameters in the project. Doing this, the probability that requirements will be met increases.

Contingency factors were applied in this manner throughout the entire project, the contingencies used on the top level requirements in performing the final design are shown in Table 8.1.

Table 8.1: Contingency Management

Parameters	Requirement	Contingency	Target Value
Maximum M	35 kg	–10%	31.5 kg
Minimum V_{max}	15 m/s	+10%	16.5 m/s
Minimum RoC	10 m/s	+5%	10.5 m/s
Minimum Endurance	60 min	+10%	66 min
Minimum Endurance at T_{max}	10 min	+10%	11 min

As can be seen in the following chapters the requirements in most cases are easily met, except for the rate of climb which will be elaborated further in chapter 15. In Chapter 10 the final design points used in the detailed design phase are elaborated further.

The data obtained in this chapter is used to assist in further development and will reduce risks the design of the UAV can run in to.

Chapter 9

Configuration selection

Now the final concept has been chosen this concept has to be further developed into a final design. The first step in this process is to determine the complete configuration. Several different wing, floater and motor configurations were considered. Each different configuration is further developed, then compared to the other options and finally the final configuration is chosen. This final configuration will be further developed into a detailed final design.

First the wing configuration is explained, after that the floater configuration and finally the motor configuration.

9.1 Wing configuration

Several different wing lay-outs are considered from aerodynamic point of view. This assessment was done with aide of MATLAB and XFLR5 software packages. The methodology was as follows: different layouts were generated using MATLAB, using baseline wing dimensions and stability equations as an input. These layouts were then imported in XFLR5 and compared, based on aerodynamic efficiency, i.e. the $\mathrm{C_L/C_D}$ ratios. The baseline wings were designed an aspect ratio of 20 wing loading value of 160 $\mathrm{N/m^2}$, consistent with earlier calculations. The different lay-outs that were considered are as follows:

- Conventional The conventional lay-out consists of a main wing and a combination of horizontal stabilizer and vertical tail located behind the main wing, this configuration can be find in Figure 9.1a. In this case the horizontal stabilizer provides negative lift, to provide longitudinal stability. This means the main wing has to provide more than nominal lift to compensate for this, thus increasing induced drag. Furthermore, for the conventional wing layout two different tail configurations were considered: a T-tail or a V-tail. V-tail demonstrated marginal efficiency increase when compared to a T-tail.

- Canard The canard lay-out consists of a main wing, a horizontal stabilizer in front of the wing and a vertical tail located behind the main wing. The horizontal stabilizer provides positive lift, which may lead to reduction in drag when compared to the conventional lay-out. The downside of this lay-out is the reduction of the travel margin available for the c.g. location, compared to conventional lay-out. This means that the mass distribution throughout the aircraft has to be adjusted such that it is balanced.

- Tandem wing The tandem wing configuration can be seen as a canard with an oversized front stabilizer. The lay-out consists of two wing of the same size, consistent with design wing loading baseline value. The benefits and deficiencies of canard layout also apply to tandem wing configuration. Tandem wing has an additional benefit of smaller possible wingspan for the same lift, wing loading values and aspect ratios.

The tandem wing configuration was selected as the optimal configuration, when taking into account the C_L/C_D, the wingspan and the input from other subgroups. According to XFLR5 evaluation it demonstrated about about 5-10% performance increase over conventional layout and was comparable with the canard configuration.

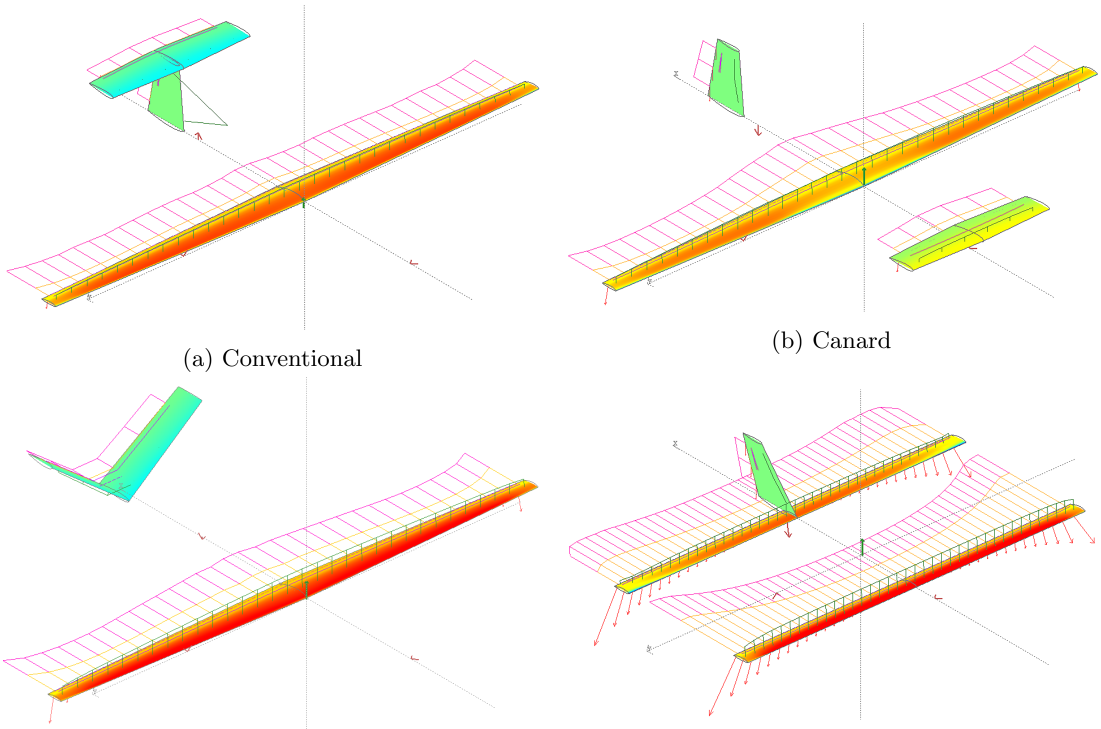

(a) Conventional

(b) Canard

(c) V-tail

(d) Tandem wing

Figure 9.1: Different wing configurations, showing C_P, Lift and Drag distributions. Made using XFLR5

9.2 Floater configuration

Another important configuration to determine is the floater configuration. There are three basic options for this, a catamaran, trimaran or sponsons configuration. A catamaran configuration is a configuration where two main, equally sized bodies provide the buoyancy of the craft. The payload can be stored either in these two bodies, or a small body in the middle of the aircraft can be used for this. This body will be above the water. Next, a trimaran configuration has one main body providing the buoyancy with two floatation devices, or floaters, at each side of the hull connected to the wing. These floaters help to provide transverse stability to the aircraft. Lastly, sponsons can be used as a floatation device. In this configuration, there also is one main floating body but with floatation devices added to the bottom of the fuselage, providing more area in the water, hence more stability.

The different configurations all have its own advantages and disadvantages. The catamaran configuration is preferable for the payload, as the camera can be put in a small hull in the middle of the aircraft, far away from the water. Also, this structure is the simplest structure, making it preferable for manufacturing & maintenance. Trimaran, after some basic CATIA investigation, turned out to be the configuration with the lowest wetted surface area. This means this will be the configuration that is preferable for take-off, as this aircraft will require the least take-off power. Also, this aircraft will be the best in hydrodynamic stability. The floaters can be put far away from the hull, creating a big counteracting moment when the craft rolls. Lastly, sponsons were preferred for aerodynamics, as this configuration will create the least aerodynamic drag. Also, this configuration would be best for structures, as the bigger bottom area gives a better load distribution for landing impact.

After a trade-off, rating the three configurations on take-off power, hydrodynamic stability, aerodynamics, structures, payload and manufacturing and materials, the trimaran configuration turned out to be the best, followed by the sponsons configuration and the catamaran configuration.

9.3 Motor configuration determination

The motor lay out determination is mainly based on the possibility of water ingestion and efficiency during cruise. As mentioned in section 15.1.1 an electric motor running at respectively low powers is inefficient [18], since the power requirement during cruise is much lower than during take off the risk of a low efficiency in cruise is high. But this efficiency can be increased by using multiple motors of which only one is used in cruise and the other kicks in when higher power is needed, therefore two motors will be used in the design. With the amount of motors known the exact location of the motors is left to be determined, the main parameter in motor location determination is clearance from water and the possibility of water ingestion in the electric motor. Therefore at least a high motor mount is required, besides that water spray will be the least at the front of the aircraft during take off and landing and the fuselage can be used like an cover against water spray. This is why the motors are both placed at the top of the fuselage behind each other.

A draw back of this location is a thrust induced pitching moment and the back motor being in the flow field of the front motor which makes the second motor less efficient. However locating the motors somewhere else than the fuselage would also require a high mount for water clearance which also at this location induces a pitching moment and the risk of water spray ingestion would increase. Besides that the two motors in the symmetry plane of the aircraft would not generate a yawing moment in case of a engine failure. Considering the positive and negative effects of this location, the positive effects are considered to out weigh the negative ones and the decision is made to place the two motors inline on the top of the fuselage.

Chapter 10

Mass and power budgets

This chapter lists the budget breakdown tables for mass and power and explains some rationale behind the current design estimates. The budgets are to provide an insight in relative mass and power usage of the UAV system components, both for the reader and as a book-keeping tool for the design team.

In the early development stages a contingency of 10% was established for budgets. In the current versions of the budgets, still not all contributing factors may be accounted for; on the other hand, most items in the budgets incorporate an extra safety factor to account for uncertainties still present in the design. It is decided to aim for a contingency factor of 10% for the energy budget in this stage of the design process. The mass budget was aimed at a 5-10% contingency; but due to mass iterations in the last days of the project, the current total mass is estimated at 8.75 kg. This includes a contingency factor of 1.5 on the hull mass, which is added to accommodate future weight increase for detailed design and payload integration. Even with this contingency, the estimated mass remains below the design mass at an effective contingency of 14%. Conclusively, there is some headroom to iterate to a more efficient design by, for example, decreasing the design wing loading which in turn increases endurance.

Mass budget is presented in Table 10.1. Note that the UAV design weight is 100N, which is why the design mass in kilograms ends up at 10.19kg. The power budget is presented in Table 10.2; the energy budget is presented in Tables 10.3 (consumption) and 10.4 (generation).

The UAV batteries are sized for a nightly mission consisting of climb to cruise altitude and a loiter period of one hour. During daytime, solar energy is generated in flight, which extends the cruise time to 1.77 hours - depicted in Table 10.4. A contingency factor of 1.1 is applied on the required energy in order to take care of uncertainties. Table 10.3 gives the energy consumed by all systems in the aircraft on an average day in one flight cycle; Table 10.4 gives the total energy available on an average day in one daytime flight cycle.

Table 10.1: Mass budget

part	mass [kg]	mass [% of design total]	comments
Structure			
Wings	1.9	19	
Fuselage, including vertical tail	1.33	13	
Floaters	0.03	< 0.5	
Coatings	0.5	5	excludes PV coating
Structural connections	0.5	5	
Control & power			
PV cells	0.2	2	258 cells
Maximum Power Point Tracker	0.16	2	2 units
Electric Speed Controller	0.12	1	2 units
Motors	0.34	3	2 units
Batteries	2.7	26	5 units
Control	0.04	< 0.5	
Autopilot	0.01	< 0.5	
Sensors	0.2	2	Camera. Other sensors are included in autopilot
Communication	0.45	4	Antennas, radio modem, R/C receiver
Wiring	0.3	3	
Subtotal	8.75 kg		
Design mass	10.19 kg		
Effective contingency	14%		

Table 10.2: Control and communications power budget

Part	Power [W]	Comments
Control	30	5 servos
Autopilot	2	Lisa/M & camera control board
Sensors	2.1	Camera & gimbal system
Communication	6.5	Radio-modem&-antenna, RC receiver&-antenna
Total power required	40.6	

Table 10.3: Energy consumption on an average day in one flight cycle

Description	Energy [Wh]
Energy required for aircraft control and imaging	83.2
Energy required for climb	144.9
Energy required for cruise	325.5
Subtotal	553.6
Contingency	10%
Total energy required for one mission cycle	608.9

Table 10.4: Energy generation on an average day in one flight cycle

Description	Energy [Wh]
Generated Solar energy during flight	176.3
Battery capacity installed	432.9
Total energy available	609.2

Chapter 11

Environment

The final design is dependent on the environment in which it will be operating. Therefore an investigation in the environment around Curaçoa is performed. First of all, the weather around Curaçoa will be discussed in Section 11.1. Further, the waves will be discussed in Section 11.2. Then the coatings are looked into in Section 11.3 and at last the surroundings are elaborated in Section 11.4.

11.1 Weather conditions

The environment the UAV is going to fly in is vital for many design processes. To be able to analyse the environment, a literature study is done to create a clear weather survey for Curaçao. First of all, the top level requirement that the UAV has to be able to operate in an environment with sea state code four is elaborated and afterwards the Curaçao weather conditions are discussed.

11.1.1 Sea state code

One of the top level requirements for the UAV is that it has to be able to take-off and land on water while being exposed to sea state four conditions. These sea state codes are produced by the WMO. The WMO (World Meteorological Organization) is a specialised agency of the United Nations and its emphasizes on the state and behaviour of the Earth's atmosphere, its interaction with the oceans, the climate and the resulting distribution of water resources [19].

In WMO's Manual on Codes international codes for meteorological data and other geophysical data relating to meteorology are elaborated [20]. The sea state codes are defined as: 'The state of the sea is the state of agitation of the sea resulting from various factors such as wind, swell, currents, angle between swell and wind, etc'. The international code on the sea state is visualised in Table 11.1:

As can be seen in Table 11.1 the UAV needs to be able to operate in waters with wave heights of up to 2.5 meters. When compared to the Beaufort scale of wind, WMO's manual states that wave heights of 2-2.5 m correspond to wind speeds of 8-10.7 m/s and a Beaufort scale of 5. On open sea these weather conditions result in moderate waves with many foam caps formed. With increasing wave height, the period of the waves increases as well.

Table 11.1: State of the sea [19]

Code figure	Descriptive terms	Height* in meters
0	Calm (glassy)	0
1	Calm (rippled)	0 - 0.1
2	Smooth (wavelets)	0.1 - 0.5
3	Slight	0.5 - 1.25
4	Moderate	1.25 - 2.5
5	Rough	2.5 - 4
6	Very rough	4 - 6
7	High	6 - 9
8	Very high	9 - 14
9	Phenomenal	Over 14

* Notes:

(1) These values refer to well-developed wind waves of the open sea. While priority shall be given to the descriptive terms, these height values may be used for guidance by the observer when reporting the total state of agitation of the sea resulting from various factors such as wind, swell, currents, angle between swell and wind, etc.

(2) The exact bounding height shall be assigned for the lower code figure; e.g. a height of 4 m is coded as 5.

11.1.2 Curaçao weather conditions

Following on the sea state code, the weather statistics for Curaçao are analysed. This way, one can see if the sea and wind conditions specified in Section 11.1.1 indeed match the conditions on Curaçao and other conditions important to the mission can be looked into. Solar, wind, temperature and precipitation statistics will be examined.

Sun: First of all, solar statistics are important to look into. Information on the amount of sun hours and the cloud coverage on Curaçao are vital for trade-offs on the area of the solar panels and indirectly on many other subsections of the UAV. For the analysis of these statistics, the yearly weather reports from the Meteorological Department Curaçao are consulted. The measurements recorded by this department are done at Hato Airport, Curaçao. First of all, these reports show that in 2012 the amount of hours between sunrise and sunset do not vary by a great extent. The shortest time in between sunrise and sunset in 2012 is 11:25 hours, while the longest time is 12:51 [21].

Between these hours, the amount of (direct) sunlight is measured. The average amount of sun hours is 8:36 hours. The minimum and maximum monthly average varies a lot though. The maximum amount of sun hours has been recorded in August 2005, 10:29 hours. The minimum amount of hours measured in this period is in November 2004, during this month the average daily sun hours were recorded to be 5:23 [22]. This result seems a bit off range in comparison to the other values, as after this minimum, the lowest amount of sun hours recorded was 6:34. However, this value has to be taken into account as a worst case scenario.

Lastly, cloud coverage is examined. Looking at the reports by the Meteorological Department Curaçao, the average cloud coverage is 47%. The lowest monthly average recorded is 32%, in February 2007, and the highest monthly average dates from May 2004, with 64% cloud coverage.

Wind and air: Next up is to analyse the wind and air statistics on and around Curaçao. A lot of the statistics found on this are gathered on the island Curaçao. However, the mission the UAV is designed for will not take place on Curaçao itself, but around the island. Also, the altitude will not correspond to the altitude the wind measurements are investigated. For both of these situations a solution needs to be found.

First we will look at the wind statistics on Curaçao. The average wind speed generally lies in the range of 4 to 8 m/s. More relevant for the design of the UAV is to look at the maximum gusts the aircraft will have to endure. The highest gusts ever recorded was 25.7 m/s [22]. To convert the measurements, taken by the Meteorological Department Curaçao, into wind speeds at higher altitudes the Wind Profile Power-Law can be used [23].

Next, air statistics on Curaçao will be looked at. The air pressure measured varies slightly from 1.010 to 1.015 bar. The average air humidity on Curaçao is 78%. The humidity varies from 74% in August to 89% in March.

Temperature: In addition, the temperatures on Curaçao will be analysed. The Meteorological Department Curaçao uses averages of 24 hours measurements to get to their results. The average temperature over a month are almost constant, they vary between about 26 to 29°C. The absolute minimum temperature ever measured was 20.3°C. The absolute maximum temperature measured is 38.3°C [22]. The minimum temperature was measured in January, while the maximum temperature was measured in September.

Precipitation: Finally, the precipitation on Curaçao is analysed. Since precipitation can influence the solar panels or damage the structure, it is one of the weather conditions to be examined.

When the years 1971-2000 and 2005-2008 are considered an average of 564 mm of rain falls each year on Curaçao. On average half of this yearly amount falls in the months October, November and December[22]. Further, the average number of rainy days a year is 71. When the total average of rainfall is compared to the maximum precipitation in one day, it can be concluded that often a third up to half of the total rainfall in one month, falls in a single day. Therefore short and heavy rains that can damage the solar panels and the entire structure need to be taken into account. The highest amount of rain fallen in one day in this period is 118 mm.

11.2 Waves

To elaborate on the weather survey of Curaçoa discussed in Section 11.1, the behaviour of the waves can be investigated. In order to define the attitude of the waves in the different sea states, the wave height and the wave period for these states are plotted against each other [24]. This plot can be found in Figure 11.1.

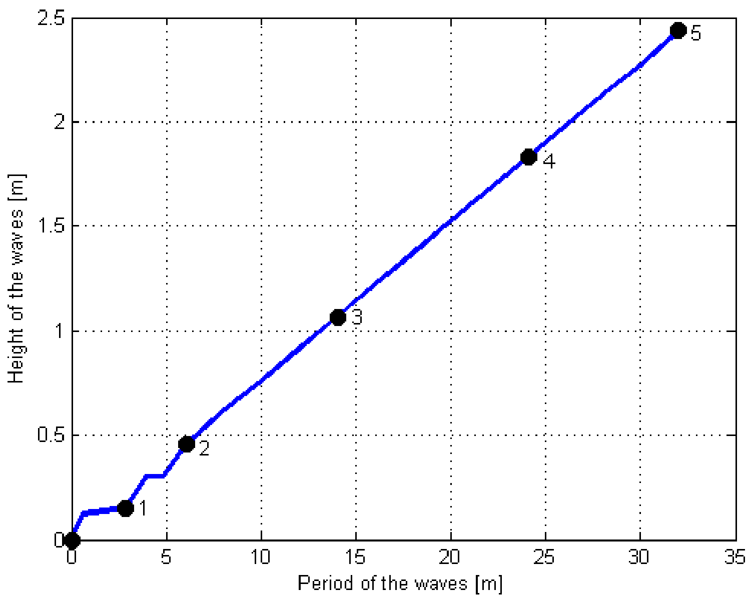

Figure 11.1: The behaviour of the waves

The black dots in Figure 11.1 indicate the start and end of a sea state. E.g. point 4, at a period of 24 m, is the start of sea state 4 conditions and point 5, at a period of 32 m, indicates the end of the sea state 4 category.

For sea state conditions 0 and 1, between points 0 and 2, it can be seen that the wave periods are very short. This results in a rough and uneven attitude of the UAV. Therefore, it needs to be secured that the UAV travels or idles in the same direction of the wave swell.

For sea state conditions 2, 3 and 4, between the points 2 and 5, the wave period is much longer in comparison with the lower sea state conditions, so the attitude of the UAV will change much more gradually. This means that this uneven and rough environment will not be a problem. Therefore the UAV will not necessarily have to be directed in the same direction as the wave swell for these conditions.

11.3 Coatings

Another important aspect to consider when designing an amphibious vehicle is the effect of the everyday environment on the craft and to find solutions to these problems. One of the ways to do this is to apply coatings to the craft to make sure it is protected against these effects. These effects will include seawater and rain. The coatings will have to be selected carefully to make sure they protect the structure entirely, without adding too much weight and to limit the performance of the craft as little as possible. The following coatings will have to be applied:

Exterior coating: First of all, a basic coating for the whole exterior of the aircraft should be applied. The coating selected for this is a coating by Sherwin Williams Protective & Marine Coatings. The coating selected is their MIL-E-1115D coating [25]. This coating is meant for general exterior shipboard use and protects the structure against sea water. Two mils of coating will be used on the UAV. One mil stands for one thousandth of an inch, so 0.0254 mm. This means 0.0508 mm of coating will be used on the UAV.

Exterior primer: When using a coating, it is advised to use a primer first. A primer is put on materials before putting on the exterior coating, to ensure better adhesion of the coating and for durability and protection of the material. The recommended primer for the selected coating is the Sherwin Williams TT-P-645 primer [26]. 3.5 mils of primer are used for optimal primer performance.

Solar panel coating: The solar panels will also have to be protected. However, the exterior coating can not be used for the solar panels, as a big part of the sunlight will be reflected by the coating, significantly decreasing the performance of the solar panels. For this application, special solar panel coatings can be found. As the solar panels already come with an anti-reflective coating, all that is needed from this coating is protection from the environment. For this purpose, the Sheldahl G430300 coating is selected [27]. To be protected two mils of this coating will be applied to the UAV.

Battery coating: The batteries are one of the components of the UAV with the most hazardous materials. Because of this, an extra coating will be added to them, to make them watertight and protect the environment in case of a situation in which the batteries could get in contact with water or, even worse, the UAV would sink. To do this, the Anti-Seize Technology Battery Protector and Sealer is selected [28]. This coating seals the batteries, but also protects the battery from acid fumes generated when charging the battery. Therefore the coating protects the battery from excessive corrosion and will prolong the life of the battery. Two mils of battery coating will be applied.

Battery cleaner: Before applying or reapplying the battery coating, the battery will have to be cleaned. The Anti-Seize Technology Battery Cleaner is recommended for this, to neutralize acid deposits left over from charging or maintenance of the battery [29]. This cleaner comes with an indicator that will turn red in the presence of acid and will turn yellow when the residuals have been neutralized.

11.4 Surroundings

Other than the everyday weather conditions the UAV can cope with by using coatings, there are many other aspects in the environment to consider. Many other parts of the surroundings can possibly influence the craft. Some of these things are easy to cope with, some will require small design changes and others will require severe prevention methods. The following aspects are analysed:

Weather: Although the weather around Curaçao is generally nice and sunny, there will be situations where the UAV will have to be able to endure various weather conditions. Some of these conditions are:

- **Rain:** Rain will of course always be something the UAV will have to undergo. As can be seen in Chapter 11.1, the average amount of rainfall per year is 564 mm. However, the daily amount of rain can be up to 118 mm. This means the UAV will have to be able to withstand the impact and fatigue caused by long rain showers.
- **Lightning:** Lightning is not a very common weather condition on Curaçao, but it is a condition that happens once in a while, so it does need to be taken into account. One of the ways to prevent damage is to be able to handle the thunder strike with the help of a conductive material, like aluminium or carbon fibres. However, one will have to make sure that there are no holes in the carbon or aluminium structure, where the lightning could 'escape' into the structure via a non-conductive material [30]. There are generally two parts of an aircraft that are most vulnerable to lightning strikes, fuel tanks and the electronics. As the UAV will be solar powered, the fuel tanks will not be a problem, as there will be none. During the design, it will have to be made sure that the electronics can not be harmed by lightning. If, for any reason, this can not be realised, the UAVs will have to return to base in case of lightning.
- **Extreme weather conditions:** Lastly, there are always weather conditions that are just not realistic to design the UAV for. Storms, hurricanes and possibly even tornado's, will have such severe influences on the flight performance that it is not safe for the aircraft to fly. Even though there are no human lives at stake, in these circumstances the UAV has a much higher chance to crash, and economically this is of course not viable. Depending on how extreme the weather is, the UAVs will either be called down to land on the ocean or called back to base.

Ocean life: Curaçao has a varying, widely spread ocean life. Many different types of fish swim around in the Curaçao ocean, so the possibility of fish hitting the UAV have to be taken into account. The hull and floaters will be designed for landing impact, so it can safely be assumed that the fuselage will be able to cope with this. There are also many different types of sharks living in the Curaçao ocean. However, almost all shark attacks reported were at places where overfishing was an issue, or where sharks were driven to the boat by blood or for example fish bait was in the water around the boat. Thus, it is assumed that a shark attack on the UAV is very unlikely. Lastly, algae might attach to the aircraft, negatively influencing the aerodynamic and hydrodynamic properties and will increase the weight. During the weekly maintenance, this algae will have to be cleaned off of the craft.

Birds: Birds are a main concern for any aircraft. Birds flying into propellers of an aircraft have led to many crashes of aircraft in the past. One of the ways to be able to cope with this is by using two propellers and making sure that the aircraft can safely land for maintenance on one motor. The rest of the structure also needs to be able to handle the impact of a bird flying against it. Thus, the structure is to be designed taking this into account.

Currents/waves: Another issue to take into account is the UAV floating away from the desired position. Currents could be the cause of this, although currents usually only act a bit under the waves, so for the UAV, with a low immersed depth, currents will probably not have a big effect. Waves however, can be the cause of the UAV to drift off as well. To be able to cope with this, the navigation/communication system will have to measure its position at all times. When the UAV detects that it is significantly far away from its desired position, the UAV will either have to propel and float back to its desired position, or it will have to take off and fly there.

Other traffic: Next, other vehicles, both marine and air, have to be taken into account. If one of the UAVs would crash into either a boat or another aircraft, consequences could very well be catastrophic. There are several ways to prevent this. One of them would be to scout for other traffic using the cameras. This is however not the perfect option as the camera system will be designed to look for objects a lot lower than the UAV, not at the same altitude. Another option to consider is to place a radar system somewhere on the ground, warning the UAV in case another vehicle comes close.

Theft: Lastly, theft is a major concern. These UAVs will be valuable and this attracts the interest of thieves. There are several solutions to consider to be able to prevent theft and/or make it attractive. The following are analysed:

- **GPS:** GPS can be a vital instrument in stopping thieves and/or tracking them down. First of all, the GPS signal will probably need to be encrypted in some way, to prevent thieves getting the positioning information and using this to their advantage. Then, when the device would be stolen, it will have to be made sure that the GPS keeps sending out info. Also, it has to be made sure that the GPS device is not easily turned off by the thieves. This could be done by making the GPS device physically not easily accessible.
- **RC:** Another aspect to take into account is the radio control of the UAV. One of the requirements was that there should be a two kilometre range over which the UAVS should be able to be radio controlled. However, prevention measurements have to be made to make sure this radio controlled signal can not just be used by anyone that has the right frequency. Thus, some sort of encryption should be added to the signal.
- **Valuable parts:** One will have to make sure that the valuable parts of the UAV are not easy separated from the rest of the UAV. For example, making the solar panels detachable would be preferable for maintenance, but would also allow thieves to quickly get to the UAV, take out the solar cells and leave again.
- **Warning stickers:** Stickers are not a very effective way of preventing theft, however it might scare thieves off if they see that the designers did think about several methods to prevent theft. This makes the UAVs not look like a ‘simple target’, similarly to stickers at houses telling you which alarm system they have.
- **Alarm signal:** A perhaps excessive measure to take, but a possibly effective one, is to have an alarm signal go off when the UAV gets stolen. It might scare off the thieves and will make it easier for the coast guard to track the UAV that is being stolen.
- **Other UAVs:** Then, the last aspect that can help in preventing theft; the use of other UAVs. Constant surveillance at all points is of course impossible, but similarly to how the UAVs look for ships doing illegal drug trafficking or illegal immigration, the UAVs can help to recognise ships trying to steal a UAV, notifying the coast guard in the process.

Chapter 12

Aerodynamics and flight dynamics

This chapter will explain the design choices made and the design of the UAV with respect to the aerodynamics and flight dynamics. First the selection of the final configuration will be described. Then the airfoil selection will be done. Following that the lay-out of the wings and vertical tail will be detailed. After that the performance of this lay-out will be described, this consists of performance coefficients and the stability analysis.

12.1 Airfoil selection

The initial configuration for aerodynamic performance design is tandem wing layout, with two equal wings and a total area of 0.625 m^2, aspect ratio of 20 and a wingspan of 2.5 m, see Chapter 9. First of all the wing airfoil has to be selected, according to design requirements. A number of different airfoils were evaluated using XFLR5 software. The selection was driven by optimal performance in steady cruise flight, i.e. the best lift to drag ratio.

12.1.1 Wing airfoil

An initial set of wing airfoils was picked according to its maximum thickness ratio in order to allow sufficient rigidity to the wing structure. Furthermore this set had been narrowed down according to a set of requirements, listed as follows:

- Airfol efficiency in cruise

  The main design focus of the airfoil and wings is to provide a high lift to drag (C_l/C_d) ratio. The UAV will spend most of the airborne time in cruise, so this is a leading design regime. The airfoils are evaluated for cruise Reynolds number of 200000, corresponding to cruise at an altitude of 2000 m. Attention must be paid that the airfoil is not prone to a very large efficiency drop due to imperfections on the wing surface, like dirt and water spray.

- High $C_{l_{max}}$

  A high $C_{l\ max}$ is needed to be able to land at low velocity. No flaps will be implemented, for simplicity, so the $C_{l\ max}$ must be sufficiently high in order to allow a soft landing. Furthermore, there has to be a sufficient margin before the airfoil stalls completely such that the landing is safe.

- Sufficient stall angle margin

  The difference in angle of attack, between the α_{cruise} and α_{stall} should be sufficiently high that a minor change -due to for example a gust- in angle of attack will not stall the wings.

The list of analysed airfoils was narrowed down to three: the Eppler 582, Eppler 584 and Clark YS. In Figure 12.1 and 12.2 different properties are shown. The different different dashed lines denote different Reynolds numbers, they range from 100000 to 400000. All these airfoil analyses are done using the XFOIL direct airfoil analysis of XFLR5.

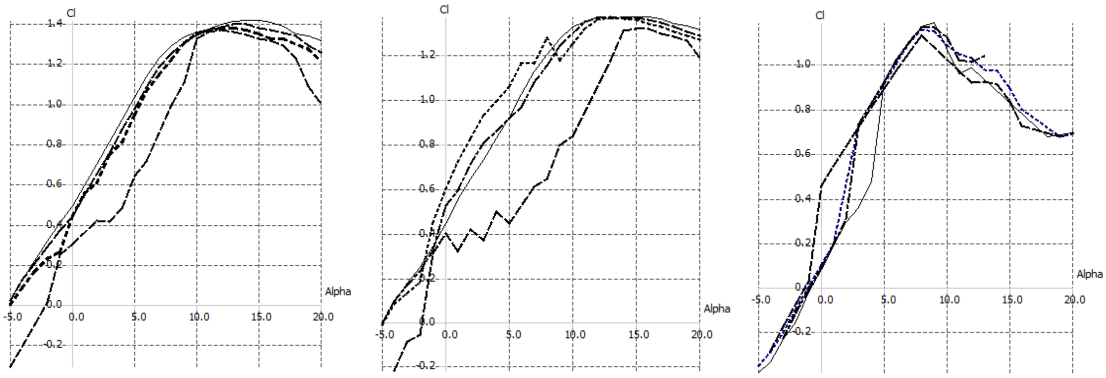

(a) Eppler 582 (b) Eppler 584 (c) Clark YS

Figure 12.1: $C_l - \alpha$ graphs for the different airfoils

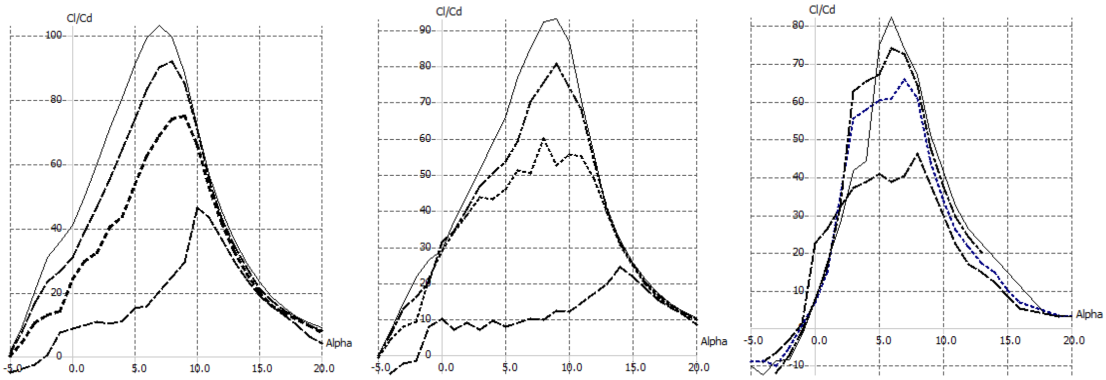

(a) Eppler 582 (b) Eppler 584 (c) Clark YS

Figure 12.2: $C_l/C_d - \alpha$ graphs for the different airfoils

As can be seen the Eppler has the highest C_l of the three airfoils and is only outperformed at low Reynolds number by the Clark YS for C_l/C_d. Designfoil was used to evaluate the effect of imperfections the wing. All the airfoils performed similarly with noticeable, but not dramatic, drop in C_l/C_d. The Eppler 582 airfoil meets all the requirements, at a Reynolds number of around 200 000 -that is at landing conditions- the $\mathrm{C}_{\mathrm{l}_{\mathrm{max}}}$ is 1.4. The $\mathrm{C}_\mathrm{l}/\mathrm{C}_\mathrm{d}$ at a Reynolds number of 250 000 -cruise conditions- is approximately 50. The α_{stall} at cruise is 14°, compared to a α_{cruise} of 3.5 °. Maximum thickness of 14.7% of the chord length is sufficient for a rigid wing structure. Figure 12.3 shows additional data about the Eppler 582 airfoil. The Eppler582 demonstrated the best performance for the purpose of designed UAV.

12.1.2 Vertical tail airfoil

A vertical tail has different requirements compared to the main wing.

- Low drag

  The main requirement for a vertical tail is to have as little drag as possible, in normal fight.

- Force when side-slipping

  The vertical tail should not provide a force in the Y-direction, unless there is a side-slip angle.

The first requirement means that the airfoil will be a thin airfoil and the second requirement means that the airfoil will be symmetric.After an analysis of several different NACA symmetric airfoils, such as

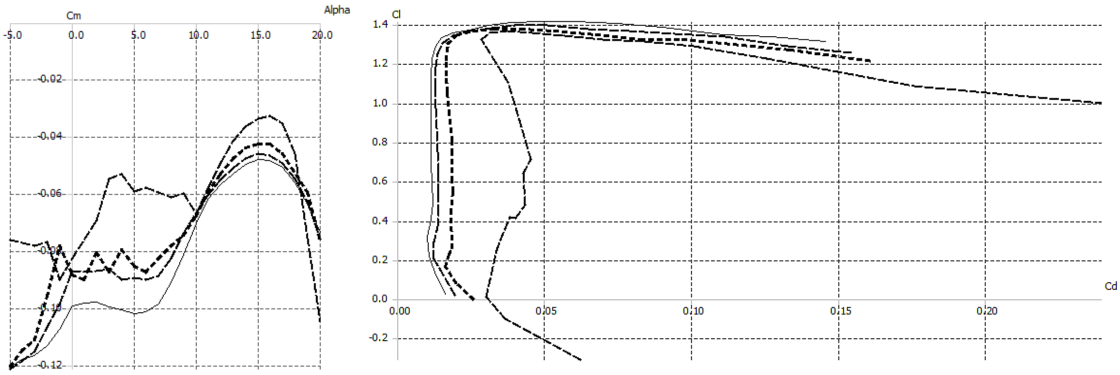

(a) $C_m - \alpha$

(b) $C_l - C_d$

Figure 12.3: Additional airfoil property graphs for the Eppler 582

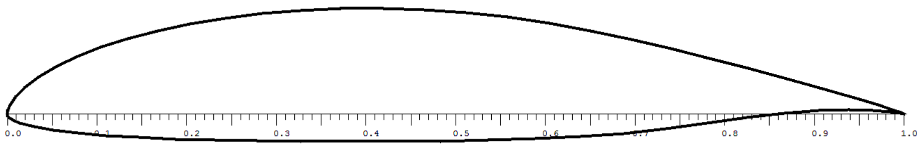

Figure 12.4: The Eppler 582 airfoil

the NACA0015, NACA0012 and the NACA0009, the NACA0009-smoothed is chosen. This airfoil can be seen in Figure 12.5.

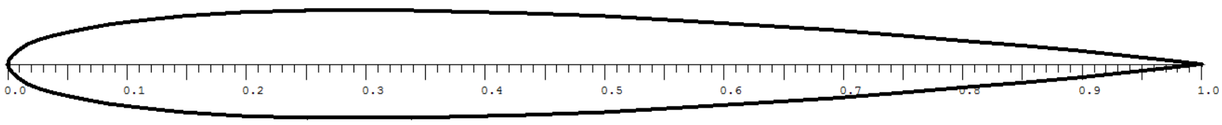

Figure 12.5: The NACA 0009-smoothed airfoil

12.2 Wing and tail lay-out

12.2.1 Wing and tail lay-out

From Chapter 7 an initial wing lay-out had been selected. This layout is further evaluated and developed in this chapter. The methodology is as follows: dynamic and static stability of the aircraft are evaluated, the wing and tail geometry is adjusted according to design requirements while all other components remain unchanged. The total surface area of 0.625 m^2 for both wings serves as initial baseline. The wing sweep, aspect ratio, surface area ratio, taper ratio and other parameters are varied and optimized for optimal performance considering component weight, aerodynamic characteristics and stability of the aircraft.

Initially the structural component weight had been considered as the key factor in selecting the wing aspect ratio. However, it was found that the wing weight is largely influenced by manufacturing constraints, such as the minimal manufacturable skin thickness. Therefore the wing aspect ratio had been optimized based on space available for placement of solar arrays. Furthermore, changes in surface area ratio of individual wings while maintaining a fixed total area were found to have minimal impact on the total drag (in the order of 0.01N). The baseline aspect ratio was initially set at 20 for both wings. Later it was discovered that such dimensions are not optimal for placement of solar arrays. The PV cells have dimensions of 31.9 by 74 mm and a spacing of 1 mm between them . Also the front and the rear of a wing can not be covered with solar panels due to the curvature, manufacturing constraints or moving parts in these regions. Therefore, the wing dimensions had been adjusted such that the front wing would have 4 rows of PV cells and lower aspect ratio, since the front wing would normally be more loaded than the aft one due to higher lift coefficient and loads on floaters attached to it. The aft wing was dimensioned to have 3 rows of PV cells, while maintaining the baseline aspect ratio. This resulted in approximately the same wing span for both wings, with a total surface area of 0.64 m^2. The front wing area in that case is 0.376 m^2 with an aspect ratio of 17.3 and a span of 2.55 m. The aft wing area is 0.264 m^2 with an aspect ratio of 20 and a span of 2.30 m. The taper of both wings is set to one. This is done to maximise the number of PV cells on the wings. The PV cells have a certain, fixed dimension, introducing taper would reduce the amount of solar cells on the wing.

The wing sweep is set at 0°quarter chord sweep. This is done to optimise the generated lift slope, since an increase in sweep angle leads to a decrease in maximum lift generated. Reasons for implementing a wing sweep would be to compensate for negative compressibility effects in the transonic speed regimes or to provide stability. The UAV is designed to fly at relatively low speeds so the compressibility effects can be neglected. Furthermore, analysis has shown that wing sweep is not required for stability.

12.2.2 Stability analysis

Angle-of-Attack Derivatives: The most decisive derivatives considering the aircraft longitudinal stability are aerodynamic angle-of-attack derivatives: C_{D_α}, C_{L_α} and C_{m_α}. The drag due to angle of attack derivative C_{D_α} is crucial for evaluation of aircraft power requirements, the lift due to angle of attack derivative C_{L_α} determines the lift characteristics of the aircraft while the C_{m_α} determines the longitudinal static stability of the UAV in flight as well as its dynamic behaviour. For aircraft to be statically stable the derivative C_{m_α} that describes the moment around it's Y-axis and it must have a negative sign. Physically this can be interpreted as follows: when the aircraft pitches nose down(negative) a positive moment is generated, which counter-acts this motion and brings the aircraft back to original flight speed and attitude. Additionally, the front wing has to operate at a slightly higher lift coefficient than the aft wing, thus it will also stall first. When the front wing stalls, it will lose its lift and the nose will drop, pitching down and lowering the angle of attack of the wings and with the pitch down the UAV will gain speed again and become stable again. The C_{m_α} is influenced by general wing layout, amount of lift each wing generates and centre of gravity location with respect to aircraft neutral point. The distance between the wings is designed in accord with longitudinal stability considerations. This is done using Equation 12.1 and 12.2.

$$\frac{\overline{x}_{np} - \overline{x}_{ac_1}}{\overline{x}_{ac_2} - \overline{x}_{np}} = \frac{C_{L_{\alpha_2}}}{C_{L_{\alpha_1}}}(1 - \frac{d\varepsilon}{d\alpha})\frac{S_2 l_h}{S\overline{c}}\frac{V_2}{V_1}^2 \tag{12.1}$$

$$\overline{x}_{np} - \overline{x}_{cg} \approx 0.05 \tag{12.2}$$

In these equations $\overline{x}_{np}$, $\overline{x}_{ac_1}$ and $\overline{x}_{cg}$ are the locations of the neutral point, aerodynamic centre of the front wing and centre of gravity, as fractions of the mean aerodynamic chord (MAC). In all further calculations MAC stands for the mean aerodynamic chord of the front wing and S stands for front wing planform area, unless otherwise noted. $\overline{x}_{ac_2}$ is the location of aerodynamic centre of the aft wing, also as a fraction of MAC. $C_{L_{\alpha_2}}$ and $C_{L_{\alpha_1}}$ denote the change in Lift due to a change in angle of attack for the horizontal stabilizer -in this case the aft wing- and the front wing, respectively. The $C_{L_{\alpha_1}}$ was estimated analytically to be 5.35 rad^{-1} and verified with XFLR5 to be 5.33 rad^{-1}. Likewise, the analytical calculation gave a lift gradient $C_{L_{\alpha_2}}$ of 5.43 rad^{-1} for the aft wing and 5.44 rad^{-1} was found using XFLR5. The $C_{L_{\alpha_2}} \frac{d\varepsilon}{d\alpha}$ is the airflow downwash gradient from the front wing, due to a change in angle of attack, it was estimated at 0.0835. S_2 is the aft wing surface area, S_1 is the front wing surface area, l_h is the distance between aerodynamic centres of the front and rear wings and $\frac{V_2}{V_1}$ denotes the difference in airflow velocities over front and rear wings. The velocity ratio is due to interaction between fuselage and the wings. The distance between wings is adjusted such that the centre of gravity is located in front of the neutral point, in this case the wing system generates a negative pitching moment gradient C_{m_α} around the centre of gravity. For the distance between the aircraft neutral point and the c.g. a safety margin of 5% of wing MAC is selected. The pitching moment gradient C_{m_α} of the entire aircraft was found to be -0.4553 rad^{-1}. Contributions of different components to this coeficient are demonstrated in figure 12.6.

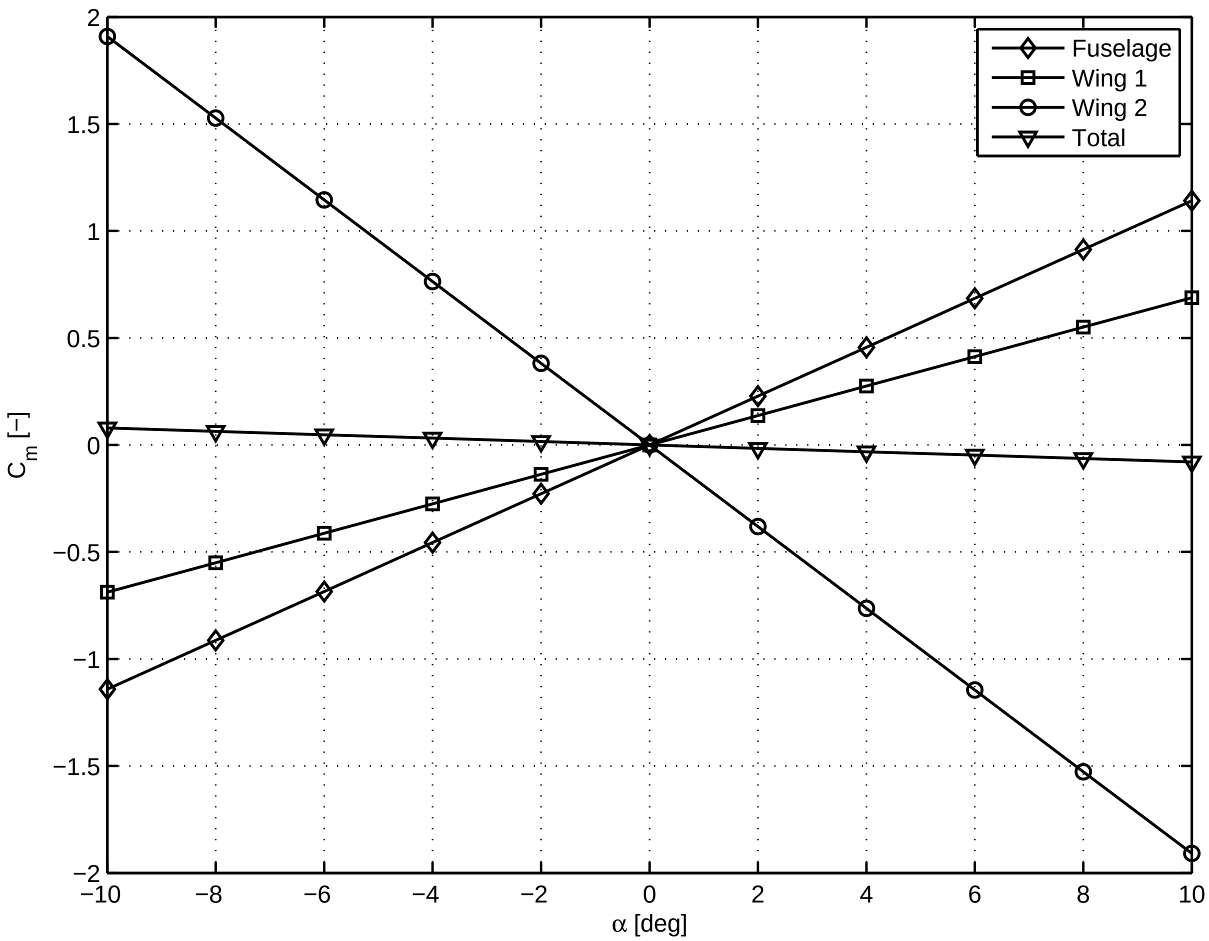

Figure 12.6: Various contributions to C_{m_α}

In case of a tandem wing, the front wing is designed to operate at a higher lift coefficient than the back wing. To achieve this the front wing can have a different airfoil, or with the same airfoil it needs to have a higher incidence angle. These incidence angles stem from the total sum of aerodynamic moments of the aircraft. Taking moment equilibrium around the aircraft c.g., each wing generates a certain amount of negative pitching moment due to airfoil camber and there is a moment generated due to different amounts of lift generated by the front and the aft wing. The distance between the wings had been optimised such that the the difference between the wing lifting coefficients is minimal. When the wings are spaced 0.62 m apart the neutral point is located 0.2572 m aft of the front wing, thus the centre of gravity has to be located 0.2174 m aft of the front wing a.c. Summing up the moments gives a required lift coefficient C_{L_1} of 0.698 for the front wing and C_{L_2} of 0.5598 for the aft wing. This corresponds to incidence angles of 2.30 degrees and 1.04 degrees for the front and aft wings respectively.

Dihedral angle is derived from two cases; ground clearance and stability. For ground clearance a check is done to see if the wingtip is still clear of the ground with a bankangle of 5 degrees [31]. In this case the critical wing would be the front wing, since it has the largest span. Taking a ground clearance of 7 cm and a wingspan of 255 cm, the maximum angle that that the plane can rotate is now found to be 3.2 degrees. This requires a dihedral angle of 1.8. For the rear wing with a wingspan of 230cm an angle of 1.6 degrees is required.

12.2.3 Tail layout & static lateral stability

The derivatives C_{Y_β},C_{l_β} and C_{n_β} describe the aircraft directional stability with respect to side-slip angle β. C_{Y_β} is the coefficient that describes the side force acting on the aircraft. C_{l_β} is used to calculate the moment generated around aircraft X-axis and the C_{n_β} is the moment around aircraft Z-axis due to side-slip. These influence the aircraft static, weathercock stability and the its dynamic motion modes. Side-slip angle derivatives are influenced by wing geometry and placement, i.e. wing effective dihedral, position of the wings with respect to the centre of gravity, fuselage dimensions and size and location of the vertical tail.

The vertical tail is added in order to provide lateral stability during flight. Since the engines will be on the centreline of the UAV they will provide no additional moment about the z-axis in case one of them fails. Thus the vertical tail is designed mainly to provide stability whilst side-slipping.

If the aircraft is subject to a side-slip angle in the airflow, it is desirable to generate a force, such that it will counter-act the side-slipping motion and position the aircraft in line with the airflow. A parameter which governs this behaviour is designated C_{n_β}. The main contributing factors to this effect are the fuselage and the vertical tail. Their individual contribution to the C_{n_β} can be found in Equation 12.3 and 12.4 [31]

$$C_{n_{\beta_f}} = -57.3 K_N K_{r_l} (\frac{S_{f_s} l_f}{Sb}) \tag{12.3}$$

$$C_{n_{\beta_v}} = -(C_{Y\beta_v})(l_v cos(\alpha) + z_v sin(\alpha)) \tag{12.4}$$

In these equations K_N is a coefficient depending on the shape of the fuselage, it is mainly dependant on the way the side-surface area is distributed. K_{r_l} is dependant on the Reynolds number along the fuselage. S_{f_s} and l_f are the side area and length of the fuselage, respectively, S and b are the surface area of the wing and the wingspan. $(C_{Y\beta_v})$ is the coefficient of the force in Y-direction, due to the vertical tail, l_v and z_v are the horizontal and vertical distance between the c.g. and the aerodynamic centre of the tail.

After several iteration it was found that the optimal configuration for vertical stabilizer is a single vertical fin with a surface area of 0.1 m^2, placed at a distance of 1.38 m aft of center of gravity. Vertical tail aspect ratio is set to 2 and the tail has a taper ratio of 0.5. Both vertical tail and fuselage contributions to aircraft stability are shown on figure12.7. Together with the fuselage the yaw angle derivative C_{n_β} comes down to 0.0405. The positive sign indicates that the aircraft is directionally stable. Parameters contributing to C_{n_β} are illustrated in figure 12.7.
To the wing parameters up, Table 12.1 shows all the important dimensions and characteristics of UAV lifting surfaces.

Table 12.1: Wing parameters

Parameter	Wing 1	Wing 2	Vert. fin
x $[m]$	-0.2174	0.4058	1.3764
z $[m]$	-0.1	-0.1	0.1994
S $[m^2]$	0.3762	0.2643	0.1
A $[-]$	17.2833	20	2
b $[m]$	2.55	2.2993	0.4472
$\bar{c}$ $[m]$	0.1475	0.115	0.2319
$\bar{Y}$ $[m]$	0.6375	0.5748	0
$sweep_{0.25}$ $[°]$	0	0	0
Γ $[°]$	1.8	1.6	0
i $[°]$	2.21	1.16	0
λ $[-]$	1	1	0.5
C_{L_α} $[rad^{-1}]$	5.3488	5.4288	2.5516
$C_{L_{max}}$ $[-]$	1.3777	1.3748	1.0347
C_{D_0} $[-]$	0.0164	0.0193	0.0066
e $[-]$	0.9259	0.9132	0.8

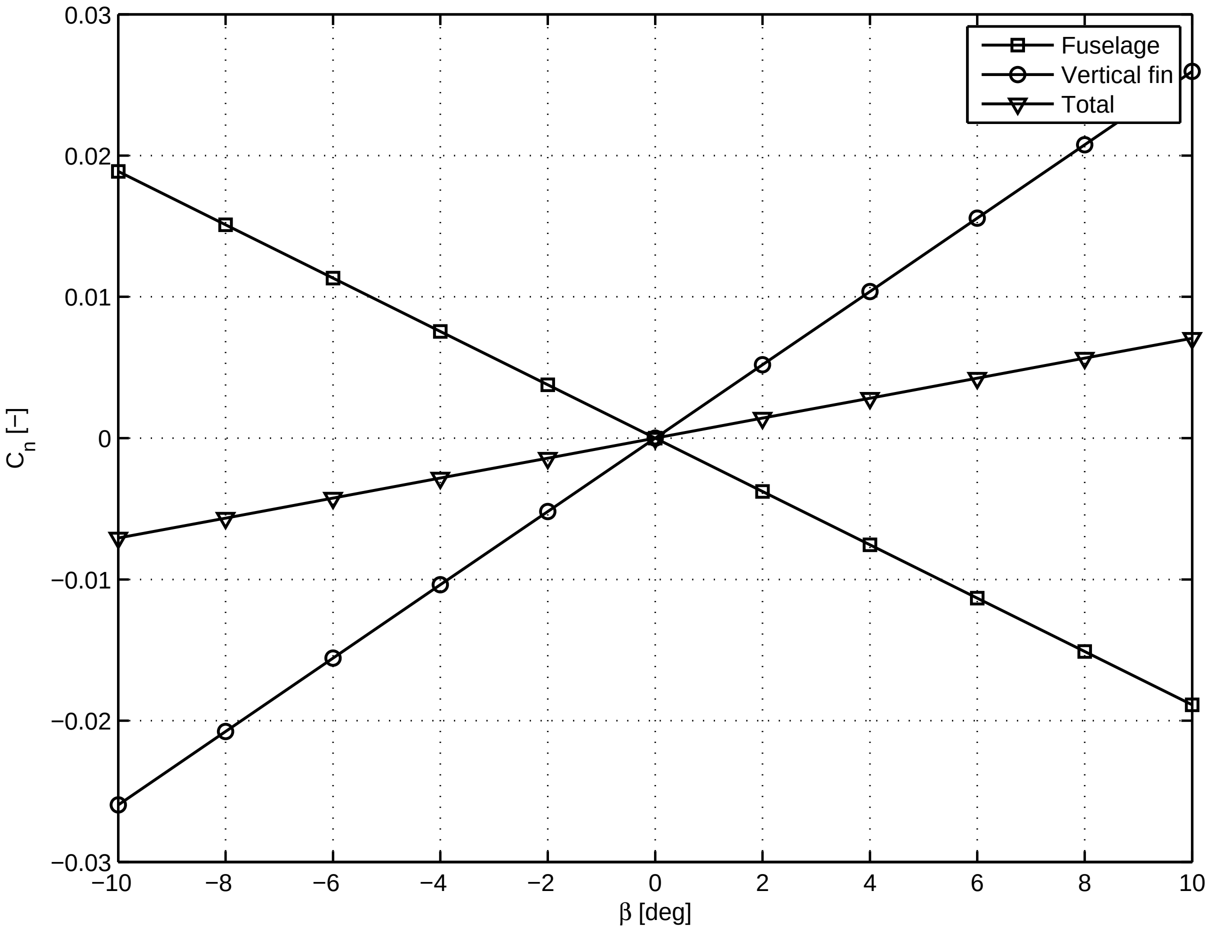

Figure 12.7: Contributions to C_{n_β}

12.2.4 Drag estimation

Drag generated by both wings, fuselage and the vertical fin all add up to total aircraft drag force generated in flight. The contribution of each component can be written as follows:

$$C_{D_{total}} = C_{D_{0_1}} + C_{D_{i_1}} + C_{D_{0_2}} + C_{D_{i_2}} + C_{D0_{fuselage}} + C_{D0_{verticalfin}}. \tag{12.5}$$

For the front and aft wings the coefficients C_{D_0} were calculated to be 0.0164 and 0.193 respectively, using airfoil analysis of XFLR5. The vertical fin was found to have a C_{D_0} of 0.066. Drag due to fuselage was estimated using Roskam method [32] that used fuselage wetted area and maximum front cross section as an input. It was found that the fuselage contributes 0.0191 to the total drag coefficient. The drag contribution of each component had been adjusted for component area divided by the front wing area, the total drag distribution per component and the lift to drag polar are shown in Figure 12.8.

It was found that in cruise the aircraft total drag coefficient including induced drag for each wing amounts to $C_{D_{cruise}}$ of 0.0681, which is consistent with XFLR5 simulation results. For a Velocity of 18.0 m/s, which would be optimal for aircraft endurance, the maximum lift-to-drag ratio of entire aircraft would become 19.2, while in cruise at 22 m/s this ratio is 17.0. These values are well above typical L/D ratios, found for seaplanes(12-16 [33]) and most conventional aircraft but lower than performance aircraft such as long endurance Rutan Voyager which has a lift-to-drag ratio of 27 [34]. This may attributed to the fact that base drag of wing airfoil increases at lower Reynolds numbers, which is unavoidable given the aircraft dimensions and operational speed range. Furthermore, about 30% of total drag force is due to fuselage drag. Large fuselage is necessary because the aircraft is required to float, so this leads to less-than-optimal drag characteristics. Furthermore, typicall operational velocities had been summed up in table 12.2

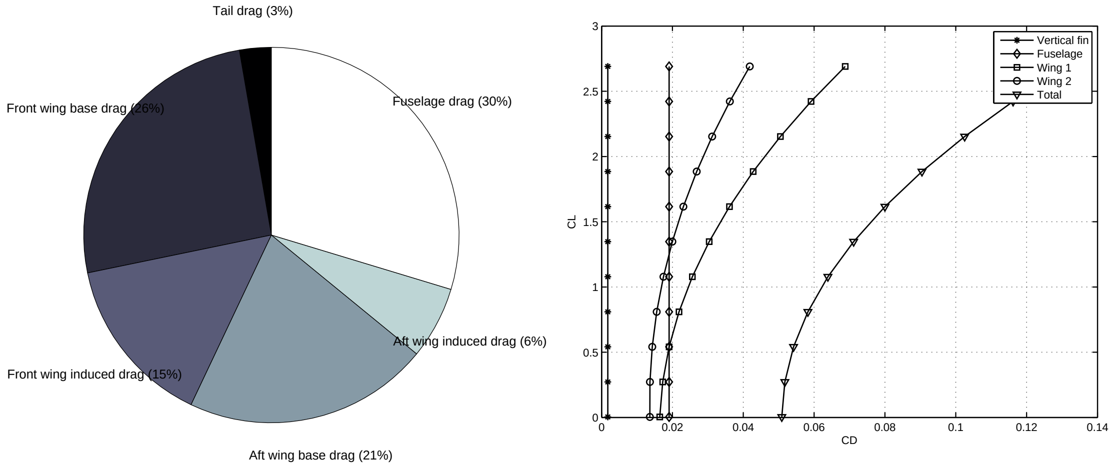

Figure 12.8: Various drag components and a total drag polar

Table 12.2: Different speeds for the UAV

V_{stall} [m/s]	B
$V_{min,manoeuvre}$ [m/s]	b
V_{land} [m/s]	b
$V_{approach}$ [m/s]	b
V_{climb} [m/s]	b
V_{max} [m/s]	b
$V_{max_{structurally}}$ [m/s]	b

12.2.5 Dynamic stability

Coefficients C_{Y_p}, C_{l_p} and C_{n_p} identify the roll rate derivatives, including the side-force in the Y-direction and moments l and n around X and Z axes respectively. The side force coefficient C_{Y_p} is mainly influenced by vertical tail geometry while the moment coefficients C_{l_p}(roll damping derivative) and C_{n_p} are mainly influenced by wing geometry. These derivatives have an impact on dynamic stability modes. Pitch rate derivatives C_{D_q}, C_{L_q} and C_{m_q} describe the forces that act on the aircraft in pitching flight. Drag due to pitch C_{D_q} is normally neglected. the lift derivatiev C_{L_q} and pitch damping derivative C_{m_q} are influenced by wing geometry and location with respect to centre of gravity. The yaw rate derivatives are mainly influenced by layout of the vertical tail. The stability derivatives had been calculated using Roskam method [31] that combines a number of analytic and empirical formulas. An overview is given in tables 12.3 and 12.4.

After all the coefficients are calculated, the eigenvalues of dynamic motions can be computed using methods provided in [35]. These eigenvalues correspond to the eigenmodes of the aircraft. From these eigenvalues it can be verified whether the aircraft is dynamically stable.

From the symmetric eigenvalues two different eigenmodes can be distinguished: the short period oscillation and the phugoid. As the name suggests the short period oscillation is (usually) a fast, highly damped motion. The short period oscillation can usually be seen when a step input is applied to the elevator. When it deflects upwards, it causes the lift on the rear wing to decrease, this increases the pitch rate. The increase in pitch rate will cause an increase in angle of attack on the, which causes the lift to increase and the pitch rate to decrease and the cycle repeats after this. The eigenvalues of the short period were found to be $\lambda_{1,2} = -0.0153 \pm 0.0016i$. The value of the short period is highly damped and it takes 0.3038 seconds for the motion to half in amplitude.

The phugoid is a slower, less damped motion. The phugoid can usually be seen after an impulse input

Table 12.3: Symmetric stability derivatives

V	=	22 m/sec	m	=	10.1937 kg	$\overline{c}$	=	0.1475 m
S	=	0.3762 m^2	lh	=	0.6232m	μ_c	=	178.9888
K_Y^2	=	8.9982	x_{cg}	=	1.7391 $\overline{c}$			
C_{X_0}	=	0	C_{Z_0}	=	-1.0912	C_{m_0}	=	0
C_{X_u}	=	-0.0844	C_{Z_u}	=	-2.1825	C_{m_u}	=	0
C_{X_α}	=	0.7474	C_{Z_α}	=	-9.1068	C_{m_α}	=	-0.4553
$C_{X_{\dot{\alpha}}}$	=	0	$C_{Z_{\dot{\alpha}}}$	=	-1.6636	$C_{m_{\dot{\alpha}}}$	=	-4.5758
C_{X_q}	=	0	C_{Z_q}	=	-6.052	C_{m_q}	=	-12.0652

Table 12.4: Asymmetric stability derivatives

V	=	22 m/sec	S	=	0.3762 m^2	b	=	2.5500 m
C_L	=	1.0912	μ_b	=	6.2004			
K_X^2	=	0.0074	K_Z^2	=	0.0375	K_{XZ}	=	0.0458
C_{Y_β}	=	-0.6569	C_{l_β}	=	-0.3989	C_{n_β}	=	0.0405
C_{Y_p}	=	-0.0431	C_{l_p}	=	-0.8655	C_{n_p}	=	-0.0933
C_{Y_r}	=	0.2974	C_{l_r}	=	0.2025	C_{n_r}	=	-0.1157

on the elevator. This will increase the pitch rate, which will cause the plane to gain altitude, because all the other factors of the airplane are kept equal, the airplane will loose velocity. The decrease in velocity also means a reduction in lift. Because the lift decreases, the pitch rate decreases and the the airplane will eventually be loosing altitude and gaining speed. This gain in speed will in cause the lift to increase and the pitch rate to increase and the cycle repeats. [35] The eigenvalues for the short period were $\lambda_{3,4} = -0.0001 \pm 0.0043i$ The phugoid period had been caculated to be 66.27 seconds, with 39.5 seconds to half the amplitude.

There are three different asymmetric modes which can be distinguished, namely the aperiodic roll, the spiral motion and the Dutch roll. The aperiodic roll is a damped aperiodic motion. It is seen when a step input is applied to the aileron. When a positive deflection is given, the airplane will start to roll to the left. This means the left wing will go down and gets a higher effective angle of attack. This means the lift increases. The right wing will go up and it is subject to a lower effective angle of attack. This means the lift will decrease. This difference in lift forces thus gives an opposite moment to the roll direction, this means the roll motion is damped. The eigenvalue of the aperiodic roll mode is $\lambda_1 = -4.7275$. Aperiodic roll is highly dampened, it takes 0.0170 seconds for this motion to half the amplitude.

The spiral motion is a slow and usually an undamped motion. The spiral motion starts when the airplane has a roll angle. This causes the lift vector to be tilted, this means the vertical part of the lift vector decreases, which means the airplane will loose altitude. The horizontal part of the lift vector will cause the aircraft to perform a turn. When this motion is undamped, the altitude will keep decreasing and the turn rate will increase. Spiral mode eigenvalue is $\lambda_2 = -0.0442$. The eigenvalue is negative, thus the spiral motion is convergent. It takes 1.8160 seconds for it to half in amplitude.

The Dutch roll is a both a yaw and roll movement. The Dutch roll can be observed when an impulse input is given to the rudder. This will cause the aircraft to yaw. When a positive deflection is given the aircraft will yaw to the left. This means the right wing will see a higher airspeed and the left wing will see a lower speed. This causes a difference in lift between these. This lift difference will cause a roll, in this case a roll to the left is initiated. This roll cause yaw to the right (adverse yaw). Now the cycle will start over again. The eigenvalues for the Dutch roll are $\lambda_{3,4} = -0.0887 \pm 0.2930i$[35], this corresponds to a period of 66.3 seconds and time to half the amplitude of 0.9062 seconds.

12.3 Control surfaces

In order to execute every required scenario (Appendix A: requirements 1.3.a-1.3.f) the UAV must have full attitude control and it has to be able to perform various manoeuvres. Control surfaces provide this stabilisation and control by redirecting the air stream when deflected and thus producing an unbalanced force that causes the airplane to rotate about the corresponding axis. In essence, this has to be done about three axes with every axis through the centre of gravity (c.g) and perpendicular to each other: roll control about the X-axis, pitch control about the Y-axis and yaw control about the Z-axis as can be seen in Figure 12.9. The positive angular directions seen in this figure follow common conventions and will be used in this report. The X-axis follows the longitudinal axis of the fuselage, the Z-axis points downward and the Y-axis is parallel to the wings. In Subsection 12.3.2, 12.3.3 and 12.3.4 the roll, pitch and yaw control will be discussed respectively. In every of these subsections, the specific control requirements are investigated and from them the control surface geometry, position and deflection will be derived. In Subsection 12.3.5 the implementation of these surfaces along with their infrastructure in the UAV will be discussed. In this design, conventional control surfaces that are proven concepts and their simplicity. The calculation of the geometry, size and position of the control surfaces follow the method of Sadraey [36].

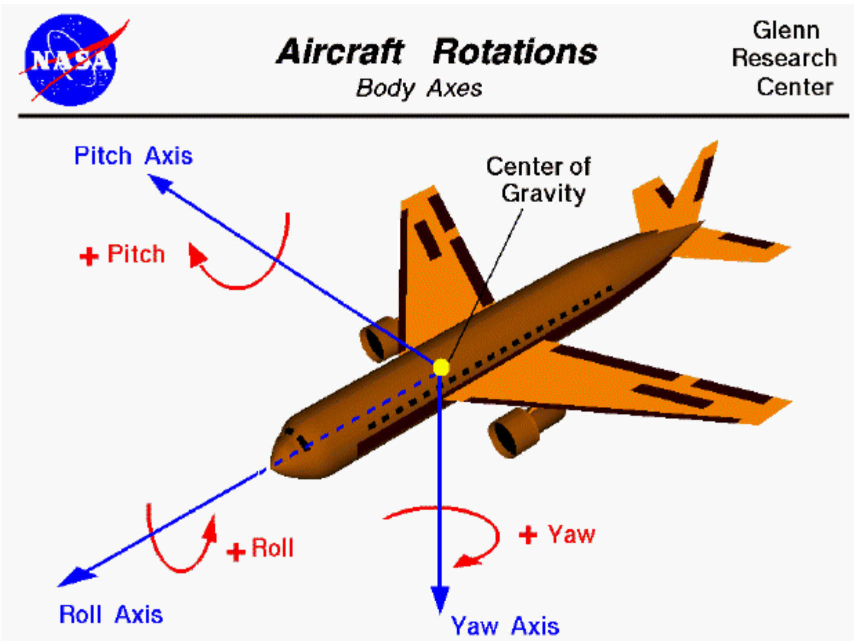

Figure 12.9: Aircraft rotations: body axes [37]

12.3.1 Placement

Firstly, because of the tandem wing design, a choice has to be made on what set of wings the ailerons will be placed and on what set the elevators will be placed. Smaller control surfaces are preferred structurally and aerodynamically. Because the ailerons will create a rolling moment around the X-axis, increasing the distance from the c.g. in the Y direction will cause a reduction in the required surface area. The elevators create a pitching moment around the Y-axis and thus a larger distance from the Y-axis in the X direction will reduce their required surface area. As the front wing has a larger span than the aft wing and the aft is located further from the c.g. in X direction, the ailerons will be placed on the front wings and the elevators on the aft wings.

12.3.2 Roll control

The rotation of an aircraft around its longitudinal X-axis is called the roll or bank and is generally controlled with the use of ailerons. This hinged section at the trailing edge of each wing can have a certain positive (downward) deflection or negative (upward) deflection. The ailerons on the two wings are connected (physically or electronically) to each other in opposition; when one aileron goes up, the other one goes down and vice versa. As there are no official control regulations concerning UAVs, the main roll requirement is derived from the rate of roll requirement from the European Aviation Safety Agency (EASA) Certification Specification for Very Light Aircraft (CS-VLA) [38]. It has two turn requirements; for take-off and approach configuration. The former states that the aircraft must be able to roll "*from a steady 30 degree banked turn through an angle of 60 degrees, so as to reverse the direction of the turn within 5 seconds from initiation of roll*". This has to be done at 1.2 stall velocity (V_{stall}) and at maximum take-off power. The latter requires the aircraft to perform the same turn within 4 seconds at 1.3 V_{stall} with the engine operating at idle power and at level flight power. Other requirements concerning flaps and landing gear and can be ignored, because of their absence in this design. Furthermore, the design should be low-cost, easily manufacturable and able to withstand operational loads.

Five values have to be derived when designing the ailerons:

- Aileron planform area (S_a)
- Aileron chord (c_a)
- Aileron span (b_a)
- Maximum up and down deflection ($\pm\delta_{a,max}$)
- Location of inner edge (measured from the wing root) of the aileron along the wing span (b_{a_i}/b)

As this is an iterative process, some initial values have to be set. The inboard and outboard positions of the aileron as a function of the wing span (b_{a_i}/b and b_{a_o}/b) are set at 70% and 95% respectively. The ratio between aileron-chord to the wing chord (c_a/c) is set at 30%.

First, the aileron rolling moment coefficient derivative ($C_{l_{\delta_a}}$) is calculated to compute the change in lift due to the deflection of the ailerons. This is done using Equation 12.6. In this equation, $C_{L_{\alpha_{w1}}}$ is the slope of the lift curve due to the front wing and S_w1 is the front wing surface area. b_{w1} is the front wing span and c_{w1} is the front wing chord. y is the location in Y direction and the integral is taken from b_{a_o} to b_{a_i}. τ_a is the aileron efficiency factor that is derived from the relative aileron chord length of 30% and is found to be 0.52 [36].

$$C_{l_{\delta_a}} = \frac{2C_{L_{\alpha_{w1}}}\tau_a}{S_{w1}b_{w1}} \int_{y_i}^{y_o} c_{w1} y dy \tag{12.6}$$

With the stated parameters, a value of 0.2868 1/rad for $C_{l_{\delta_a}}$ is produced. With the δ_a it determines the rolling moment caused by the aileron deflection. In order to calculate the aircraft rolling moment (L_A) when the ailerons are at maximum deflection, a tentative value for $\delta_{a,max}$ is selected of 20 degrees (or $\pm$0.349 rad) . With Equation 12.7 and 12.8 the aircraft rolling moment coefficient (C_l) and the aircraft rolling moment (L_a) are calculated respectively. For the two CS-VLA requirements, two values of the aircraft rolling moment are calculated; for a velocity of 1.2 V_{stall} for take-off and 1.3 V_{stall} for approach.

$$C_l = C_{l_{\delta_a}} \delta_a \tag{12.7}$$

$$L_a = \frac{1}{2}\rho V^2 C_l b_{w1} \tag{12.8}$$

This gives a value of 16.6 Nm for $L_{a_{TO}}$ and 19.5 Nm for $L_{a_{app}}$. As previously stated, the aircraft starts to roll because a change in lift is produced by the aileron deflection. In opposite direction, a rolling drag force acts in the YZ plane. This drag force increases with the roll rate, which makes the rolling motion non-linear. When the ailerons are deflected the aircraft starts to roll until the the rolling moment caused by the drag force is equal to the moment caused by the aileron deflection. From that instant, the aircraft has a constant roll rate (P_{SS}) about the X-axis. This steady-state roll rate is calculated with Equation 12.9 where C_{D_R} is the front wing/aft wing/vertical tail rolling drag coefficient and y_D is the drag moment arm.

$$P_{SS} = \sqrt{\frac{2L_a}{\rho(S_{w1} + S_{w2} + S_{vt})C_{D_R} y_D^3}} \tag{12.9}$$

Values of C_{D_R} vary from 0.7 to 1.2 [36] and for now is selected at 1 and the drag moment arm is assumed to be at 40% of the wing span. P_{SS} is now calculated as 17.4 and 18.9 rad/sec for take-off and approach velocity respectively.

The bank angle (ϕ_{SS}) at which this roll rate is achieved is calculated in Equation 12.10. Here, I_{xx} is previously calculated as 1.01.

$$\phi_{SS} = \frac{I_{xx}}{\rho y_D^3 (S_{w1} + S_{w2} + S_{vt})C_{D_R}} ln(P_{SS}^2) \tag{12.10}$$

ϕ_{SS} is found to be 47.1 and 48.4 rad. Now, the roll acceleration ($\dot{P}$) that is produced by the aileron rolling moment until the aircraft has reached P_{SS} is calculated in Equation 12.11.

$$\dot{P} = \frac{P_{SS}^2}{2\phi_{SS}} \tag{12.11}$$

The roll rate now is 2.9 and 3.3 deg/s^2. Now, the time required to achieve the required bank angle (Θ_{req} of 60 degrees can be calculated using equation 12.12.

$$t_{turn} = \sqrt{\frac{2\Theta_{req}}{\dot{P}}} \tag{12.12}$$

With the initial values that were stated at the beginning of this subsection, the required time for a 60 degree turn for the V_{TO} and V_{stall} is 6.4 s and 6 s respectively; these values do not fit the turn requirement. In Figure 12.10 the turn times for different inner-aileron-position-to-half-wing span ratios can be found. The inboard and outboard aileron position, along with its chord length are changed while considering constraints defined by the placement of the solar cells. After several iterations it is concluded that with the aileron characteristics that can be seen in Table 12.5 that the turns at V_{TO} and V_{stall} can be achieved in 4.3 and 4.0 s respectively.

Table 12.5: Final aileron parameters

Parameter	**Value**	**Unit**
b_{a_i}	0.77	m
b_{a_o}	1.245	m
c_a	6.1	cm
$\delta_{a,max}$	30	°
t_1	4.3	s
t_2	4	s

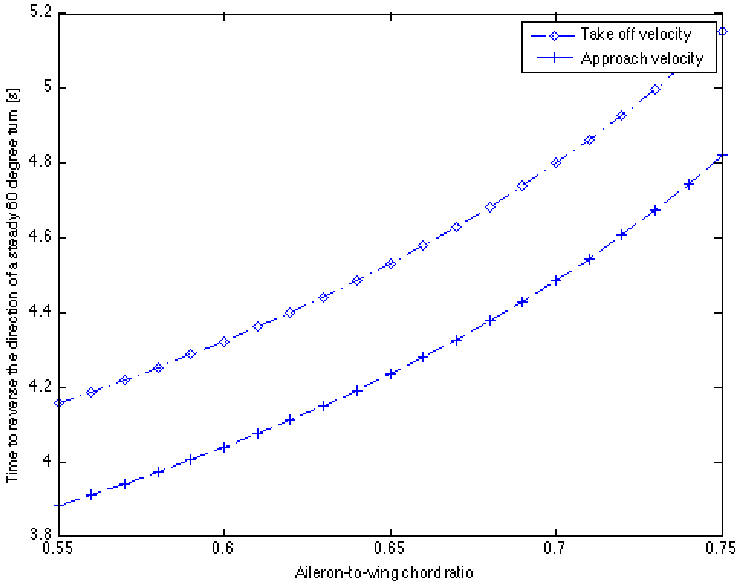

Figure 12.10: Turn times for different inner-aileron-position-to-half-wing span ratios

12.3.3 Pitch control

The rotation of an aircraft about its Y-axis is called the pitch and it is usually controlled with the use of elevators. These are control surfaces that are mounted on the horizontal tail, or in this case, the aft wing. By convention a downward deflection is positive and will produce a positive lift force, causing the UAVs pitch angle to decrease (nose-down). The elevators should meet a couple of requirements:

- Aircraft should be able to meet take-off requirements
- Aircraft should be able to maintain horizontal flight at all required velocities
- The elevator design should be low-cost, easily manufacturable and able to withstand operational loads

First, some initial values have to be set to start analysing the UAVs ability to meet the requirements. The elevator-span-to-aft wing-span ratio is set at 0.4. The elevator-chord-to-aft wing ratio is set at 0.3, which gives a elevator effectiveness ratio (τ_e) of 0.2 [36]. In the following equations, the subscript $_h$ represents the horizontal tail which in the tandem wing UAV is the aft wing.

Take-off will be done without the use of the elevator, as can be read in Chapter 13 so only one requirement remains. In order to meet the horizontal flight trim requirements, the required elevator deflection is calculated at every velocity the UAV will fly. The required deflection is calculated in Equation 12.13 [36]. Here, T represents the thrust force required and z_T is the distance in Z direction from the thrust to the c.g.

$$\delta_e = -\frac{\left(\frac{T z_T}{q S C} + C_{m_0}\right) C_{L_\alpha} + (C_{L_{cruise}} - C_{L_0}) C_{m_\alpha}}{C_{L_\alpha} C_{m_{\delta_e}} - C_{m_\alpha} C_{L_{\delta_e}}} \tag{12.13}$$

Because the UAVs angle of attack at cruise velocity is 0, $C_{L_{cruise}}$ is equal to C_{L_0}. C_{m_α} and C_{L_α} are calculated previously at -0.51 and 5.3 1/rad respectively, Chapter 12. The elevator effectiveness parameters $C_{L_{\delta_e}}$ (rate of change of lift coefficient with respect to elevator deflection) and $C_{m_{\delta_e}}$ (the rate of change of aircraft pitching moment coefficient with respect to elevator deflection are calculated in Equations 12.14 and 12.15.

$$C_{L_{\delta_e}} = C_{L_{\alpha_h}} \eta_h \bar{V}_h \frac{S_h}{S} \frac{b_e}{b_h} \tau_e \tag{12.14}$$

$$C_{m_{\delta_e}} = -C_{L_{\alpha_h}} \eta_h \bar{V}_h \frac{b_e}{b_h} \tau_e \tag{12.15}$$

In Equation 12.15, $\bar{V}_h$ represents the horizontal tail volume coefficient, calculated in Equation 12.16. , where l_h represents the distance between the aerodynamic centre of the aft wing and the c.g. S_h denotes the surface area of the aft wing and MAC is the wing chord.

$$\bar{V}_h = \frac{l_h S_h}{SMAC} \tag{12.16}$$

When the initial values for δ_e are evaluated for different velocities the minimum and maximum aileron deflection is -43 and 7.4 degrees. Generally, the maximum deflection for elevators is approximately 25 degrees. After considering the surface area required for the solar cells, the parameters found in Table 12.6 are determined. The required elevator deflections for various velocities are plotted in Figure 12.6. The position in Y direction on the aft wing has no consequences on the performance and is determined in Subsection 12.3.5. A maximum of 10 degrees is used for the deflection to decrease the servo travel angle, this increases the resolution of the control surface.

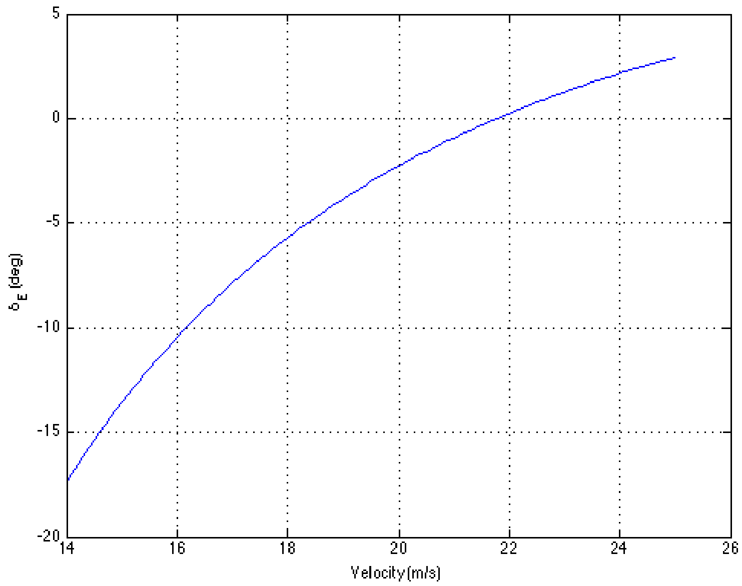

Figure 12.11: Elevator deflection required for horizontal flight at different velocities

Table 12.6: Final elevator parameters

Parameter	**Value**	**Unit**
c_e	3.5	cm
b_e	27.5	cm
$\delta_{e,min}$	-20	$^\circ$
$\delta_{e,max}$	10	$^\circ$

12.3.4 Yaw control

The rotation of the UAV about its Z-axis is called the yaw and it is usually controlled by the rudder. The rudder is a control surface located on the vertical tail and its deflection can cause a yawing moment (N_Y). Also, because the rudder is placed higher than the c.g., it can cause a rolling moment. The rudder is used for directional control and for directional trim e.g. in the case of cross wind. When designing the rudder, four parameters must be determined:

- Rudder area (S_R)
- Rudder chord (c_R)
- Rudder span (b_R)
- Maximum rudder deflection ($\pm\delta_{R,max}$)

For simplicity, a rectangular rudder is chosen for the UAV. The positive rudder deflection is, following convention, when the rudder is deflected to the left when looking alon.

There are 6 different rudder design requirements, the type of aircraft defines the most critical requirement. According to Sadraey [36], for a model aircraft, the coordinated turn requirement is the critical requirement. It states that the UAV has to be able to do "*a turn where the components of forces along the aircraft body-fixed y-axis sum to zero. In addition, it is desired that the aerodynamic side force (F_{Ay}) is equal to zero*". The calculations are done for the minimum controllable velocity of 11.2 m/s and the maximum controllable velocity of 25 m/s. Equation 12.17 for the coordinated turn is derived from Newton's second law:

$$F_{A_{y_t}} = 0 = F_C - W \sin\phi \tag{12.17}$$

From the load factor (n) of 2.5, the bank angle (ϕ) of 66.4 degrees is calculated using Equation 12.18:

$$\phi = \arccos\left(\frac{1}{n}\right) \tag{12.18}$$

The centrifugal force (F_C) during the coordinated turn can be calculated with Equation 12.19.

$$F_C = m\frac{V^2}{R_t} \tag{12.19}$$

When Equation 12.19 is substituted in the right hand side of equation 12.17, a value of 14.0 and 69.5 m is found for the turn radius (R_t) for the minimum and maximum controllable velocity respectively.

The aerodynamic side force ($F_{A_{y_t}}$) is set to 0 in equation 12.20. By definition, the sideslip angle (β) is 0, C_{y_r} is previously calculated as 1.18. $C_{y_{\delta_a}}$ is negligible in conventional aileron arrangements [31] and $C_{y_{\delta_r}}$ is calculated in Equation 12.21

$$F_{A_{y_t}} = \frac{1}{2}\rho V^2 S\left(C_{y_\beta}\beta + C_{y_r}\frac{Rb}{2V} + C_{y_{\delta_A}}\delta_A + C_{y_{\delta_R}}\delta_R\right) \tag{12.20}$$

$$C_{y_{\delta_r}} = C_{L_{\alpha_v}}\eta_v\tau_r\frac{b_r}{b_v}\frac{S_v}{S} \tag{12.21}$$

In Equation 12.21, $C_{L_{\alpha_V}}$ is previously calculated to be 3.3. The initial values for the rudder span ratio and chord ratio ($\frac{b_r}{b_v}$ and $\frac{c_r}{c}$) are 0.5 and 0.28, based on reference aircraft. The latter value gives a value of 0.5 for the rudder efficiency factor (τ_r) [36]. R_{SS} represents the steady-state yaw rate and is calculated in Equation 12.22.

$$R_{SS} = \frac{g\sin\psi}{V} \tag{12.22}$$

Now, when setting $F_{A_{y_t}}$ to 0, the required elevator deflection δ_r is calculated to be 8.7 and 1.7 degrees for the minimum and maximum controllable velocity. Maximum deflection is selected at 15 degrees, this value is comparable to reference aircraft [36]. The deflections required are significantly smaller than the other control surfaces for the need of rudder deflection is usually less with small aircraft. In order to further investigate rudder performance, one could calculate the aerodynamic rolling moment during turn and the aerodynamic yawing moment. Control derivatives required for these calculations are commonly calculated from wind tunnel testing. The final rudder parameters are found in Table 12.7.

Table 12.7: Final rudder parameters

Parameter	**Value**	**Unit**
C_r	3.5	cm
b_r	33.8	cm
$\delta_{e,max}$	±20	°

12.3.5 Integration

The control surfaces need to be structurally implemented in the UAV. Servos will produce the required torque to deflect the control surfaces and will be placed as close to the surface as possible. A program called 'Servo Calculator' [39] is used to calculate the required torque for the servos that deflect the control surfaces. From the required torque, the suitable servo can be found. The inputs for this calculator are:

- Maximum airspeed
- Control surface chord
- Control surface span
- Maximum deflection

When given the final parameters, the maximum torques required for each control surface can be calculated, summarized in Table 12.8. Possible servos that are selected to fit the requirements are listed. A safety factor of 2 is applied because of the simplified calculations of the required torque.

Table 12.8: Control servo torque requirements

Control surface	**Torque required [N cm]**	**Possible servo**	**Servo torque [N cm]**	Width [cm]
Ailerons	16.5	Spektrum SPMSA7020	33.4 [40]	2.7
Elevators	3.1	Spektrum SPMSA2020	8.4 [41]	2.3
Rudder	2.0	Spektrum SPMSA2020	8.4 [41]	2.3

With these selected servos, the supporting structure for the control surfaces can be estimated. Every control surface has to be connected at the two ends of the span and an axis of rotation must be supported in the wing. The structure will have the same shape as the wing and the chord will correspond to the control surface chord. At one end of the control surface a servo will be placed and the other end has to be supported so that it can rotate freely. For the aileron, this results in a structure with span length of 4 cm on the end supporting the servo. For the elevators and rudder the structure will require a span length of 3.5 cm. At the supporting end, a structure of 3 cm will suffice to allow free rotation.

12.4 Conclusion

In Section 12.1 the airfoil was selected; it is the Eppler 582. In Section 12.2 the wing configuration was determined, it is as follows in Figure **??**. The dimensions and other parameters are as stated in Section 12.2. Section 12.2 explained the performance of this configuration and showed that the stability coefficients and the eigenmodes are stable. Also some drag calculations were performed in this section. For the stability coefficients and the drag calculations, the individual contributions of the differents parts of the UAV have been determined, as well. The final technical drawings are shown in Figure 12.12.

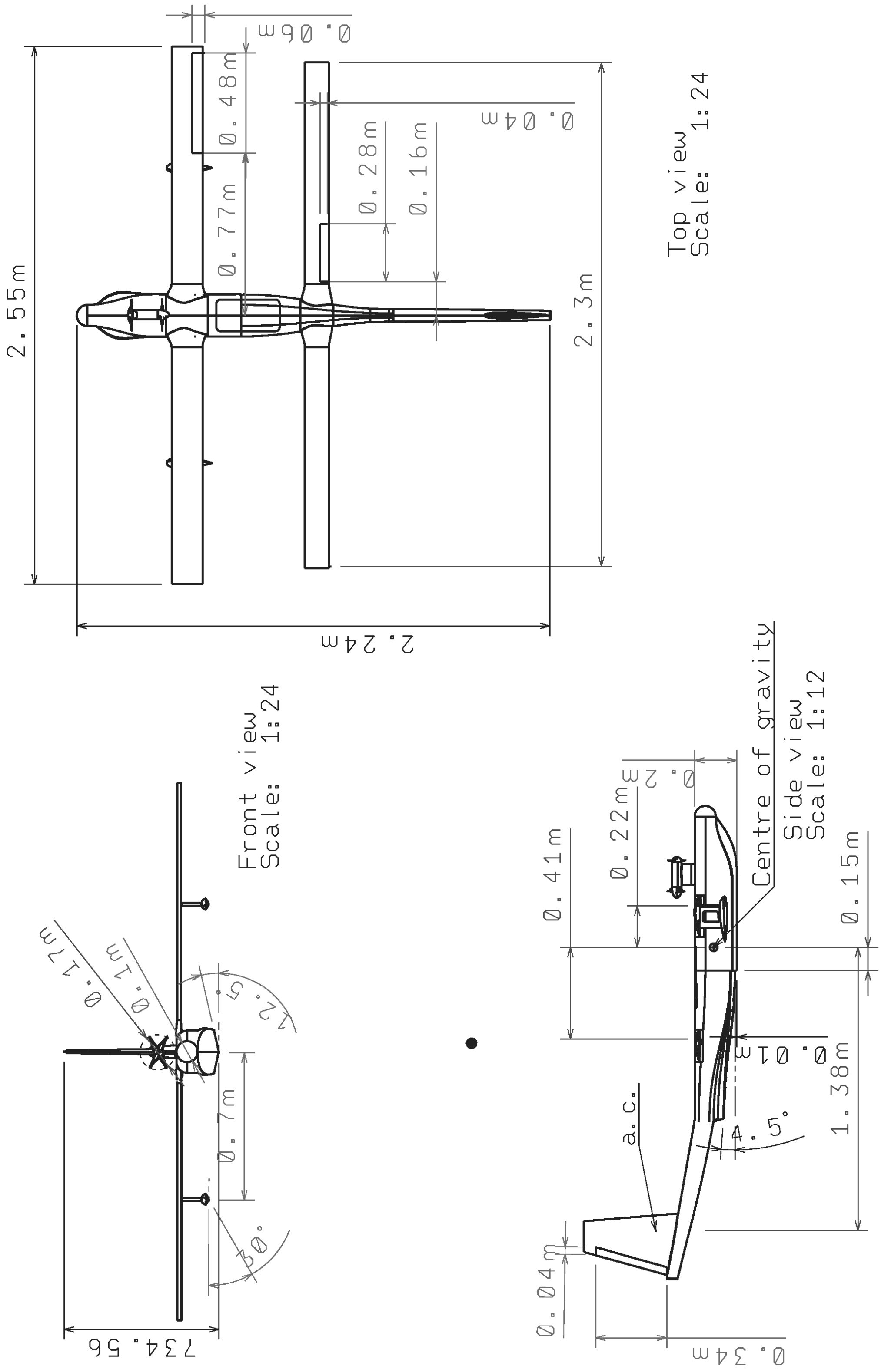

Figure 12.12: Dragonfly technical drawings

Chapter 13

Maritime

Now that aerodynamic characteristics of the product have been designed, the maritime specifications can be designed. First of all, the basic hull parameters will be elaborated in Section 13.1, then the loads acting on the UAV during landing and take-off will be analysed in Sections 13.3 and 13.2. When these loads are known, the stability of the UAV will be secured in Section 13.4. Following on this, the floaters will be designed in Section 17.5.3. Finally, the main design parameters are concluded in Section 13.6.

13.1 Hull parameters

The fuselage has to be able to perform in a marine environment as well as an aerial environment, so it is an important design feature. To be able to perform in a marine environment the hydrodynamic properties of the fuselage need to be optimised. In order to optimise the shape, several parameters need to be looked into.

First of all, the fuselage needs to act as a boat hull and it needs to be buoyant in order to float. Archimedes' principle states that the upward buoyant force exerted by the water must equal the force of the weight pressing down on the water [42]. The equation for the buoyant force can be seen in Equation 13.1 [43].

$$F_B = \rho_{water} g \nabla \tag{13.1}$$

In this equation, F_B represents the buoyancy force, ρ_{water} is the density of seawater, g is the gravitational acceleration and ∇ is the water displacement. In order to validate Archimedes' principle the buoyancy force must equal the weight of the body acting on the water. The final design has a mass of 10.2 kg. Therefore, the hull will cause a water displacement of $9.95 \cdot 10^{-3}$ m^3.

With the required water displacement known, the bottom part of the fuselage can be designed. To do this, different hull parameters need to be explored. The basic hull parameters are visualised in Figure 13.1.

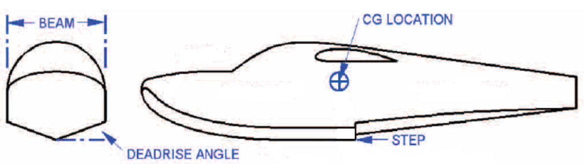

Figure 13.1: Basic hull parameters [44]

The first parameter that is explored is the beam of the hull. The beam corresponds to the width of the hull, as can be seen in Figure 13.1. The beam is critical for achieving a good water performance. If the fuselage has too much beam, it adds weight and drag and it may start skipping on the water at higher speeds [44]. Skipping occurs if sufficient hydrodynamic lift is produced to take-off before the wing provides adequate aerodynamic lift, causing a hydrodynamic instability. Due to this instability the UAV is launched in the air with a speed below minimum flying speed, which will result in a stall and can lead to a crash

[45]. If the beam is too small, the UAV will be immersed deeper in the water to cope with the necessary water displacement. This will result in the hull producing more spray and a higher hump resistance. Spray is undesirable since it can be directed into the propeller causing corrosion and erosion of the blades. A higher hump resistance indicates a higher maximum drag and therefore a longer take-off run. This hump resistance occurs just before the UAV has enough speed to provide the lift to start raising itself out of the water [44]. In order to design a beam, the required beam can be related to the wing area and maximum lift coefficient as can be seen in Equation 13.2 [46].

$$b_h = K\sqrt{S} \tag{13.2}$$

In Equation 13.2, b_h equals the beam of the hull, K equals the beam coefficient and S equals the wing area. The beam coefficient can be obtained from Figure 13.2.

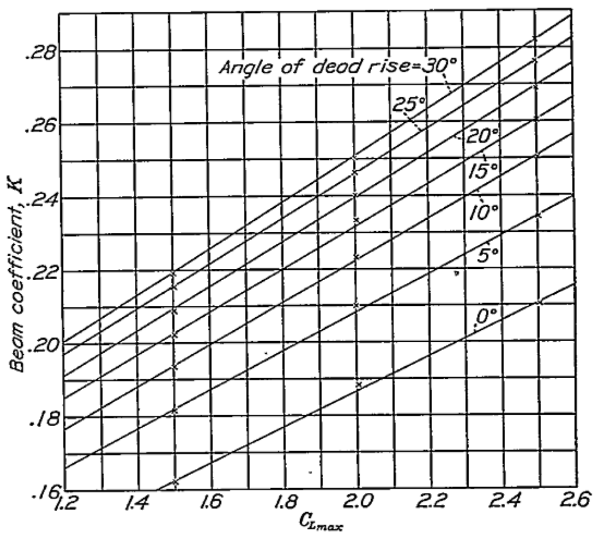

Figure 13.2: Beam coefficient as a function of $C_{L_{max}}$ and deadrise angle [46]

The beam coefficient is a function of the maximum lift coefficient, $C_{L_{max}}$, and the deadrise angle, β. The deadrise angle is the angle of inclination of the bottom surface of the hull with respect to the horizontal [47]. The deadrise angle is very important for the hydrodynamics of the hull. A small deadrise angle results in a lower hydrodynamic drag and a higher hydrodynamic lift. A major disadvantage of a small deadrise angle is that it produces a lot of spray. A high deadrise angle directs spray more towards the sides and therefore away from the engines. Also, a higher deadrise angle results in lower impact loads. Typical deadrise angles for aviation seaplanes vary from 15 to 25 degrees [44]. Since the desired value for the deadrise angle for hydrodynamic drag and landing impact are opposing, iteration within these two cases has to be performed.

Equation 13.2 gives the required beam for a hull. As was stated before, a lower value than the required beam is highly undesirable. Most of the seaplanes have a higher beam than the required beam, because there is no assurance that the required beam is the beam that gives the best dynamic performance. Therefore the required beam can be seen as a lower limit [46].

The next important parameter in the design of the hull is the step. The step is an abrupt break in the longitudinal direction of the hull [48]. The step of a seaplane positively affects the balance of the seaplane in the water and helps to control the trim angle and thus the aerodynamic angle of attack. As the speed increases, hydrodynamic lift is produced, causing the hull to be raised on the step. This phenomenon is called planing. Further, the step is necessary to break the suction of the water and to keep the UAV balanced at trim angles desirable for short take-off [49]. With adequate step height, usually 7 to 12 % of the beam, the UAV will be able to have a stable take-off and landing. Also, experiments have showed that including this step height may help in avoiding catastrophic skipping [45].

To conclude the basic hull parameters, the c.g. location can be analysed. When the fuselage is designed, the optimal c.g. location is just before the step and usually along a line of 2 to 10 degrees from the vertical, in front of the step [44].

Now that the hull parameters are defined, the landing, take-off and stability of the UAV can be defined and calculated.

13.2 Take-off

Having set the basic parameters of the hull, the first phase to analyse is take-off. Compared to taking off from land, taking off from water is more challenging to design for. When increasing speed to get out of the water and get airborne, large drag loads will be encountered by the structure. These loads will have to be analysed in order to be able to see if take-off is the critical parameter for the sizing of the motors. Both the drag during take-off and the power required at that point will be evaluated. To do this, the method described in Daniel Savitsky's paper 'Hydrodynamic Design of Planing Hulls' [50] is used, although slightly adapted to fit into the take-off of a UAV. Savitsky's paper uses the imperial unit system, so to make sure the calculations are correct imperial units are used during the calculation. Before and after the set of equations, the units where converted from and to SI-units. All of the calculations were performed using MATLAB.

Savitsky's method starts with the determination of the velocity coefficient. This coefficient is determined using Equation 13.3.

$$C_V = V/\sqrt{gb_h} \tag{13.3}$$

In this equation, V is the velocity, g is the gravitational acceleration and b_h is the hull width. Next, the lift coefficient for a deadrise surface(C_{L_β}) should be computed. This is done using Equation 13.4.

$$C_{L_\beta} = \frac{\Delta}{\frac{1}{2}\rho_{water}V^2{b_h}^2} \tag{13.4}$$

In Equation 13.4, Δ is the weight of the body in pounds and ρ_{water} is the water density. After determining this coefficient, the C_{L_0} can be defined using Equation 13.5. This is the lift coefficient at constant trim angle (τ), wetted length to beam ratio (λ) and velocity coefficient (C_V).

$$C_{L_\beta} = C_{L_0} - 0.0065\beta {C_{L_0}}^{0.60} \tag{13.5}$$

After this, the wetted length to beam ratio (λ) of the hull can be computed. This is done using Equation 13.6.

$$C_{L_0} = \tau^2(0.0120\lambda^{\frac{1}{2}} + 0.0055\lambda^{\frac{5}{2}}/{C_V}^2) \tag{13.6}$$

Next, the average bottom velocity is to be determined. Savitsky performed experiments with flat plates and the drag these plates endure to approximate this bottom velocity. The results of these experiments are shown in Figure 13.3. Using MATLAB, these figures are extrapolated to give an approximation for all values for λ, τ and β.

In Figure 13.3, $\frac{V_l}{V}$ represents the ratio of the average bottom velocity (V_l) over the forward planing velocity (V). Then the Reynolds number for each point in time is calculated, using Equation 13.7.

$$Re = \frac{V_l \lambda b_h}{\nu} \tag{13.7}$$

As previously introduced, V_l represents the average bottom velocity, λ is the wetted length over beam ratio and b_h is the average hull width. In addition, ν represents the kinematic viscosity. Using this Reynolds number, the friction coefficients (C_f) can be computed. This is done using Equation 13.8 [51].

$$C_f = \frac{0.00665787}{(\log_{10}(Re) - 4.3762)^{0.042612*\log_{10}(Re)+0.56725}} \tag{13.8}$$

Now all the variables to calculate the drag are present. The drag in the longitudinal direction of the body, D_f, can be obtained using Equation 13.9.

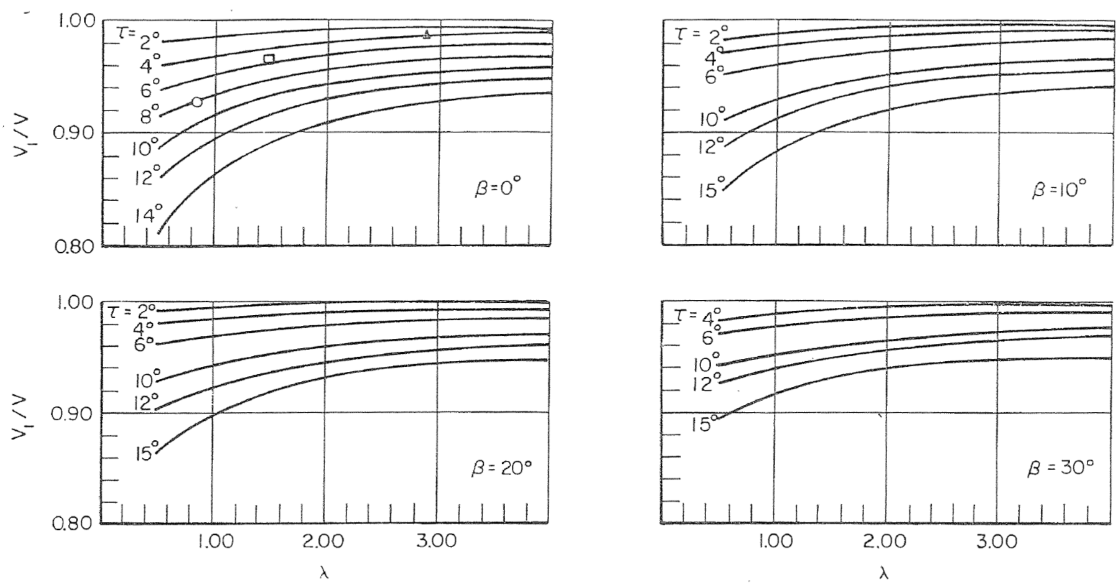

Figure 13.3: Graphs relating the (average bottom) velocity, λ, τ and β

$$D_f = \frac{\rho {V_l}^2 \lambda {b_h}^2 C_f}{2cos(\beta)} \tag{13.9}$$

Finally, the drag in the direction of the velocity of the UAV is calculated using the trim angle and the component of the weight that will act as drag.

$$D = Wtan(\tau) + D_f/cos(\tau) \tag{13.10}$$

This drag force concludes Savitsky's method for determining the drag of a planing boat, or in this case a planing amphibious aircraft. All of the parameters needed for these calculations are either known or can be set, iterating to an optimal design. However, there is one exception. One last input that has to be determined is the trim angle of the hull at equilibrium condition, so the trim angle which the hull will be at during the take-off stage. These equilibrium trim angles are determined in the subsection concerning longitudinal stability, Section 13.4.1.

Using these new trim angles (visualised in Figure 13.8), the set of equations will be run one more time, to get the final drag of the UAV during take-off. To get a complete picture of the drag however, the aerodynamic drag during take-off will have to be incorporated as calculated in Chapter 12.

The final drag curve can be seen in Figure 13.4.

Two clear peaks in this curve can be identified. At the start of the take-off phase, friction drag will be dominant. Later, wave drag will become dominant, causing the drag to go up again. Around 10 m/s, the trim angle gets around 2 degrees and the lift starts acting, causing the effective weight to go down and thus the drag will go down.

After iteration and exchange of data and calculations between the aerodynamic and hydrodynamic aspects, the hull width determined was 20 cm. For aerodynamic reasons, this high width results in a smaller side area and therefore a more favourable tail design. The wedge angle was put to be 10 degrees, the biggest value possible in this configuration, as a higher wedge angle is preferable for impact damage. The centre of gravity with respect to the step of the hull was put 15 cm in front of the step at a height of 10 cm.

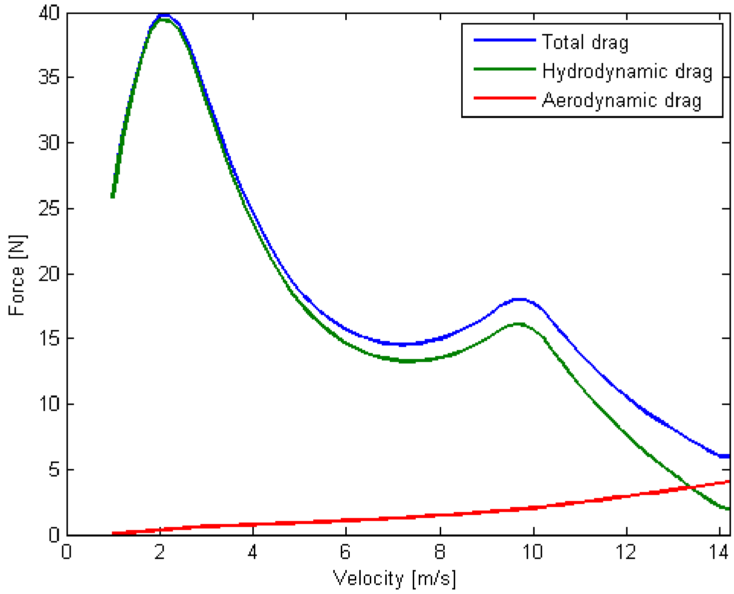

Figure 13.4: The drag curve for take-off

13.3 Landing

After the take-off has been evaluated, landing can be analysed. The top level requirements state that the UAV has to be able to land on water. When the UAV lands, the behaviour of the surroundings and the behaviour of the UAV need to be analysed. Further, the UAV needs to be able to withstand the impact loads it will undergo during landing.

13.3.1 Landing behaviour

When the UAV lands, the environment and the attitude of the UAV have important roles in the landing procedure. First of all, the landing terrain is not smooth and not homogeneous. Also, waves and currents are not easily predictable. The UAV should land in the direction of the wave swell to increase the effective wave period. Doing so, the entire landing procedure will be less rough. It has to be made sure that the autopilot detects the behaviour of the waves and directs the UAV in the required landing attitude.

The best landing conditions for the UAV occur when the UAV lands with minimum airspeed, in the correct pitch attitude and without side drift. The objective is to touch down on the step, with the stern touching or nearly touching the water. Landing on the step minimises the impact forces. The pitch angle should be rather low at landing to prevent from being tossed back into the air at dangerously low airspeeds. Also, a low pitch angle is preferable for piercing through the tops of the waves [48].

Now that the landing behaviour is analysed, the impact loads can be calculated. Since the landing attitude of the UAV is assumed to be in the same direction as the wave swell, all calculations are performed taking this landing attitude into account.

13.3.2 Impact

In order to define what the strength of the structure needs to be, it is important to know the impact loads and pressures that the UAV will be subjected to when it touches down on water.

To find the impact pressure, a wedged-shaped body with a constant beam is considered. When this body hits the water the maximum pressure between the body and the water can be calculated using Equation 13.11 [47].

$$p_{max} = \frac{\rho V_0^2}{2}\pi cot(\beta) \tag{13.11}$$

The maximum pressure, p_{max}, can be determined with the use of the water density, ρ_{water}, the vertical velocity, V_0, and the deadrise angle, β. The velocity in this equation was taken to be 0.656 m/s, which is the highest vertical speed the aircraft can reach. Then the two unknowns, maximum pressure and deadrise angle, can be plotted against each other. This plot is generated using MATLAB visualised in Figure 13.5.

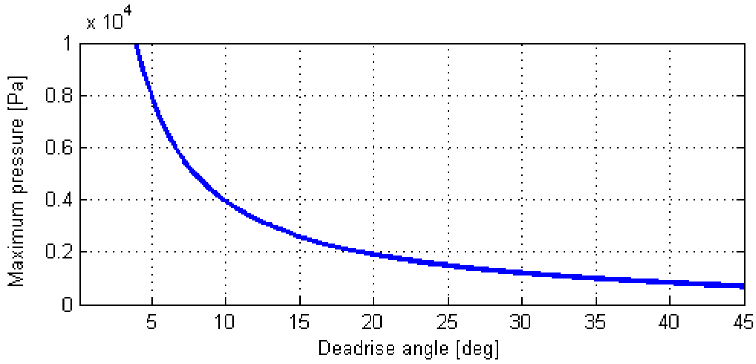

Figure 13.5: Maximum pressure as a function of the deadrise angle

Together with the drag, the impact loads are the main design parameters for the deadrise angle. As can be seen in Figure 13.5, higher deadrise angles are favourable for lower impact pressures. With this input, the deadrise angle was designed to be 10 degrees, as is elaborated in Section 13.2. The maximum pressure for the designed deadrise angle will be $3.93 \cdot 10^3$ Pa.

With the deadrise angle known, the impact loads can be calculated. This calculation was performed with the use of Equation 13.12 [52].

$$F_i = \frac{1}{2}\pi \rho_{water} V_0^2 S_w \left(1 + \frac{\pi \rho_{water} S_w^2 cos^2(\beta)}{8m}\right)^{-1} cos(\beta)cot(\beta) \tag{13.12}$$

To elaborate on the maximum pressure equation, Equation 13.12 calculates the force of impact with the use of the wetted area, S_w, and the mass, m. This result is computed and a visualisation of the impact load as a function of half of the immersed beam can be found in Figure 13.6.

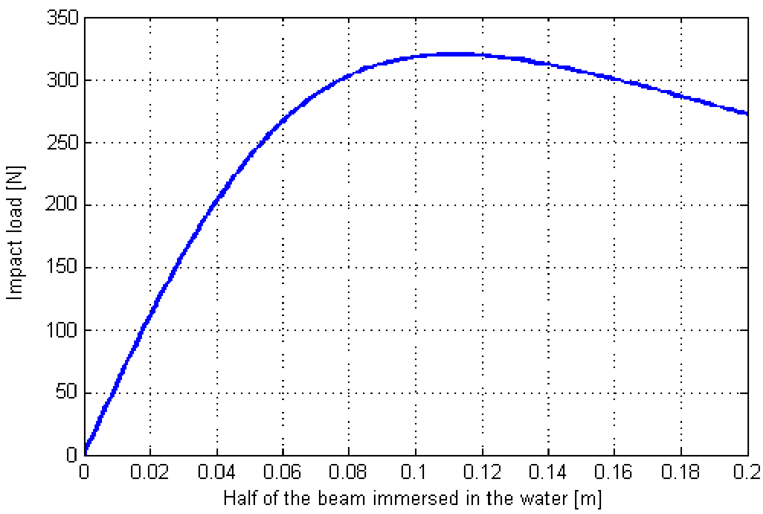

Figure 13.6: Impact loads as a function of the immersed width

With the designed beam width of 0.2 m, the impact load will be 318.4 N. This load is a very important design parameter for the structure, since the has to be able to withstand these forces.

13.4 Stability

Now that the hull parameters and the take-off and landing conditions have been evaluated, the stability will have to be determined. First, longitudinal stability will be analysed, in Section 13.4.1. Next, transverse stability will be looked into, by designing the floaters. This can be found in Section 13.4.2.

13.4.1 Longitudinal stability

First, an overview of all the forces and moments acting on the hull of the UAV during take-off will be presented in Figure 13.7. This figure is taken from Savitsky's paper and adapted to the UAV by adding a lift force and by changing the thrust force from the under-water propellor of a boat to the propellor on top of the hull for the UAV.

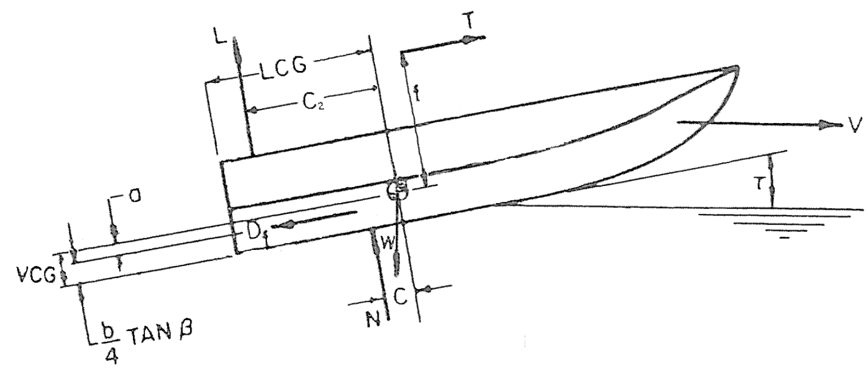

Figure 13.7: The forces acting on the UAV during take-off and their moment arms [50]

In this figure, the position of the centre of gravity (c.g.) is portrayed with the use of parameters LCG, the longitudinal position of the c.g. and VCG, the vertical position of the c.g.. Next, the following forces are presented: L is the lift force, T is the thrust force, W is the weight force, N is the normal or buoyant force, that the water exerts on the hull and D_f is the drag force. The forces' moment arms are shown by: c_2 for the lift force, f for the thrust force, c for the normal force, a for the drag force and the weight force has no arm as it acts from the c.g.. Lastly, $\frac{b}{4}tan(\beta)$ is the vertical distance from the bottom of the hull to the c.g., τ is the trim angle and V shows the direction of the velocity.

The moment arms of the normal force and the drag force can be calculated with the use of Equations 13.13 and 13.14 [50].

$$c = LCG - C_p \lambda b_h \tag{13.13}$$

$$a = VCG - \frac{b_h}{4} tan(\beta) \tag{13.14}$$

Here, C_p presents the distance of the centre of pressure (hydrodynamic force) along the keel, forward of the transom. The other moment arms, f and C_2, are known by design. The weight force is also known. The drag force is computed in Section 13.2, the lift force is taken from aerodynamics (Chapter 12) and the thrust and normal force can be computed using Equations 13.15 and 13.16.

$$T = D_f + W sin(\tau) \tag{13.15}$$

$$N = W cos(\tau) - L \tag{13.16}$$

Now that all the forces are known, the moment (M_{tot}) around the c.g. generated by these forces can be computed, by multiplying the forces by the moment arms, and then adding these moments together. This is done using Equation 13.17.

$$M_{tot} = D_f a + Tf + Nc + LC_2 \tag{13.17}$$

As all of the forces except the weight force depend on the velocity and the trim angle, for each velocity the equilibrium trim angle can be obtained. This is done by checking at which trim angle the total moment generated around the c.g. equals zero. At this angle the UAV will be in equilibrium and therefore it will be longitudinally stable. Performing these calculations, leads to the trim angles at each velocity, shown in Figure 13.8.

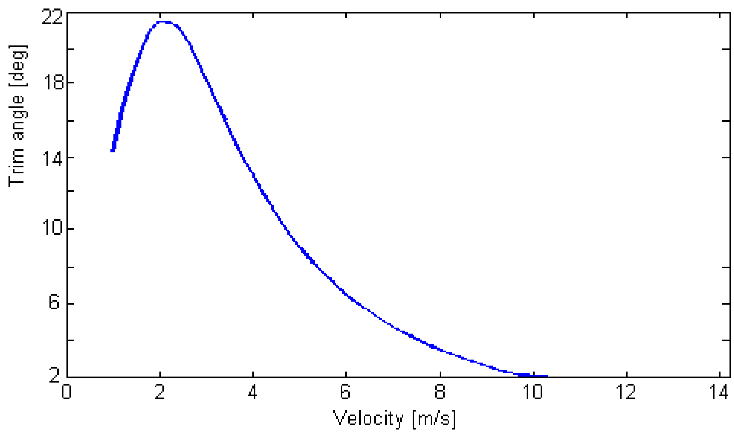

Figure 13.8: The trim angles at take-off

It can be seen that the theoretical trim angles at low velocities will be relatively high. Practically, these angles will be a lot lower. It is incorporated in the hull design that at the end of the hull, the width is decreased into a point. This way, when the UAV trim angle increases, the average hull width will decrease, decreasing the trim angle at this point. When the trim angle will be higher than 12 degrees, the back part of the fuselage will get in the water, moving the normal force to the back and opposing the angular moment of the plane, also decreasing the final trim angle.

Having obtained these trim angles, one can visualise the final drag curve of the UAV during take-off. This curve is shown in Section 13.2.

13.4.2 Transverse stability

Now that the longitudinal stability is assured, the next thing to define is the transverse stability. In order to be stable on water and to prevent the wings from hitting the water, the UAV needs to have floaters on both sides of the hull. These floaters can be mounted either on the fuselage or on the wings, dependent on the desired floater characteristics. To create the same righting moment, floaters near the hull will require more volume than wing mounted floaters. This means that mass-wise, floaters far away from the hull are favoured. However, the structural loads on the wing will be higher when the floaters are farther away from the wing. Thus, a compromise is to be made. The first step in defining the floater placement and size, is the determination of the righting moment of the hull.

The righting moment of he hull is the reacting moment of the hull when rolling in the water. When the hull is heeled, the centre of buoyancy (c.b.) moves to the new centre of the displaced volume. The buoyancy force, acting upwards in the moved c.b., then creates a couple with the gravity force acting downwards at the c.g. causing the hull to retain its static equilibrium position. To calculate the righting moment Equation 13.18 is used [42].

$$M_R = mgy_{GZ} \tag{13.18}$$

In Equation 13.18 M_R is the righting moment, m equals the mass of the UAV, g is the gravitational acceleration and y_{GZ} is the lever arm as can be seen in Figure 13.9a.

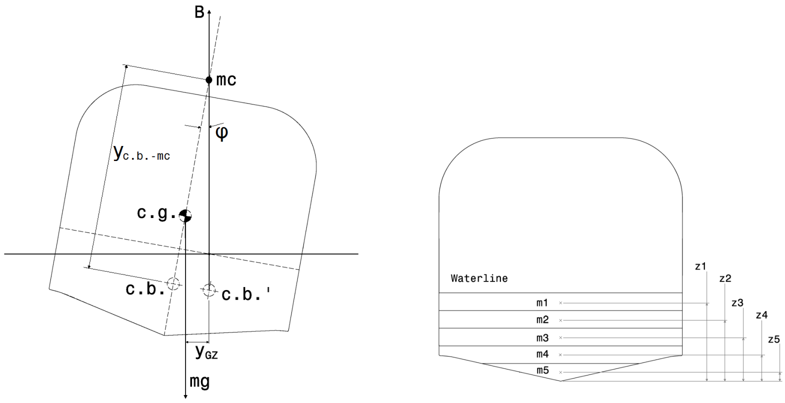

(a) The hull in rolling motion

(b) Mass and height distributions of a hull's displaced volume

Figure 13.9: Transverse stability

In order to define the righting moment, several parameters needs to be determined. The first parameter that has to be calculated is the height of the c.b.. This height can be assumed by dividing the displaced volume in different sections as can be seen in Figure 13.9b. When the displaced volume is divided in vertical sections, each section has a different centre of mass and with Equation 13.19 the height of the c.b. can be assumed. The more sections that are used for the calculation, the more accurate the approximation will be.

$$z_{c.b.} = \frac{m_1 z_1 + m_2 z_2 + m_3 z_3 + m_4 z_4 + m_5 z_5}{m_1 + m_2 + m_3 + m_4 + m5} \tag{13.19}$$

In this equation the height of the c.b. is given by $z_{c.b.}$, m_i is the mass of section i and z_i is the corresponding height of m_i. $z_{c.b.}$ is calculated in the same vertical plane as the c.g. and is assumed to be 0.0432 m above the lowest point. With the height of the c.b. and c.g. known, the transverse stability relations can be calculated. The transverse stability relations define all the relations needed to calculate the righting moment. The first relation is the fundamental stability formula, which results in the distance between the c.b. and the metacentre (mc). The mc is the intersection between the vertical line through the moved c.b. and the symmetry plane of the hull, as can be seen in Figure 13.9a. This relation to determine this distance can be found in Equation 13.20.

$$d_{c.b.-mc} = \frac{I_T}{\nabla} \tag{13.20}$$

The fundamental stability formula states that the distance between the c.b. and the mc, $d_{c.b.-mc}$, with I_T representing the transverse moment of inertia and ∇ being the water displacement. The transverse moment of inertia can be calculated by dividing the waterline cross-section into different ordinates with a constant ordinate spacing, s, as can be seen in Figure 13.10. Then the product of the multiple beam widths to the power three can be calculated using Simpson's rule, as can be seen in Table 13.1.

Simpson's rule is a method for numerical integration to calculate the area under a curve. With the sum of products known, this area and subsequently the transverse moment of inertia, I_T, can be calculated. These calculations are given in Equation 13.21 and Equation 13.22 respectively.

$$A = \frac{s}{3}(\text{Sum of products}) \tag{13.21}$$

$$I_T = \frac{2}{3}A \tag{13.22}$$

The ordinate spacing, s, in Equation 13.21 was taken to be 0.127 m. This spacing corresponds to the length of the waterline divided by 10 creating 10 ordinates. The transverse moment of inertia was

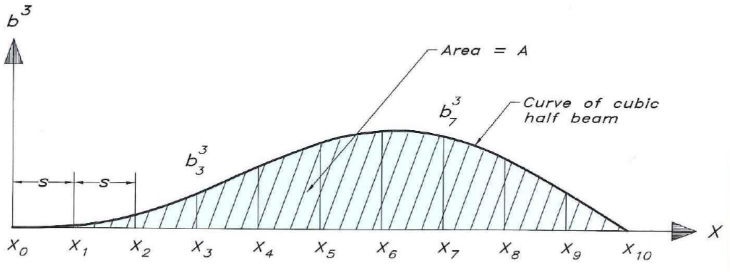

Figure 13.10: Waterline cross-section with ordinates [42]

Table 13.1: Simpson's rule

Ordinate No.	Ordinate value		S.M.	Product	
0	b_0^3	[0.0]	1	b_0^3	[0.0]
1	b_1^3	$[1.20 \cdot 10^{-3}]$	4	$4\ b_1^3$	$[4.80 \cdot 10^{-3}]$
2	b_2^3	$[1.01 \cdot 10^{-3}]$	2	$2\ b_2^3$	$[2.02 \cdot 10^{-3}]$
3	b_3^3	$[1.00 \cdot 10^{-3}]$	4	$4\ b_3^3$	$[4.00 \cdot 10^{-3}]$
4	b_4^3	$[1.00 \cdot 10^{-3}]$	2	$2\ b_4^3$	$[2.00 \cdot 10^{-3}]$
5	b_5^3	$[1.00 \cdot 10^{-3}]$	4	$4\ b_5^3$	$[4.00 \cdot 10^{-3}]$
6	b_6^3	$[9.82 \cdot 10^{-4}]$	2	$2\ b_6^3$	$[1.96 \cdot 10^{-3}]$
7	b_7^3	$[7.49 \cdot 10^{-4}]$	4	$4\ b_7^3$	$[3.00 \cdot 10^{-3}]$
8	b_8^3	$[3.57 \cdot 10^{-4}]$	2	$2\ b_8^3$	$[7.15 \cdot 10^{-4}]$
9	b_9^3	$[3.77 \cdot 10^{-5}]$	4	$4\ b_9^3$	$[1.51 \cdot 10^{-4}]$
10	b_{10}^3	[0.0]	1	b_{10}^3	[0.0]
				Sum of products	$[2.25 \cdot 10^{-2}]$

calculated to be $7.06 \cdot 10^{-4}$ m^4. Together with a water displacement of $9.95 \cdot 10^{-3}$ m^3, $d_{c.b.-mc}$ will be $7.10 \cdot 10^{-2}$ m. Then, the distance from c.g. to the metacentre, which follows from the subtraction of the distance between c.g. and c.b. and the $d_{c.b.-mc}$, will be $1.42 \cdot 10^{-2}$ m. To calculate the righting moment, the only parameter missing is the lever arm, which can be calculated with the use of Equation 13.23 [42].

$$y_{GZ} = d_{c.g.-mc} sin(\phi) \tag{13.23}$$

The roll angle, ϕ, was assumed to be maximum for the case that the wing nearly touches the water. With a wing length of 1.255 m and a clearance of 0.0962 m, the maximum roll angle will be 4.31 deg. From Equation 13.23 it follows that the lever arm, y_{GZ}, has a value of $1.07 \cdot 10^{-3}$ m.

The righting moment, as defined in Equation 13.18, will be 0.107 Nm. This is a positive righting moment, which indicates that if the hull starts to roll, it creates a positive moment to return to its static equilibrium. However, when the angle of roll is to high, the wings will hit the water. To decrease the likelihood of this event occurring, floaters can be added to the wing. The design of these floaters will be elaborated in Section 17.5.3.

13.5 Floaters

To increase the transverse stability floaters can be added to the UAV. First the size and distance of the floaters are designed for in Section 13.5.1 and afterwards the impact loads on the floaters are evaluated in Section 13.5.2.

13.5.1 Floater design

The size and distance of the floaters from the vertical axis of symmetry can be calculated by Equation 13.24 [53].

$$B_f y cos(\phi) = N M_R \tag{13.24}$$

Equation 13.24 states that the buoyancy moment created by a submerged floater, calculated by multiplying the buoyancy force (B_f) by the floater distance (y), must equal the righting moment of the hull (M_R) times a safety factor (N). This safety factor is included to allow for all additional disturbing moments, created by for example gusts and waves. Literature study in various seaplanes showed that a safety factor of two is satisfactory for assuring transverse stability [53]. The maximum roll angle of 4.31 degrees, is assumed again. These parameters define the floater size and the floater distance from the axis of symmetry of the hull. The relation between the floater size and floater distance from the hull can be seen in Figure 13.11.

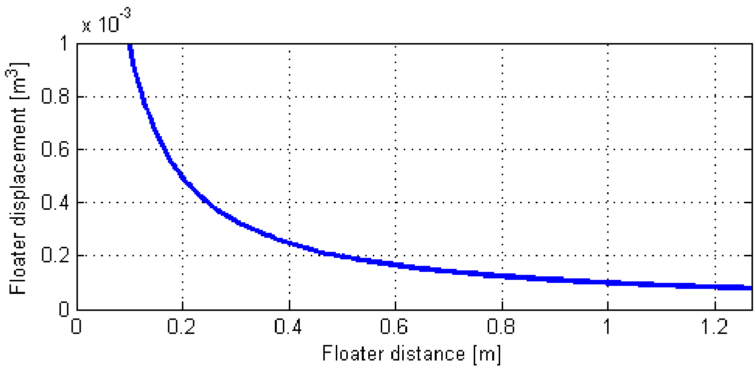

Figure 13.11: Floater displacement versus distance from axis of symmetry

From Figure 13.11 it follows that the required float displacement, and therefore the size, is inversely proportional with the distance from the vertical axis of symmetry. From a structural point of view it is favourable to minimise the distance. From iteration, the optimal distance was found to be 0.7 m from the axis of symmetry. With this distance, the structure is still able to cope with the corresponding loads and the floater size is minimised. A larger distance was not possible because this would mean the floaters would interfere with the ailerons, decreasing the aileron efficiency.

The three main functions of a floater are that it needs to be aerodynamically shaped to reduce the drag in the air, it needs to cope with the required water displacement and it needs a wedge-shaped bottom surface to reduce impact loads. To reduce the impact loads a deadrise angle of 30 deg was given to the floaters. Since the floaters will not touch the water at higher speeds, this high deadrise angle will not influence the maximum drag at the hump resistance which occurs at significantly higher speeds. To reduce the aerodynamic drag, the floater was designed to have a airfoil shape and after iterations with minimal wetted surface, minimal size while still providing adequate water displacement, the NACA0025 airfoil was chosen for the floaters. Then, to cope with the required water displacement, $1.41 \cdot 10^{-4}$ m^3 at 0.7 m from the axis of symmetry, the dimensions of the floaters can be seen in Figure 13.12.

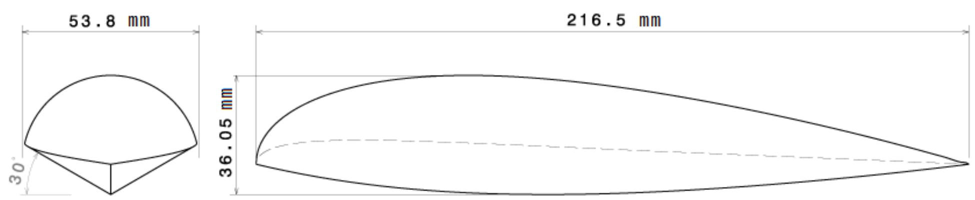

Figure 13.12: Floater dimensions [mm]

With the hull, floater position and floater size designed, the stability of the UAV, in both longitudinal and transverse directions, is achieved and the floater impact can be evaluated.

13.5.2 Floater impact

With the floater dimensions known, it can be calculated what the impact loads are on these floaters. First the vertical impact is calculated and then the horizontal wave impact is estimated.

The vertical impact was calculated using the same method used to calculate the hull impact in Section 13.3.2. For a floater with dimensions as shown in Figure 13.12 and a wetted area of $1.98 \cdot 10^{-2}$ m^2, the vertical impact can be seen in Figure 13.13.

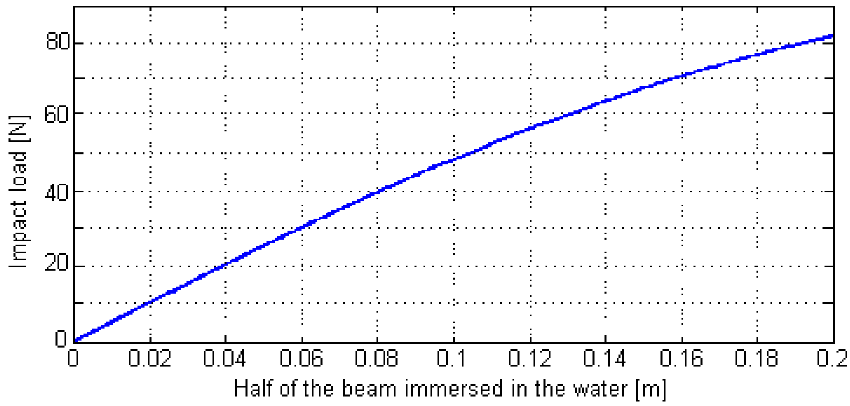

Figure 13.13: Vertical impact on the floaters

As can be seen, for a half width of the floater of 0.0269 m, the vertical impact for the floater is 13.96 N. This impact load will have to be taken into account when designing the wing.

The other impact load is the horizontal impact load. This load needs to be calculated to define the torque applied to the wing when the floater hits a wave in a horizontal attitude. Further, the supporting structure between the floater and the wing is dependent on this load. Since no actual equations were wound for this impact load, the load is assumed to be the skin friction drag with a safety factor applied.

In order to calculate the skin friction drag, several parameters need to be determined and calculated. The calculation for the skin friction drag is given in Equation 13.25.

$$D_f = C_f \frac{1}{2} \rho_{water} V^2 S_w \tag{13.25}$$

This equation determines the skin friction drag (D_f) with the use of the skin friction coefficient (C_f), density of seawater (ρ_{water}), the horizontal speed (V) and the wetted area of the floater (S_w). The wetted area of the floater was assumed to be the wetted area of the submerged floater. This area, determined using CATIA, was found to be $1.98 \cdot 10^{-2}$ m^2. Then the skin friction coefficient can be calculated using Equation 13.8 as was used in Section 13.2.

The only parameter needed to calculate the skin friction coefficient, C_f, is the Reynolds number, Re, which can be calculated using Equation 13.26 [42].

$$Re = \frac{V L_f}{\nu} \tag{13.26}$$

In this equation, V is the velocity, L_f is the length of the floater and ν is the kinematic velocity, which is $1.0 \cdot 10^{-6}$ m^2/s for salt water at 20 °C. With a floater length of 0.217 m and assuming a horizontal impact velocity of 18 m/s, the Reynolds number will be $3.90 \cdot 10^6$. Therefore the skin friction coefficient will be $3.39 \cdot 10^{-3}$ and the friction drag 11.2 N. With a safety factor of 1.5, since this is a very rough approximation of the impact force, the impact force can be assumed to be 16.7 N.

With these impact forces known, the wing structure can be designed.

13.6 Maritime conclusion

To conclude the this maritime chapter, the main resulting parameters of the hydrodynamic design will be presented in this section.

First of all, for the determination of the deadrise angle it was found out that the hydrodynamic drag during take-off was critical in comparison to the impact forces when landing. Therefore the deadrise angle was agreed to be lower than typical deadrise angles for general aviation seaplanes, namely 10 degrees.

The required minimum beam was dependent on the deadrise angle and could be determined by using Equation 13.2 and Figure 13.2 from Section 13.1. With the maximum lift coefficient and the wing area known from Chapter 12 to be 1.4 and 0.64 m^2 respectively, the beam coefficient is found to be about 0.19 and therefore the required minimum beam will be 0.15 m. After iterations with the design, the actual beam was determined to be 0.20 m.

The total length of the fuselage in order to be stable in both water and air, was found to be 2.35 m. Further, the centre of gravity in longitudinal direction was found to be 0.15 m in front of the step and in vertical direction it is 0.1 m above the lowest point of the hull.

For the final shape of the hull, the water displacement is $9.95 \cdot 10^{-3}$ m^3. This leads to a waterline height of approximately 7 cm.

Furthermore, it has been determined that the propellers should be designed to be able to overcome the drag presented in Figure 13.4, with a maximum drag of about 40 N. Also, the hull should be designed to withstand an impact load of about 318.4 N, while the floaters should be able to handle 13.96 N in vertical direction and 16.7 N in horizontal direction.

With these parameters known, the basic shape of the UAV is defined. The basic maritime parameters are visualised in a front and side view given in Figures 13.14 and 13.15 respectively.

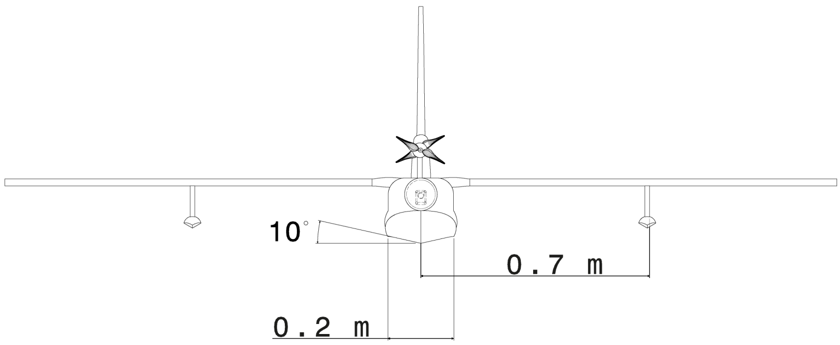

Figure 13.14: Front view of the UAV

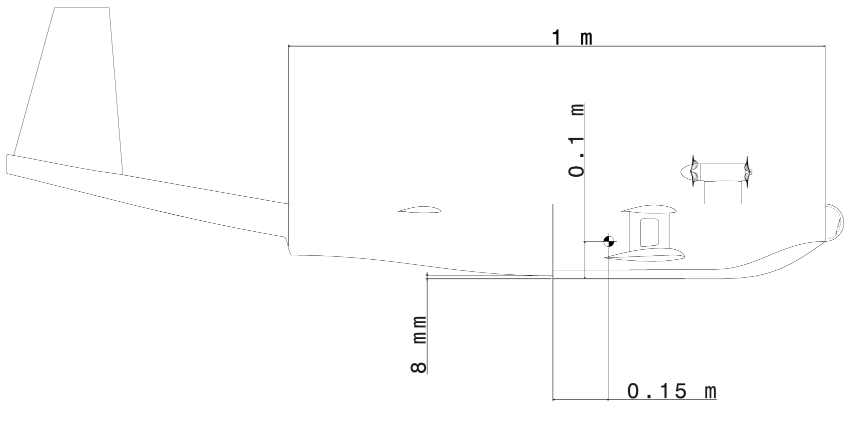

Figure 13.15: Side view of the UAV

Chapter 14

Operations

14.1 On-board communication system

In a modern sophisticated communication system, many problems should be considered. In this section, issues related to the requirements are discussed. And components are selected after the discussion. Then some other concerns about this system are mentioned.

14.1.1 Operating environment

In the following, the radio frequency environment is discussed in detail and the others are generally mentioned at the end.

The communication system is supposed to exchange telemetry commands and send visual surveillance data back from the UAV to the ground control station (GCS) across a maximum distance of 80 km. This largest distance is estimated from detailed statistical data [54] as well as the surveillance area. In short range within 2.5 km a safety link is also enabled. The criteria to select the components in the communication system can be derived by these requirements. The requirements on the communication range relates to the communication type, such as Beyond line of sight (BLOS) and Line of sight (LOS).

For BLOS communication, relay via satellite or other aircraft is necessary. However the operation cost of data relay via satellite or other UAVs is high; the cost can be reduced by applying LOS communication. The barrier of LOS can be removed by increasing the flight height of the UAV and place the receiver antenna at a higher location. When assuming the receiver antenna is on sea level altitude, the minimum flight height for a certain range can be calculated. In order to cover a range of about 80 km, the minimal required height is about 0.4 km [55]. Any higher flight altitude or higher position of the receiving antenna can ensure a LOS communication range of 80 km. The available legal frequency varies in time and district. For current LOS operations in north America, unlicensed 902MHz to 928MHz frequencies are available for industrial, scientific and medical (ISM) and a worldwide unlicensed 2.4 GHz ISM frequency is assigned. Other LOS frequencies such as 310−390MHz, 405−425MHz, and 1350−1390MHz in the United States for example require an operating license [56]. The radio frequency for UAVs in Europe is allocated by European Defence Agency (EDA) in Study on the Insertion of unmanned aircraft system in the general Air Traffic (SIGAT). The legal radio frequencies that can be applied to UAVs vary with region and time.

When the size, weight and power consumption of the components are considered as well, a low frequency also indicates a low power consumption and large antenna size. Since both telemetry downlink and television downlink are necessary, the latter is more critical to select the data rate at such a distance. This is because the operating frequency should be compromised for 80 km communication and relative large visual data rate. The data rate needed for compressed HD video is about 1 Mbps and for picture is about 80 kbps. The data rate is limited by the Shannon-Hartley theorem 14.1. This equation relates the channel capacity (C) to the signal to noise ratio and bandwidth of the transmitted signal. It is desired that the data rate R is less than the channel capacity, so that the amount of error bit can be minimised [57]. This equation is evaluated in Section 14.4.

$$C = B \ln(1 + SNR) \tag{14.1}$$

In the radio frequency environment, frequency interference can occur both between operating frequency of the on-board components and UAVs nearby using common signal channel. The former interference can be easily solved by specific operating frequencies of the components. In case of a 900 MHz radio modem, this frequency will interference with 1800 MHz, 2700 MHz frequencies and so on. However, the latter problem can be solved by implementing anti-jamming features, like beam angle of the antenna and the channel coding [56]. A narrow beam antenna provides good jamming-proof property, but such a antenna requires the highest allowed frequency band of the given antenna and additional supporting structure and mechanisms, which increase the required volume and weight. The channel coding technique converts the transmitted signal into many small parts in coded data stream, so that these small parts can be detected and corrected by outer coding and therefore protected. Extended research on anti-jamming is necessary to go deep.

The natural humidity and thermal environment in the mission area is discussed in Chapter 11. The humidity inside the UAV is designed to be low, nevertheless the electronic system can get damaged. The thermal environment inside the UAV will be higher than the external temperature due to the electric heat. However, the heat can be conducted from high temperature sources to low temperature sinks. The resistance of the components, the endurance and the conductivity of the system are determinate parameters of the thermal environment. In this mission, the temperature inside the UAV is assumed to be tolerable to the on-board components without affect their performance. This assumption can be proved by thermal dynamics calculation. This needs further work on thermal dynamics.

14.1.2 Autopilot

Autopilot together with a GPS chip can be used for UAV flying independent of ground station and stability control by ground crews. The client has a preference for the Paparazzi hardware and software system and due to its open source technology and versatility it is used in this project. There are several products that function as an autopilot in combination with Paparazzi. Currently, the autopilots available and usable in the UAV to be designed are the Lisa/M, the Umarim Lite and the TWOG [58]. They have similar dimensions and they are all COTS products. A comparison is done in Table 14.1 with these autopilots, with the properties being the cost, processor clock speed and the Random Access Memory (RAM).

Table 14.1: Autopilot comparison table [58]

Autopilot	Cost [$]	f_{clock} [MHz]	RAM [kb]
Lisa/M	250.00	72	64
Umarim Lite	249.00	60	32
TWOG	310.00	60	32

From Table 14.1 it is seen that the only significant difference is seen in the amount of RAM and a minor difference in the processor clock speed. At the Delft University of Technology (DUT), team ATMOS and the engineers in the Micro Air Vehicle (MAV) Lab have experience working with UAVs and specifically with Paparazzi. Team ATMOS also started as a DSE group and have designed and built a UAV capable of vertical landing and take-off and horizontal flight [59]. The MAV Lab is a laboratory consisting of aerospace engineers whose knowledge from electronics, mechanics, aerodynamics, navigation and control are combined for the development of MAVs [60]. Both teams have experience in using the Lisa/M autopilot. After some consideration of the several autopilots, the Lisa/M autopilot is chosen for the mission.

Control theory of Lisa/M: The Lisa/M autopilot performs as a Proportional, Integral, Derivative (PID) controller. The essence of it is a feedback control loop, as shown in Figure 14.1. This feedback loop processes the present error, accumulation of past error and predicted future error by proportional, integral and derivative calculation respectively. The present error is the difference between the current measured value and the setpoint value. This value is multiplied by a gain K_P and integrated over the time interval of each control operation with a gain K_I. As well, the derivative of this error amplitudes with a gain factor K_D. Then this calculations are further processed to generate an output value and the loop iterates. These gains can be obtained by implementing results of the aerodynamic calculation to control theory.

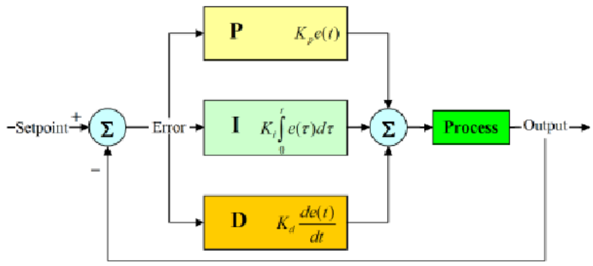

Figure 14.1: PID controller scheme[61]

One function of the Lisa/M board is to control servos of the control surface and thus the attitude of the UAV. The control loop of the attitude control system is displayed in Figure 14.2. As shown in this system, the UAV is able to carry out pitch ,roll and yaw motion by setting the angle of deflection of the control surface to desired values. The setpoints are based on the design and calculation of the control surfaces in Section 12.3. For example, in order to achieve a desired roll angle which is set in the autopilot programme as an example, the current roll angle is measured by the vertical gyroscope and then the difference between the setted value and the measured value is manipulated through PID calculation. The results are converted to electronic signal to the motor controller and eventually control the servos to deflect the roll control surfaces towards the desired value so that the required roll angle is achieved.

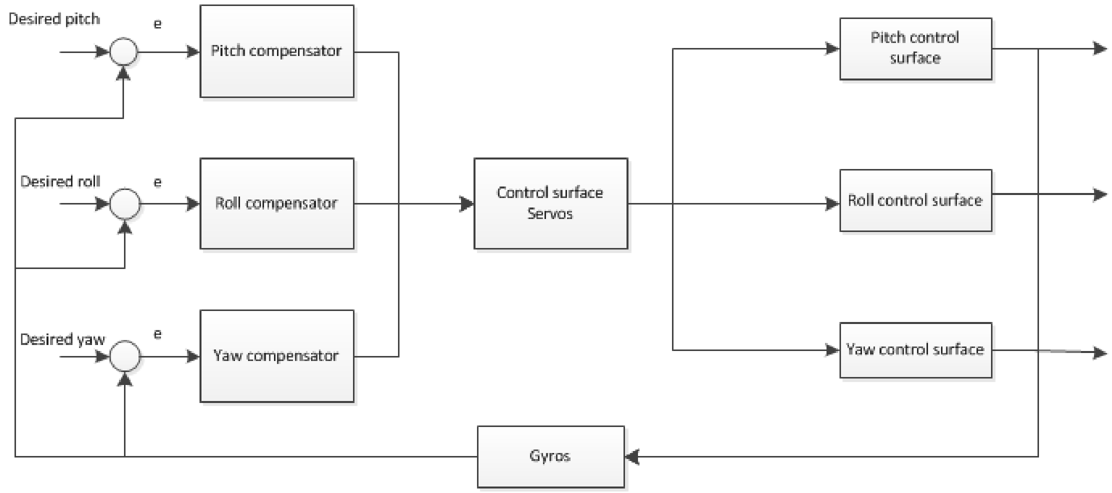

Figure 14.2: Attitude control system block diagram

In Figure 14.3, the interrelation between Lisa/M board and other on-board components is depicted. The arrows towards the Lisa/M board indicates the measured input signal of the PID controller, and on the contrary, the outwards arrows define signals from controller to components to be controlled. For example, the motor controller block contains two segments, an electronic speed controller (ESC) and a battery eliminator circuit (BEC). The input signal of the ESC is from the battery. If the power level of the battery is low, the ESC generates a signal to the Lisa/M and the Lisa/M board sets a zero motor speed via the ESC.

The types of control signal through the on-board components are shown in Figure 14.4. The signal flow is in the direction of the arrow. Two types of signals are displayed in this figure, serial signal and pulse-position modulation (PPM). The PPM frame contains a certain number of PPM signals.

GPS: The autopilot that has been selected does not have an integrated GPS module, so a separate module must be chosen to provide the UAVs location. The GPS module is selected based on a number of

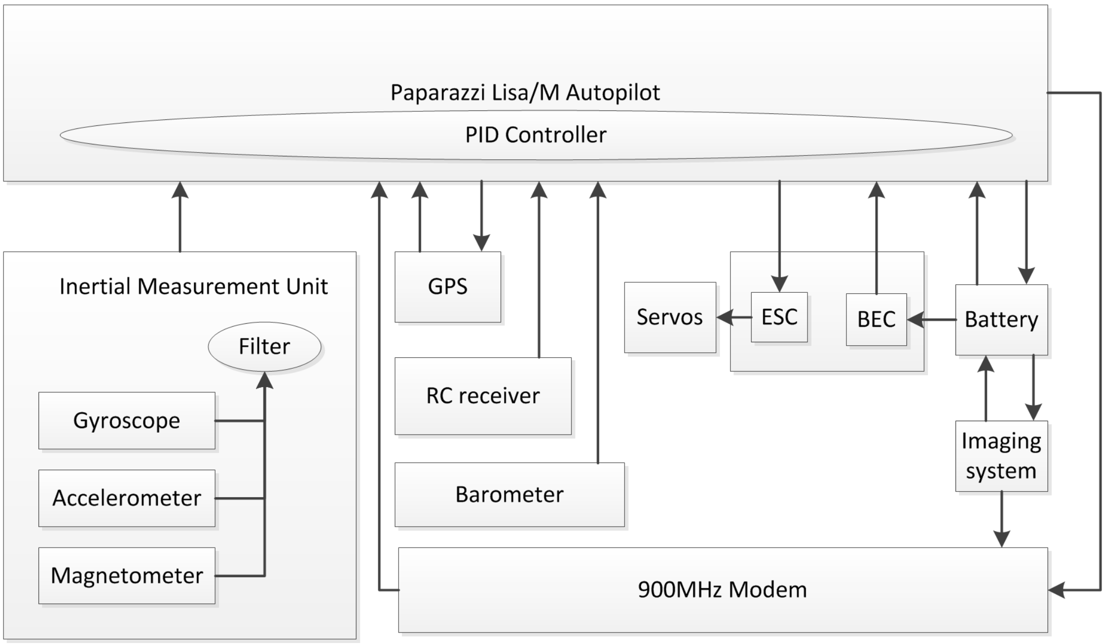

Figure 14.3: Control logic of on-board system

requirements, namely the cost, power usage, accuracy, speed and size. The UAV is supposed to perform maritime surveillance and as soon as a possibly suspicious ship or object is spotted by implementing the use of a uBlox GPS chip.

14.1.3 Other components of on-board communication system

Data-link radio modem: The data-link radio modem acts as an on-board transceiver. The data-link modem can generate or receive a radio frequency with the assistance of an antenna. A particular modem works only at one or several signal channels. As discussed above,these frequencies determine the possible data rate of the radio modem and the communication distance depends on antenna height and type. Moreover, the performance of the radio modem depends on the sensitivity and output power or receiver of the modem. With a high modem sensitivity, it can operate at a low received power and vice versa. Since a bit rate of 1 Mbps is required to be transmitted back at a critical distance of 80 km, one commercial-off-shelf radio modem that satisfies these requirements is Nano Series - n920x. This is a miniature 900 MHz wireless modem, which operates at a common frequency in the America region. The specification of this product [62] is used to test the entire communication system in Section 14.4. When the legal frequency differs in different regions, this radio modem has to be changed.

Antenna: There exist many different antennas. Generally, these antennas can be summarised into two categories. One category is the directional antennas which radiates most power in a certain directions. This type of antennas can improve the performance in such directions and reduce interference. Thus it is important that the directional antenna points towards receiver or transmitter with additional mechanisms. This increase the weight and volume of the UAV. The other is omnidirectional antennas. These antennas radiates signal powers identically in all direction. Generally, a omnidirectional antenna is relative simple to design and small in size comparing to a directional antenna. While the former is usually characterised with a higher antenna gain (6 dBi to 20 dBi) and better anti-jamming property than omnidirectional antenna (0 dBi to 6 dBi).

A relative high gain antenna is necessary to cover the 80 km communication range. The magnitude of the gain is influenced by ground receiver antenna and the sensitivity of the ground radio modem as well. This relation is revealed in Equation 14.2. However, Equation 14.4 indicates that a high power will be radiated with a high gain antenna. This value is limited by the available power. Moreover, the size of

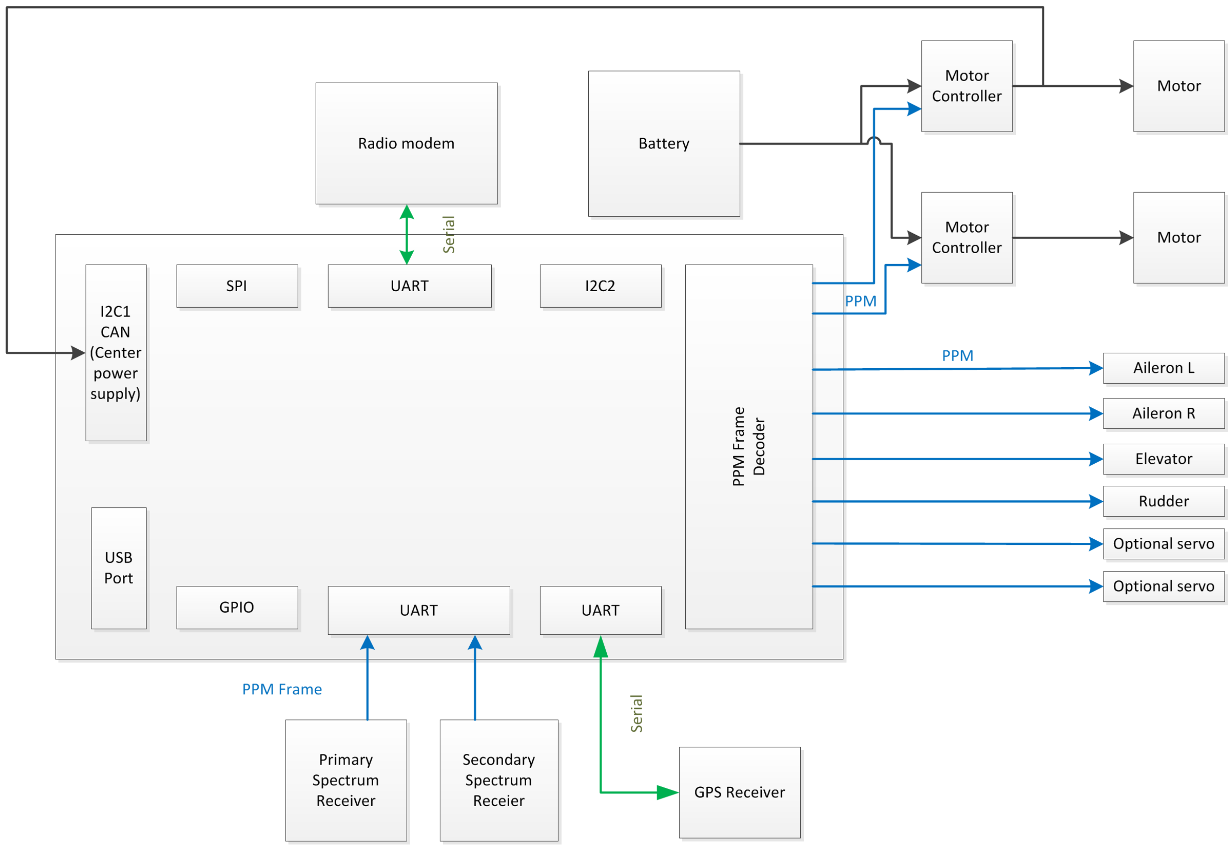

Figure 14.4: Data flow in on-board communication system

the antenna depends on both the demanded gain and type of the antenna. For the selected radio modem above, it specifies that transmitted power of the radio modem is at most 1 W with a 6 to 12 dB antenna. An antenna with a maximum gain of 6 dB can be used with a 1 W transmitter under the rule of Federal Communication Commission. If the antenna gain is increased, the power output of the transmitter must be reduced by the same amount [63]. One of the commercial-off-shelf antenna providing a 6 dB gain is about 40 cm long and weigh 600 g. The cost of this antenna is 40 dollars. Moreover, it is recommended to use a self-designed antenna for the mission.

$$\text{Sensitivity} = \text{Radiated power} - \text{Maximum Allowable Path Loss} \tag{14.2}$$

RC receiver: A RC receiver is usually used to receive safety link. The range and data rate requirements of this receiver are much lower than the on-board radio modem. For example, a $R6008SP$ $2.4GHz$ receiver is adequate. This frequency will not interference with radio modem frequency and discussed more in Section 14.1.4. With a 13 cm pigtail antenna, the communication range is extended to 3 km [64].

14.1.4 Other considerations

The discussion above are based on the mission requirements. While when considering more detailed scenarios in practice, more issues are generally described in the following.

Track and follow procedure: In the surveillance mission, the track and follow procedure can be realized by ground crews. However, this will increase the personnel effort and operational experience is of great importance. Another choice is to design a on-board tacking system so that the UAV can recognise and following potential target autonomously. The suspecting target can be recognised either by the ground crew with the visual data or by a data base on the UAV. And the tracking motion of the UAV indicates that the

UAV should be able to predict the moving target's motion and make short manoeuvre. Constant real time decision is required to optimize many parameters taking care of physical constraints on the aircraft at the same time and predict the further motion of the moving target is more difficult [65]. The on-board system and payload camera system will become more complex and thus the level of requirements of the entire UAV is higher due to the snowball effect.

Collisions avoidance system: The existing unmanned collision avoidance system is composed of functions of sensing, detection, avoidance, and communication functions. In Figure 14.5, each function's most important inputs, outputs and triggers [66] are shown. The sense of the other flight object is qualified by the field of view of the sensors. Detection function is the means to discover and manage imminent risks to the UAV. The detection range should be regulated to a specific UAV. The delays of autonomous response, LOS and BLOS control are different and should be taken into consideration. Moverover, the detection range differs at different altitude since the climb/dive rates and turn rate are a function of altitude [67]. The manoeuvring of the UAV will be performed based on the scheduled flight plan along with the level of responsibility assigned by the ground controller. This issues should be further studied and applied to the on-board system.

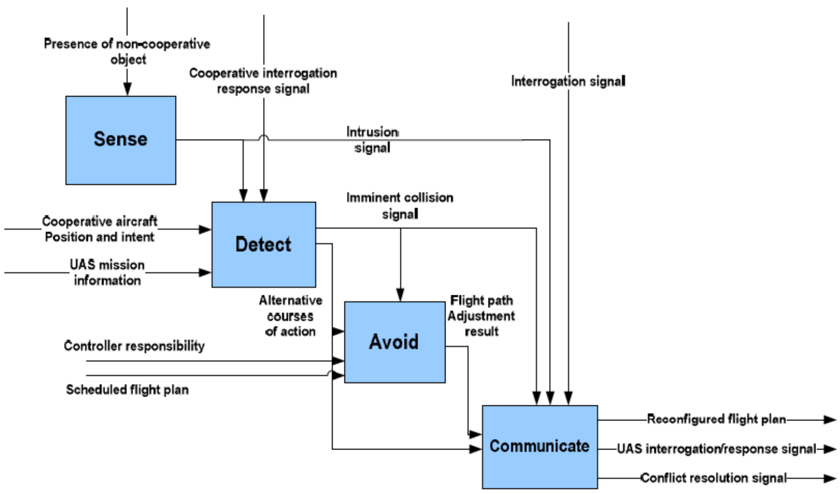

Figure 14.5: Unmanned UAV collision avoidance system [66]

Signal Encryption :

When the sensitivity of the information is high, the encryption technique prevent original information to be recovered by a third party. A commercial-off-shelf radio modem with function of encryption is common. For the selected on-board radio modem, 128 bit Advanced Encryption Standard (AES) is an encrypting option. The encryption technique is based on signal modulation knowledge but many encryption algorithms exist such as AES specified for encryption of electronic data.

14.2 Ground control system

The Ground Control Station has two functions: the first is to receive and analyse data gathered by the surveillance UAVs. Secondly, the GCS is used to send commands to the vehicles. For these purposes, feasible hardware and software options are discussed in this section, based on the relevant UAV system requirements. Since the GCS is operated by ground crews, ease of use of the system interface is also considered. GCS selection is based on current COTS (Commercial off-the-shelf) systems available on the market.

Section 14.2.1 covers the workstation (hardware) selection, after which the software selection is elaborated on in Section 14.2.2.

14.2.1 Hardware

Several ground work station concepts are used in practice, such as a conventional personal computer (PC), a rugged PC, a portable GCS, or a radio controller. These options are discussed below based on practicality, battery endurance, portability and durability of the work station.

Personal Computer: A conventional PC is suitable for a stationary GCS. The battery life of a conventional laptop type PC is about 2 hours. The operating time is considered acceptable compared to the UAV's endurance of 1 to 1.7 hours. However, when the GCS is designed to be stationary, battery life challenges can be eliminated completely. However, the normal PC is not that robust to be transferred frequently. The price of PCs is usually between $500 and $1200.

Rugged computer: A rugged computer is a PC protected by a case. Battery endurance in both portable and stationary GCS are expected to be comparable to the conventional PC. Mobility of the UAV operator is greatly increased when using a rugged pc. Cost is about $500 higher than a conventional PC.

Man-portable control station: A portable ground control system is defined as a small modular configuration that includes a ruggedly built work station as well as a remote interface box and miniature ground data terminal. A man-portable control system is based on a workstation. This integrated system is a robust design which is sized to be portable. The available operating time is similar to that of a normal PC. The price is however higher, at around $5500. A COTS product of around $5200 dollars is selected[68].

Radio controller: The radio controller is used for direct line-of-sight control of the UAV, and as such is only used when the GCS is not controlling the UAV. While in the surveillance mission, the radio controller can not work separately as a work station.

If the GCS is a stationary stationary, the battery endurance is assumed not to affect the GCS selection. In this case operational life of each option only depends on use. Although the cost of the GCS is not set as a high priority by the client, a conventional PC can be used in this case for its low price. When the GCS is required to be highly mobile, a portable control system is preferred.

The GCS has to be compatible with the UAV board communication system. This means that another radio modem and antenna operating in at a range of 80 km should be connected to the control station to receive the signal at 900 MHz, which is the UAV radio modem's operational frequency. One option is to use the same radio modem and antenna as used in the UAV. This option is tested in Section 14.4. The cost of this system is presented in Table 14.2. However, the size and power consumption of the antenna on ground are not as critical as the airborne component, so the radio modem type is generally very adaptable. The cost of this system therefore can be changed.

Table 14.2: Possible cost for ground control system

Component	Price in dollar
Man-portable GCS	5200(Portable)/1200(Stationary)
Radio modem and antenna	500
Radio controller	60
Total Cost	5760/1760

14.2.2 Software

In addition to the hardware mentioned in the previous section, a user friendly interface is preferred for the ground operator(s). The data transferred back from the UAVs should be visible on the display, such as the GPS position in the map and a primary flight display (PFD) window. Received flight data should be stored and analysed. The UAVs should be easily controllable. Since multiple UAVs will fly in the surveillance mission at the same time, the software must be able to to select and control multiple UAVs separately.

There are several options autopilot software. Paparazzi and Open Pilot are free and open source and they both have been tested in practice for years. Therefore the software license is not a problem in this project. The Paparazzi autopilot program is selected and researched to simulate missions. By tuning the parameters in the program to fulfil the mission, autopilot can be configured. The actual programming and configuration of the autopilot is beyond the scope of this design project.

14.3 Imaging system

In order to acquire visual data (Appendix A, requirement 1.2.a) the UAV has to be equipped with a photographic sensor that is able to gather visual information during flight. The criteria for the imaging system:

- The resolution must be high enough that ships can be detected and classified at cruise height
- The viewing angle must be sufficient to maximize coverage
- The size and dimensions must comply with the UAV
- The weight, power usage and cost have to be within their budget bounds
- The components and infrastructure must be COTS
- The system must be able to rotate to improve tracking

The camera system selected is the 'Lockheed Martin Procerus Technologies BTC-88 Gimbal' [69]. The system is able to pan and tilt and is specifically designed for on-board imaging of small UAVs. The main structure consists of a dome with an 88 mm diameter that supports the camera. Some important characteristics of the Gimbal can be found in Table 14.3.

Table 14.3: Relevant BTC-88 Gimbal characteristics

Property	**Value**	**Unit**
Minimum viewing angle	4.6	degrees
Maximum viewing angle	46	degrees
Horizontal resolution	752	Pixels
Vertical resolution	582	Pixels
Pan angle	360	degrees
Tilt angle	90	degrees
Cost	3150	€

The camera has to be placed outside of the UAV and be protected from water. In order to maximize aerodynamic efficiency the camera is placed on the nose with the lens pointed down, as can be seen in Figure 14.6. In this position, tilting corresponds to a rotation in the XZ-plane and panning occurs in the YZ-plane.

In order to calculate the daily coverage area of the UAV the viewing area has to be known; multiplying with the maximum daily range gives the daily coverage area. The viewing area depends on a couple of parameters:

- Cruise height (2000m)
- Viewing angle
- Pan angle range
- Required level of detail

From Table 14.3 the viewing angle and pan angle range can be determined. However, the required level of detail is a driving parameter for the viewing area. The required amount of pixels to classify a ship is 66 pixels [70]. A typical boat used to transport drugs (as described in Section 4.1) is a yola boat and typical dimensions are 10×2m. This results in a meter-per-pixel ratio of 0.55. When multiplied with the

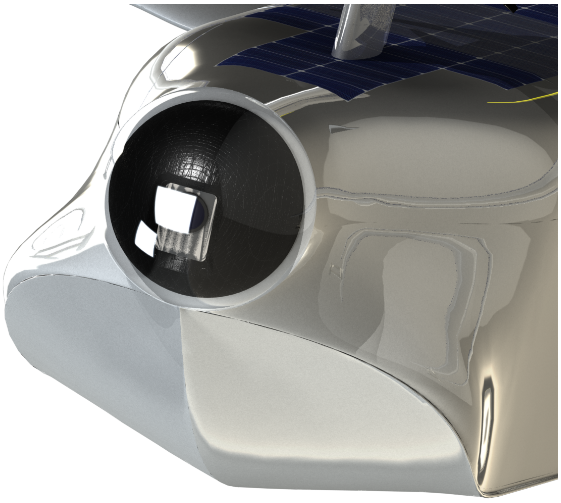

Figure 14.6: Placement of the camera dome

camera's resolution the maximum instantaneous viewing area is 414 × 320m. When pointed straight down, a maximum angle of view of 11.8 degrees is required. By panning, the camera can cover a larger area but it is limited by the maximum instantaneous viewing area. When considering the cruise velocity of 22 m/s and a pan velocity of 288 deg/s no coverage loss is assumed. When the pan angle is too large the acquired image has a level of detail that is too little to classify the object. In figure 14.7 the horizontal viewing distance is plotted against the pan angle from the normal. By using the smallest angle of view, the maximum pan angle was found to be 52 degrees. This results in a horizontal coverage distance of 5.1km. When multiplied with the daily range of 140km, the daily coverage area is 718km^2

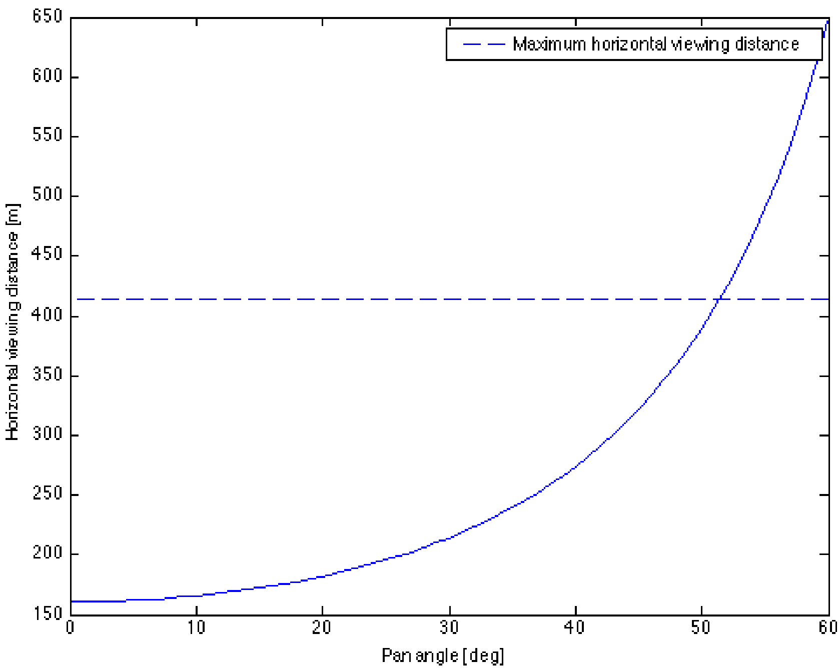

Figure 14.7: Influence of camera pan angle on the UAVs horizontal viewing distance

14.4 Communication system test

The communication between ground control system and the UAV is bi-directional as shown in Figure 14.8. The critical situation for this communication system indicates a communication distance of 100 km and a data-rate of 1 Mbps for image and video data transfer. In the case that the identified radio modem and antenna are applied to both the airborne communication system and ground control station, the power consumption and the antenna gains of both on-board communication system and ground control system can be tested at once.

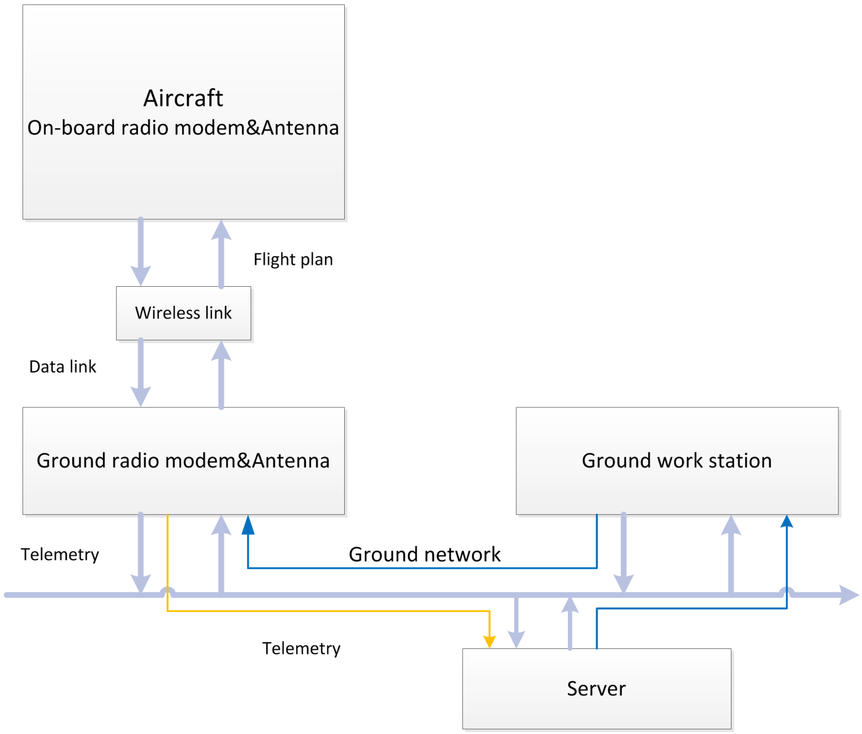

Figure 14.8: Communication between paparazzi agents[71]

The received signal power P_{RX} is the summation of received antenna gain G_{AR}, space loss G_{FS} and transmitted power P_{TX}. This can be expressed in Equation 14.3 [72]. The space loss is dominated by the distance between transmitter antenna and receiver antenna. More transmitted power is needed for a longer distance.

$$P_{RX} = G_{AR} + G_{FS} + P_{TX} \tag{14.3}$$

The transmitted power P_{TX} from the selected on-board antenna radiates omnidirectional and the power received P_{RX} at the receiver depends on the distance between the transmitter and the receiver. The radiated power in direction of the ground raido modem can be expressed as Equation 14.4. The output power for the selected radio modem in Section 14.1 is 1 W [62] and the corresponding receiver antenna gain is 6 dB. Thus the transmitted power P_{TX} is about 36 dBm. Then the radiated power in direction of the receiver antenna is 61.1 dBm.

$$P = \frac{P_{TX}}{4\pi d^2} \tag{14.4}$$

By substituting the antenna gain equation 14.5 and Equation 14.4 into Equation 14.3, Equation 14.6 can be obtained, in which λ is the wave length of the 900 MHz signal. The received power P_{RX} is about -76.78 dBm. This power is higher than the ground radio modem sensitivity 100 dBm, which can be found from reference [62], the feasibility of the ground control system is thus verified.

$$G_{AR} = 10 \log \left(\frac{4\pi A}{\lambda^2} \right) \tag{14.5}$$

$$P_{RX} = P_{TX} + G_{AR} - 10 \log \left(\frac{4\pi d}{\lambda} \right)^2 \tag{14.6}$$

Further, the noise power can be calculated with Equation 14.7. This equation indicates that the noise power depends on the data-rate (R).

$$N = 10 \log(R) - 174 \tag{14.7}$$

At this point, SNR can be derived by combining equation 14.6 and Equation 14.7. The relation is expressed in Equation 14.8.

$$SNR = P_{TR} + G_{AR} - 10 \log \left(\frac{4\pi d}{\lambda} \right)^2 + 10 \log(R) - 174 \tag{14.8}$$

Usually, an SNR higher than 10 dB will guarantee a good performance of the communication system [56]. If the SNR value is assumed to be 10, a relationship between transmitted power and the antenna gain is written as Equation 14.9. Then maximal R is evaluated to be approximately $10^{5.8}$ bit per second. This value is slight lower than the maximal data-rate of the product required. However, since the constraint of the ground control station is less constrained than for the air vehicle, the performance of the entire communication system can be improved by selecting a different ground receiving antenna. An iteration of this process with a ground antenna of higher gain can be performed until R is larger than 1 Mbps. At the end of this iteration, an 8 dB antenna on ground proved to be adequate.

$$P_{TR} + G_{AR} - 10 \log \left(\frac{4\pi d}{\lambda} \right)^2 + 10 \log(R) - 174 = 10 \tag{14.9}$$

With the SNR values known, the channel capacity C in Equation 14.1 turns out to be more than 50 Mbps. This value is much higher than $10^{5.8}$ bps, then the amount of errors in the bits can be minimised according to Shannon-Hartley theorem.

14.4.0.1 Communication regulations and protocol

All aircraft must follow the basic safety and operational rules that outlined by locally airspace. During take-off, ascent, decent and landing, the UAV operator will have to adhere to instrument flight rules and be in contact with Air Traffic Control. The telemetry and nose camera give a pilot a view of the UAVs. Pilots on ground should be familiar with the operation and regulations. Since the UAV development keeps progressing and UAV traffic is becoming heavier, the regulations are regularly updated in conferences or by organisation. For instance, cross Atlantic cooperation and coordination for UAV regulation and control coalesced at an invitation only conference between Federal Aviation Administration, the European Aviation Safety Agency and Eurocontrol, at the annual UAV International Air Show.

Since the surveillance mission is carried out in South American region, the interoperation and recognition may be required. The authority and regulations for communication system would introduce a technical based regulation in the design process of this system. For example, standardization Agreement (STANAG) defines the a group of interface regulations on both military and scientific aspects between allied member countries of North Atlantic Treaty Organization (NATO). Thus, the information format is prescribed. For our communication system STANAG 4586, 4545, 4609, 7085 and 5500 are used.

In detail design of the electronic component, the operating frequency of the components are based on certain existing standards used. For example, the form of the transmitted data are regulated for the UAV communication system. During the UAV operation, a mission plan can be uploaded to the a UAV only after the data should be modified into a format through a suitable file transfer protocol.

Because of the 1 Mbps data rate and 80 km communication range requirements, only proprietary ISM protocol can meet the requirements. The frequencies of Proprietary ISM protocol is discussed in Section 14.1. They are good choice for low power consumption, low data rate and long range wireless network [73]. However, as discussed in Section 14.1, the higher data rate R can be transmitted by allowing higher the power consumption. As discussed in Section 14.1 and Section 14.4, the 900 MHz locates in ISM frequency channel and perform properly in this communication system.

Recent years, all of the spare capacity in the usable radio frequency spectrum from 9 kHz to 60 GHz has been depleted. New serves are now only accommodated either by the removal of existing allocations or by an acceptance of frequency sharing between two compatible services [74]. In the procedure, the following organizations are likely to be involved, European Telecommunications Standards Institute, International Telecommunication Union as well as European Conference of Postal and Telecommunication Administrations.

14.5 Flight cycle

In order to get a clear view of an operational cycle, the separate components of the flight cycle will be discussed in this subsection. First, the pre-flight operations will be discussed in Subsection 14.5.1 and the actual flight cycle can be found in Subsection 14.5.2.

14.5.1 Pre-flight operations

The following actions need to be taken before the UAV can start its mission:

1. Weather conditions: check if the weather conditions do not exceed sea state 4.
2. Ground control station: start up the system, connect the UAV.
3. Mission program: make sure the desired mission is programmed in the UAV.
4. Structural integrity: check if weekly inspection is done. Further information in Section 16.5.
5. Battery: should be fully charged.
6. Motor: fully functioning, communicating with autopilot.
7. Electronics: autopilot is booted, control surfaces are controllable. Camera is functioning electronically and structurally. Communication system is tested.

After the pre-flight checks are done, the UAV is ready for take-off. The UAV should be placed in the water, preferably with its nose in the wave direction. The total pre-flight checks shouldn't take more than 10 minutes. Optionally, the UAV can be controlled manually in heavy weather within a BLOS distance but take-off is usually done autonomously.

14.5.2 Flight operations

The flight phase of the UAV can be seen in Figure 14.9. Take-off is discussed in more detail in Section 13.2, landing in Section 13.3 Cruise characteristics are listed in Table 14.4

Table 14.4: UAV cruise characteristics

Property	**Value**	**Unit**
Cruise velocity	22	m/s
Stall velocity	13.7	m/s
Daytime range	140.2	km
Night-time range	72.2	km
Altitude	2000	m

The UAVs mission will end when its program is finished and returns to base or when the operator aborts the mission from the ground control station. Also, when the UAV gets damaged while operating, it will return to base.

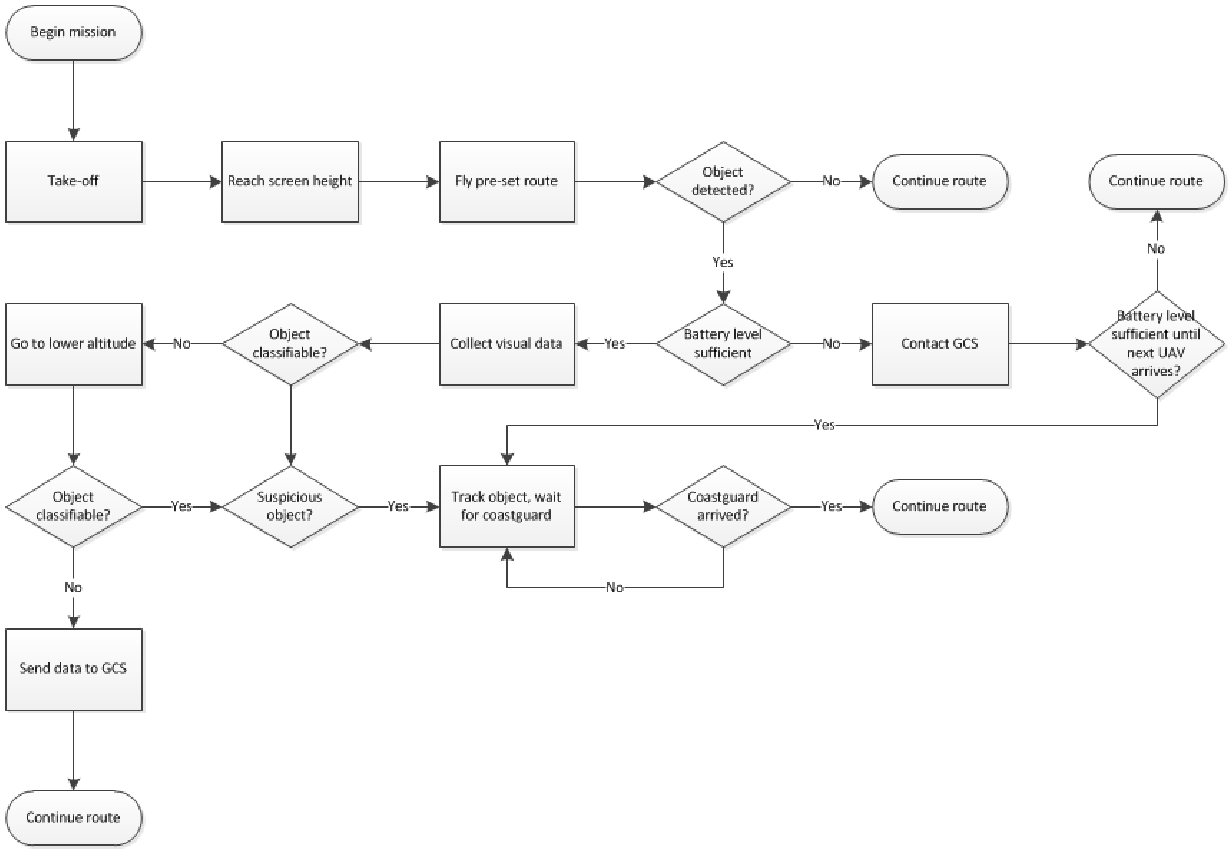

Figure 14.9: Flow chart of a UAV flight cycle

14.6 Conclusion

The solar powered amphibious UAV can be operated autonomously and controlled by the pilot on ground. During the autonomous fight, the position of the UAV is acquired by GPS and its attitude is measured by the embedded inertial measurement unit. The Lisa/M board can compute these input measurements and direct the control surface to make proper response. The imaging system can transmit an image of 752×582 pixel back via a 900 MHz radio modem and 6 dB gain antenna from at most 80 km away. The captured picture illustrates an surveillance area of 1.6 km^2. While the ground control system consisting of a portable work station, 900 MHz radio modem and a feasible antenna is capable to uplink new mission plan and thus conduct the UAV's behaver.

The autonomous flight is realized by pre-programming Lisa/M autopilot board. A general logic of autonomous flight is shown in flight cycle diagram 14.9.By implementing the control and operation system, the typical flight cycle in Section 14.9 is completable with a well designed UAV.

Chapter 15

Propulsion and power

The design of this UAV requires a full-electric drive, as stated in Chapter 1. In order to meet this requirement, electric motors are chosen to drive the propeller. Solar cells are integrated in the UAV to collect solar energy. This energy is stored electrochemically in batteries to enable operation without solar input.

This Chapter is dedicated to elaborate the propulsion and power systems of the UAV. The propeller and motor selection procedure is described in Section 15.1. Section 15.2 describes the design and selection procedure of the motor controller. The battery sizing and selection is elaborated in Section 15.3. The Chapter continues with the solar panel design in Section 15.4 and the electrical power conversion described in Section 15.5 elaborates on this. As a major outcome of this Chapter, the electrical block diagram is provided in Section 15.6.

15.1 Motor and propeller selection

The motor and propeller sizing is about the generation of propulsive power from the provided electrical power in the most efficient way, for the complete flight envelope. It is impossible to design one propeller motor combination to be optimally efficient in all of the flight conditions. But since the cruise phase of the flight is the most important, the propeller motor combination is optimised for this condition and the performance in the other phases is then assessed to make sure that the motors provide enough power during all of them.

The initial analysis of the propeller motor combination is done with help of the open source program called JavaProp [75]. When this program is provided with values for the amount of revolutions per minute (rpm) (obtained from motor data), the propeller diameter, the flight velocity and and the shaft power provided by the motor or the thrust force required, it will generate a propeller with the most efficient shape for the considered condition. The propeller diameter can then be iterated to obtain the most efficient propeller for that condition.

When the propeller is chosen, the program provides data on the propeller shape, the efficiency of the propeller and the velocity in the wake of the propeller. The propeller shape is implemented in the CATIA drawings, the efficiency and velocity data is used together with motor data in MATLAB to generate available power, thrust and climb performance values.

15.1.1 Motor selection

As stated previously, motor data is required for the determination of the propeller efficiency. But because the power available of the aircraft is both a function of motor and propeller capabilities, the motor selection requires an iteration with a check if it can provided the required power during take off while not being too over powered for the cruise phase. This is because electric motors tend to be inefficient at low input powers.

There are a lot of electric motor manufacturers which provide motors capable of delivering the power required for the UAV like, the Scorpion Power System [76], the Hyperion [77] and the Plettenberg [78]. Since all of these companies are able to deliver the right motors with comparable performance, the choice of manufacturer was made based on the amount of motor data available, which is beneficial for producing extensive power and thrust data using MATLAB. With reasoning the Plettenberg motors are considered for this aircraft. Plettenburg was the only company that published power and efficiency data for its motors at different voltage, power and rpm values.

The motor finally selected is the Plettenberg Orbit 15/14, with a maximum Shaft power of 739.5 W and a weight of 170 g each, two of these motors will be installed in the way stated in Chapter 9. Since the motor and propeller selection is very interrelated, this is the level of detail this subsection is concluded with. The next section about propeller sizing will elaborate on why this motor is the right one for this design.

15.1.2 Propeller selection

The propeller selection starts with an performance analysis of the front motor propeller running only as will be the case during cruise. This is done by first providing JavaProp with the original cruise condition data, a cruise drag of 3.9 N, which was an initial estimate based on the drag polar of the aircraft at the selected cruise speed of 22 m/s. This drag value is used for the propeller design. After including rotational speed data which is obtained from the Plettenberg motor data sheet, and the propeller diameter which is by iteration optimized for highest efficiency, JavaProp is able to generate the most efficient propeller for this configuration. JavaProp then provides efficiency and wake velocity data on the front propeller. With this efficiency data and maximum motor shaft power, the maximum power produced by the front propeller at other flight speeds by can be assessed using MATLAB. The maximum power produced by the second motor can be obtained with use of the flow wake speeds induced by the front motor the front motor generated, JavaProp provides this. When the total available thrust is enough for take off and the cruise efficiency is as optimal as possible for a certain motor, this motor propeller combination is selected for the aircraft.

The complete iteration in motor selection will not be shown here, but the way the motor and propeller selection is performed will be explained according to the chosen Plettenberg Orbit 15/14 motor.

The Plettenberg data sheet for the Orbit 15/14 motor [79] provides the rotational velocity data required for the propeller design with JavaProp, but the required shaft power in cruise needs to be available in order to determine the rotational velocity. Since the required shaft power is an output of the JavaProp program, as can be seen in the lower table in figure 15.1, an iteration is used in order to find the right shaft power required and the corresponding rotational velocity. The shaft power required for cruise turned out to be 148.88 W. According to the motor data sheet, the Plettenberg motor will have a rotational velocity of 17620 rpm when producing this shaft power, which is implemented in the input table in the same picture. After optimizing the propeller diameter for maximum efficiency, the input data used in JavaProp can be seen in figure 15.1. Hence the optimal propeller diameter is through iteration determined to be 0.179 m. The data output table in the bottom half of the figure also shows the pitch angle and the efficiency of the propeller which is used on the front motor. This propeller diameter seems to be plausible when considering the Scaneagle [8], the propeller diameter of this aircraft could not be found directly but is according to images estimated to be around 22.5 cm. Since this UAV would use 2 rotors with a diameter of 17.9 cm, this propeller design seems to be in the range of expected values.

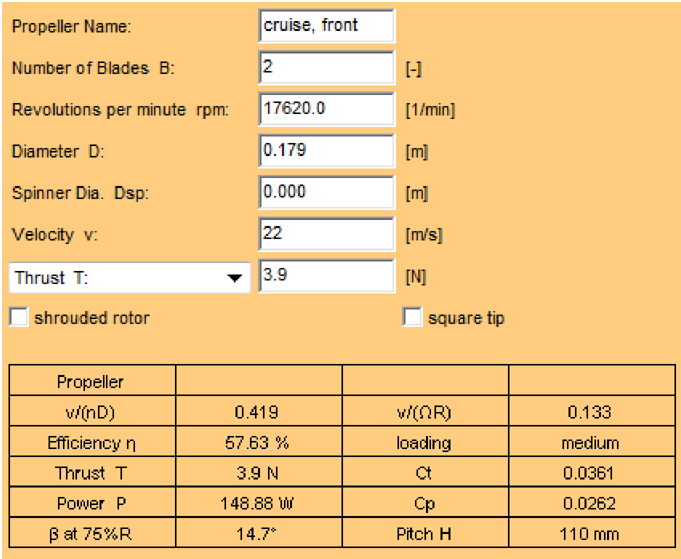

Figure 15.1: JavaProp input data for cruise condition

A note should be made to the amount of propeller blades. A rule in propeller blade design is the higher the number of propeller blades the higher the possible power absorption by the propeller but the lower the efficiency [80]. Since the power needed by this aircraft is relatively low compared to larger aircraft which use more than two propeller blades, it is concluded that using more than two propeller blades is not needed and that a maximum efficiency with respect to the amount of propeller blades is desirable.

The optimal propeller efficiency in cruise turns out to be57.6 %, this might seem to be a low value. This is due to the relatively low airspeed of the aircraft, since the propeller efficiency drops with speed [81]. Using this reference the propeller efficiency calculated seems reasonable.

The back motor will be equipped with the same rotor as the front motor since the design velocity is that the back motor can also perform on its own in cruise with a reasonable efficiency in case of a front motor or propeller break down. But it would be a loss of potential to not optimize this propeller a little for the normal conditions, in which the second motor is used to increase maximum power available. Since the airflow speed is higher due to the air acceleration of the front motor this optimization can be done by altering the pitch angle without changing the dimensions of the propeller too much. An pitch angle increase of five degrees would give the highest efficiency, but this would lower the efficiency during take-off too much since optimisation for higher speeds leads to adverse effect at the lower speeds. Therefore finally and increase in pitch angle two degrees is chosen, this makes the pitch angle at three quarters radius 16.7 degrees.

The efficiency data provided by JavaProp is given as a function of advance ratio. The advance ratio can be calculated using equation 15.1, in which V is airflow speed in [m/s], n is the amount of revolutions per second and d is the propeller diameter in [m].

$$J = \frac{V}{nd} \tag{15.1}$$

The change in local flow speed due to the front motor at maximum power is determined with JavaProp at several flight speeds and used as an input in MATLAB. With this data and the efficiency data on the two motors given as a function of advance ratio the total power available can be calculated as a function of speed, this is given in figure 15.2.

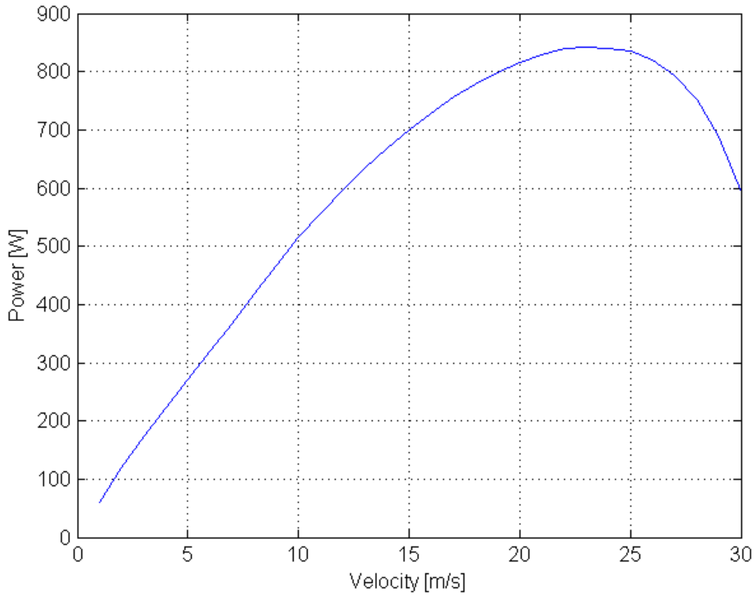

Figure 15.2: Total motor power available as function of speed

The power available during take-off should be assessed in order to be sure the aircraft is able to take off. The original design philosophy was redundancy, hence one motor was able to get the aircraft to take off. But after the motor was chosen based on this condition a more detailed water drag analysis showed that the drag turned out to be way higher than expected. Therefore the current design needs the two motors both running in order to take off. Figure 15.3 shows the total power available and the power required at take off with two motors, hence with two motors the power required in take-off is met.

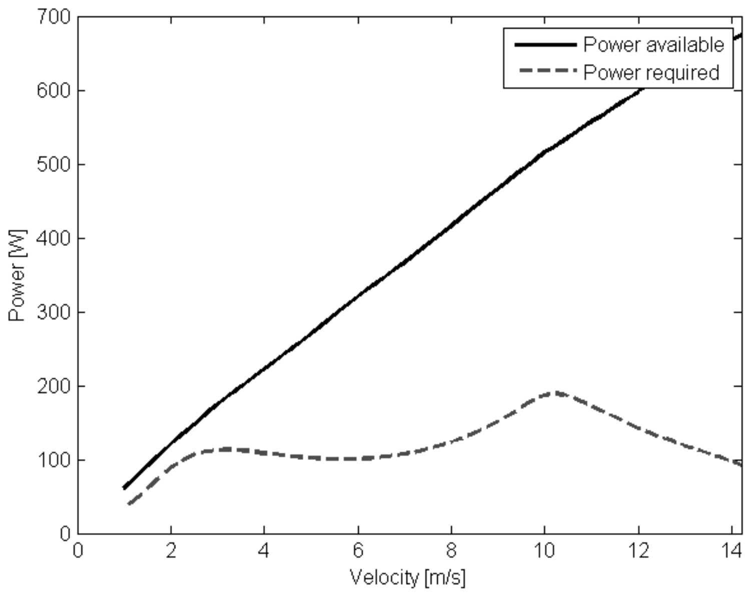

Figure 15.3: Power available and Power required in take off (both motors)

With the data on total power available the maximum rate of climb can be assessed. The requirement for the rate of climb was 10 m/s but this requirement would affect the motor size by such an extent that the motor efficiency in cruise would decrease drastically. This is due to low efficiency of high power motors at low power output, as mentioned before. Therefore this requirement was in consultation with the client set to be a non driving requirement. Thus, the motor is sized at the power required for take off and the maximum achievable climb rate is calculated with help of the data on the motors.

The rate of climb can be calculated with equation 15.2 [82], in which P is the power in W, RoC is the rate of climb in m/s and W is the aircraft weight in N. This plot ends at V is 31 m/s since the front propeller will have no efficiency left at this speed, the influence of the front rotor at the back rotor at speeds higher than 31 m/s should be assessed in wind tunnels to determine the maximum speed more exactly. But since the drag due to the front motor is expected to increase quickly, the maximum speed estimate of 31 m/s seems to be very reasonable.

$$RoC = \frac{P_{available} - P_{required}}{W} \tag{15.2}$$

The power available is plotted with respect to the power required in figure 15.4.

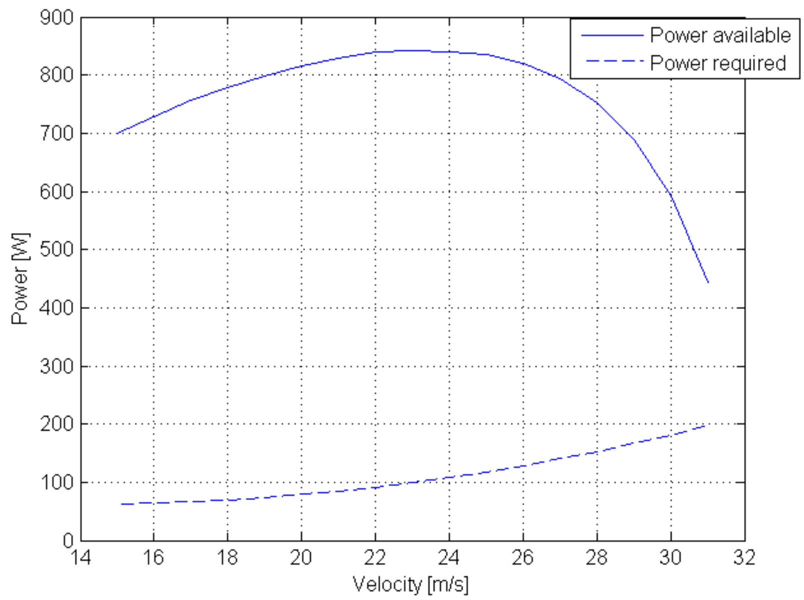

Figure 15.4: Power available and Power required as a function of speed

The maximum difference between the curves defines the flight speed at which the highest rate of climb can be achieved. This point is at 22 m/s, the cruise speed. This is not a coincidence since the cruise speed is at the speed where the drag is minimum. With a power available of 839.75 W, a power required of 93.62 W at sea level and an aircraft weight of 100 N the maximum rate of climb equals 7.46 m/s.

15.2 Motor controller

The motors considered need motor controllers in order to be able to run the motors at their desired power. Such a motor controller is called an Electrical Speed Controller (ESC). A brushless ESC can be equipped with a Battery Eliminator Circuit (BEC) which powers all the other systems in the aircraft. The usefulness of a BEC is in the power management side of the aircraft. When the battery is about to run out of power the BEC shuts down the engines and makes sure that all the other systems of the aircraft are still able to function, hence the aircraft is able to safely glide towards the ground.

Due to the benefits of a BEC, an ESC with a BEC is selected for this aircraft. Since the motor data shows that the motors will maximally drain 55 A of current [79], a 60 A ESC should be able to power these motors in all conditions. However, ESCs of this kind are generally maximally able to provided 15 W through their BEC. This value is too low to power the other aircraft systems. ESCs which are capable of handling 80 A typically have a 30 W BEC which is able to provide enough power to the other aircraft systems. Therefore, two of such ESC's will be installed in the UAV, one for each motor. An ESC which can provide the powers and currents stated above, that is also low weight is the Cobra 80 A ESC with a 33 W BEC. This ESC only weighs 0.0601 kg [83].

15.3 Battery sizing and selection

The battery is the energy provider of the complete aircraft. It is charged by the maximum power point tracker and provides its power to the ESC. In order to size the battery the required electric power should be assessed.

The power needed for flight can be split up in 2 sections. The power needed to climb to altitude and the power needed for cruise. Section 15.1.2 gives the data on power available. In order to climb in the most efficient way to the cruise altitude of 2000 m, this climb should be executed as quick as possible , with the most efficient power conversion. This condition is met in the point where the rate of climb is maximum. The difference between the power available and the power required is maximum in this point, meaning that the usage of power is as optimal as possible. With the rate of climb already obtained, the time to climb to altitude is as described in equation 15.3, in which t_{climb} is the time to climb and H is the cruise altitude.

$$t_{climb} = \frac{H}{RoC} \tag{15.3}$$

The time to climb is 0.076 hour. Knowing this time and that the maximum motor input power is 878.9 W for each motor as obtained from motor data [79], according to equation 15.4, the energy needed to climb is 133.2 Wh.

$$E = Pt \tag{15.4}$$

The cruise energy required is dependent on the propeller efficiency in cruise and the power required at cruise level 62.4 W. This number was based on a cruise drag of 2.8 N and a cruise speed of 22 m/s, this was an initial updat of the earlier considered drag of 3.9 N but in the most final stage of the project it was found that the actual drag is 5 N. Since there was no time left to update the calculations, a reconsideration of the battery capacity calculation is left as a recommendation. The calculation stated here is done with the drag of 2.8 N.

The electrical power required can be calculated with the total efficiency in this condition. A plot of the efficiency versus power required is given in figure 15.5, as can be seen the total motor and propeller efficiency at cruise power is 37 %, the cruise electrical power required is therefore 167.6 W. Since the total power has to be provided for one hour to meet the requirement, the energy required to cruise is 167.6 Wh.

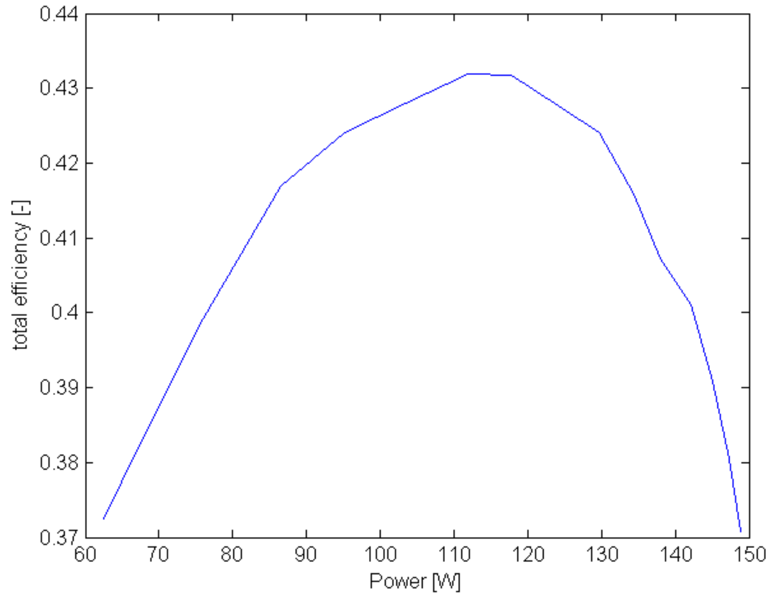

Figure 15.5: Total efficiency as a function of Power required

With these values the total electrical energy required by the propulsion system for one flight cycle considering flight at batteries only is 295.9 Wh, but the energy required by the other systems should be included in this value. The power required by the other systems is 40.6 W which should run during climb and cruise so for 1.0742 hours. Therefore the electrical energy needed by the other systems is 43.7 Wh, the total required electrical energy is then 344.4 Wh.

The only efficiencies not included right know are the electronic speed control efficiency and battery efficiency. The battery efficiency of lithium polymer batteries at 40 degrees Celsius is 96% [84] and the electronic speed control efficiency is 95% [85]. Including these efficiencies would give an required battery capacity of 376.0 Wh. Since the contingency for endurance is set at 10 % and it would be good to put a contingency at the energy required by all the systems, 10% contingency is applied on the the total energy required. This makes the total energy required increase to 413.6 Wh.

With the battery capacity required determined, the actual battery selection can take place. Earlier in this design process, Thunder Power with its G6 pro lite battery series was selected as the battery to be used, because of the high specific energy of the batteries of 163.2 Wh/kg [86]. Since the motor can achieve its maximum power at a Voltage level which is normal for 18.5 V lithium polymer batteries, lithium polymer batteries with 18.5 V output voltage are selected. This means that three batteries rated at 7.8 Ah, 18.5 V and a total weight of 2.652 kg are used to provide 432.9 Wh of energy.

15.4 Solar panel design

The batteries that drive the electric motors are recharged with solar panels. This Section clarifies the design procedure of the solar panels. As the design exercise describes a mission for the island of Curaçao, the first thing to do is to investigate the available solar energy for this geographic location.

15.4.1 Available solar energy

The Earth receives around 1367 W/m^2 of solar power outside the Earth's atmosphere [87]. This received solar power per unit area is often referred to as irradiance. The solar power that is received on different geographical locations differs from this number, because of several effects such as the albedo effect. Not all incoming solar radiation reaches the Earth's surface, but a certain percentage reflects back into space directly from the edge of the Earth's atmosphere or from the Earth's surface.

Depending on the exact location, the path that solar radiation travels also decreases solar power significantly. A geographic location is described with two coordinates, namely longitude and latitude. Latitude influences the solar power variation over the year, while longitude does not [87].

Not only the location influences the received solar power, but it also depends on the time of the year. Since the Earth's rotational axis is not perpendicular to its orbital plane around the Sun, the distance that solar radiation travels to reach a certain location varies throughout the year. The angle δ between the equatorial plane and the orbital plane is 23.45° on June 21$^{\text{th}}$ and −23.45° on December 21$^{\text{th}}$. For the Northern hemisphere, these dates are known as the summer solstice and the winter solstice, respectively. The spring equinox (20$^{\text{th}}$/21$^{\text{th}}$) March and the autumn equinox (22$^{\text{nd}}$/23$^{\text{rd}}$) September are the dates on which the declination angle δ is zero and the Sun is directly above the equator. On the summer solstice, the Sun is above the Tropic of Cancer and for the winter solstice, it is above the Tropic of Capricorn [88].

Since Curaçao is situated between the Tropic of Cancer and the Tropic of Capricorn, the intensity of the received solar radiation varies from solstice to equinox. For geographic locations above the Tropic of Cancer, i.e. the Netherlands, the solar intensity just has a peak during summer, unlike Curaçao that has peaks in spring and autumn [88].

Equation 15.5 shows the relation of the angle of incidence θ_i, the declination angle δ and the latitude ϕ [87]. Other parameters that influence the angle of incidence are the solar panel slope β, the surface azimuth angle γ and the argument of perigee ω.

$$\begin{aligned}\cos\theta_i = &((\cos\phi\cos\beta + \sin\phi\sin\beta\cos\gamma)\cos\delta\cos\omega \\ &+ \cos\delta\sin\omega\sin\beta\sin\gamma \\ &+ \sin\delta\,(\sin\phi\cos\beta - \cos\phi\sin\beta\cos\gamma))\end{aligned} \tag{15.5}$$

The declination angle δ can be represented by Equation 15.6, where n represents the day of the year.

$$\delta = 23.45\sin\left((284+n)\left(\frac{360}{365}\right)\right) \tag{15.6}$$

The slope β is the angle between the horizon and a line normal to the solar panel. If the panel is oriented parallel to the horizon, $\beta = 0°$. The surface azimuth angle γ describes the panel's orientation with respect to the geographical North and South, i.e. a panel facing South has a γ equal to zero and a panel facing North has a γ of 180°.

The argument of perigee ω describes the location of the Sun with respect to the sky. At solar noon, the Sun has the highest elevation and $\omega = 0°$. Throughout the day, it increases by 360°, starting at −180° at midnight, i.e. an increase of 15° per hour.

For level flight, $\beta = 0$ of zero degrees is assumed, $\cos\beta = 1$ and $\sin\beta = 0$. Using MATLAB®, irradiance data is generated and evaluated for Curaçao. Figure 15.6 shows how the maximum irradiance varies per month. This plot does not take cloud coverage into account, but merely shows the fluctuation in irradiance.

The acquired data is used to size the solar panels.

15.4.2 Solar panel sizing

The first step in the solar panel sizing is to perform a PV cell selection. For terrestrial applications, generally crystalline (generation I) silicon PV cells are used [88]. Other available technologies are thin-film cells (generation II) and multiple junction cells (generation III). Figure 15.7 shows the average price per Watt-peak for these three generations of PV cells.

Initially, monocrystalline silicon solar cells were selected. These cells are relatively low-cost and have efficiencies up to 20%, as can be seen in Figure 15.7. As mentioned before, these type of cells are mainly used for terrestrial/domestic applications. Sizes of such cells typically range between 10 and 17 cm [89]. Since this design has wings with a chord length below 15 cm, these cells prove to be unfitting for this UAV.

As an alternative, space grade solar cells have been investigated. Generally, these cells have smaller dimension, because they are applied on numerous spacecraft with different dimensions. The investigated PV cell technology is the S 32 Silicon Solar Space Cell by AZUR SPACE Solar Power. This particular

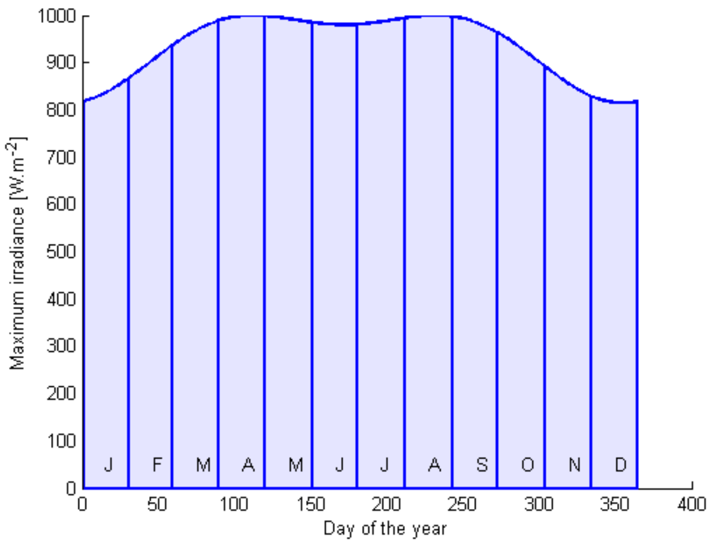

Figure 15.6: Maximum irradiance for Curaçao

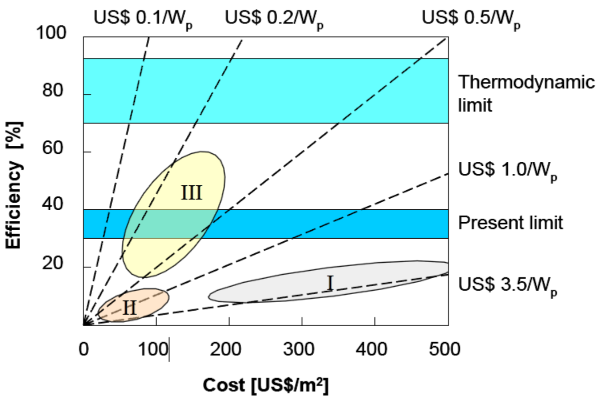

Figure 15.7: Cost per area vs. panel efficiency for three generations of solar cells [89]

type of PV cell is made from crystalline silicon, but it is slightly flexible in contrary to commonly used monocrystalline PV cells. Cell dimensions are 74.0x31.9 mm ±0.1 mm, with a thickness of 130 ± 30 µm [90]. The cells are rated at an efficiency of 16.9% and have mass of 32 mg/cm^2. Furthermore, the cells have a open circuit voltage of 628 mV and a short circuit current of 45.8 mA/cm^2. Under ideal conditions, this PV cell produces a current of 43.4 mA/cm^2 with a voltage of 528 mV. This cell is found to fulfill our requirements and therefore is incorporated into the design.

The short circuit current and the open circuit voltage are two parameters that determine the IV-curve of a PV cell. The IV-curve shows the relation of output voltage and current of a PV cell and depends on ambient temperature, irradiance and circuit loads.

The second step to size the solar panels is to calculate the total amount of cells that can physically be placed on the UAV. The restricting parameters are the wing planform and the fuselage dimensions. For the initial power budget calculations, the dimensions of the cells was not taken into account. The final panel sizing procedure does include these dimensions, which results in a certain cell configuration. The PV cell layout is optimised in MATLAB, whilst the control surfaces are kept free. The spacing between the cells is set to 1 mm, in order to optimise the cell placement, whilst the placing accuracy remains realistic. The cells have a minimum distance to the trailing edge of 4% and 6% of the chord lengths, for the front and aft wing respectively, since the cells have to be sunk into the wing structure. The layout of the cells on the wings and fuselage is depicted in Figure 15.8. Calculations in Chapter 16 verify that the cell spacing is sufficient.

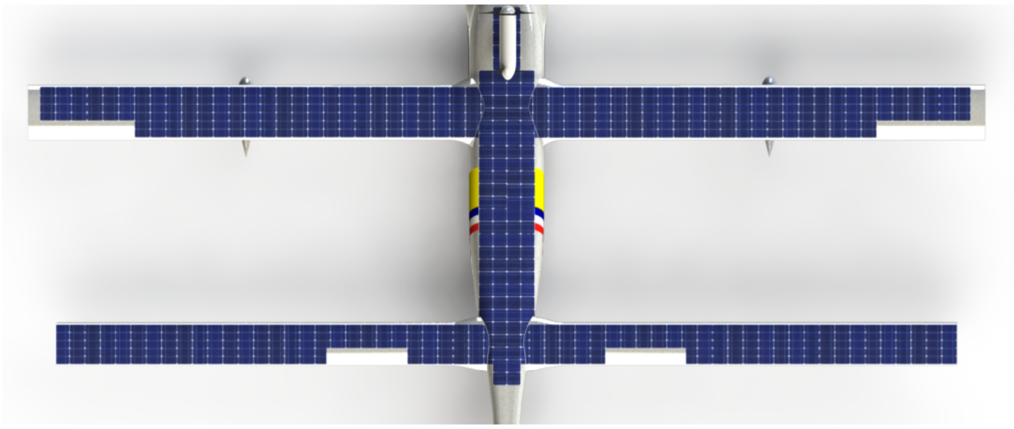

Figure 15.8: PV cell layout on the wings and fuselage

With the wing span and chord length as restricting factors, the total amount of PV cells that can be placed on the wings is found to be 182. In order to increase the amount of PV cells, the upper surface of the fuselage is covered with an additional 70 cells. This brings the total amount of PV cells to 252. The total area of the PV module is 0.64 m^2. The mass of the PV module is 0.2 kg. Wiring mass is estimated to be 3% of the total mass of the UAV, i.e. 0.3 kg.

The PV cells are connected as follows: 7 series containing 36 cells each. With this, each series produces up to 19.0 V and the total current is 7.17 A. Thus, the output power of the PV module is 136.3 W in optimal conditions.

With this output power, it is possible to calculate the battery charge time. Figure 15.9 shows the relation between battery charge time and the time of the year. Note that the battery charge time is directly influenced by the irradiation, as can be seen from the shape of the curve.

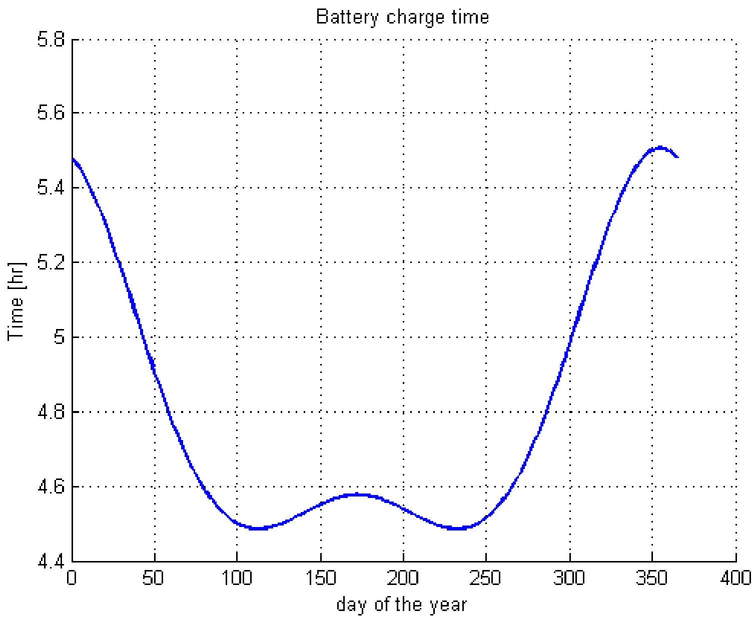

Figure 15.9: Battery charge time per day

15.4.3 Effect of water on solar panel performance

Operating under maritime conditions exposes the solar panels to water. The influence of water on the performance of solar panels is briefly investigated. It is found that the performance of crystalline panels increases by 15%, when solar panels are submerged at a water depth of 4 cm [91]. The main reason for the performance increase is the fact that solar radiation reflects less from the surface of the panels and the fact that the solar panels are cooled. The output voltage of solar panels decreases as the operating temperature increases [88]. For this reason, the performance of the solar panels is expected to remain constant, or even increase, by the presence of water on the panels.

15.5 Electrical power conversion

With the determined solar input power, the rest of the circuit can be designed. The batteries require an input voltage of 18.5 V. In order to charge a battery, the charging voltage should be higher than the battery output voltage [92]. If this is not the case, the battery acts as a power source instead of a load. Fluctuations in the charging voltage can be harmful to the battery life and should be avoided. As explained earlier, the output power of solar panels varies for different electrical loads, ambient temperatures and irradiance. To avoid these fluctuations, a maximum power point tracker (MPPT) should be incorporated in the design [88].

A MPPT is a device that tracks the maximum power point on the IV-curve of the solar panel. In general, the commercially available MPPTs are used for household applications. For this reason, they are often large in volume and have a significantly high mass [85]. For the design of an aerial vehicle, it is beneficial to use a lightweight, low-volume MPPT. Often, these type of MPPTs are custom-made for specific purposes. A company that provides COTS lightweight MPPTs is SolarMPPT, situated in Australia. This company is a spin-off of a World Solar Challenge race team, that required a lightweight MPPT. The Automax Solar MPPT is one considered option for this design [93]. Although the exact dimensions of the Automax are not specified by the manufacturer, it can be estimated from Figure 15.10 that it weighs below 50 g.

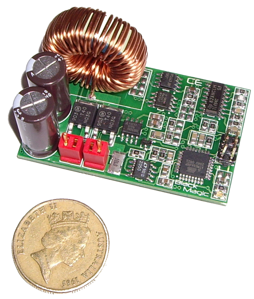

Figure 15.10: The Automax MPPT [93]

Another considered option is the Genasun GV-10 [94]. This company offers modified MPPTs with a mass of 185 g and a volume of 0.28 litres. The GV-10 is significantly heavier than the Automax, but is specified as marine-grade by the manufacturer, who also offer 5 years of warranty. For this reason, the GV-10 is incorporated in this design.

15.6 Electrical Block Diagram

The power for all the sub systems in the UAV is supplied by the batteries, which are charged by solar panels. The power flow in the complete UAV is illustrated in an electrical block diagram, which can be found in Figure 15.12.

This figure shows that the solar cells generate the electrical power, this power is maximised by the maximum power point tracker and this power charges the batteries. The batteries power the motor controllers, which are equipped with a battery eliminator circuit. The battery eliminator circuit of motor controller number two powers the Lisa/M at 5 volt, the battery eliminator circuit of motor controller number one powers the camera control board at 5 volt, and the 2 battery eliminator circuits together power the camera at 10 volt. The Lisa/M board finally powers the servos, sensors and receivers/transceiver.

The manner in which the motor controller powers the Lisa/M, camera control board and the camera at their respective voltage levels is shown in Figure 15.11. Diodes are used to regulate the current flow direction and the voltage is regulated by connecting the boards parallel to one motor controller and by connecting the camera to the two motor controllers in series.

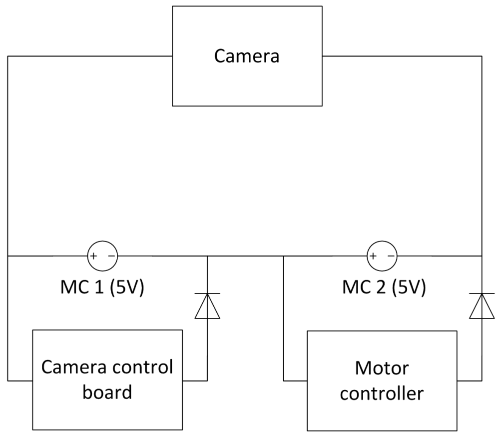

Figure 15.11: Voltage regulations on different systems

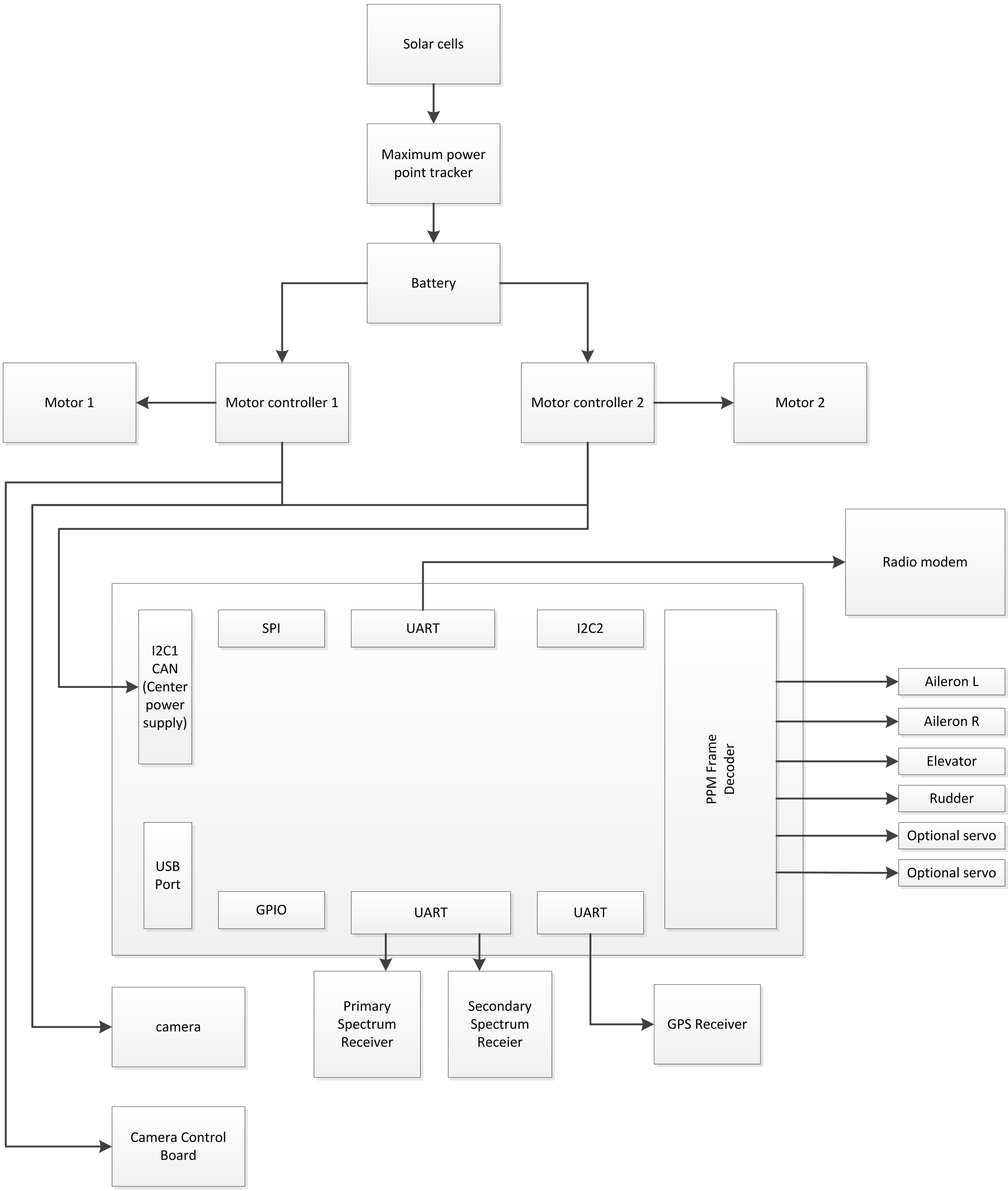

Figure 15.12: Electrical block diagram

15.7 Conclusion

In conclusion, it can be said that the research and investigations on propulsion and power have resulted in the power train of the UAV system. Starting from the motor and propeller design, the required motors were selected and adequate propellers were designed. For the design of these components, performance requirements are driving. The performance analysis results in thrust requirements for take-off and cruise flight. The design choice is made to incorporate two motors, of the type Plettenberg Orbit 15/14, whilst each single motor can perform full flight. This is done for redundancy reasons. However, due to final design iterations, the take-off drag cannot be overcome by a single motor and drag in cruise increased. As there is a significant difference in the final required thrust, i.e. 40 N for take-off and 5 N for cruise flight, the motors in the current configuration are overpowered for cruise conditions and the rotor efficiency is not as optimal as possible in cruise any more due to the cruise drag increase. Using a powerful motor for low power flight reduces the efficiency significantly, due to inertial and electrical losses. Since the redundancy requirement cannot be fulfilled any more, a different motor configuration is recommended with a low power motor for cruise and a high power motor for take-off and climb. In which the rotors should be reconsidered to increase the efficiency as much as possible considering other motors and the final drag values in cruise and take off.

Power collection is performed by PV cells. Due to the slender shape of the wings, the selected cells have to have small dimensions. The selected type of cell is the S32 solar cell of AZUR SPACE. Rated at 16.9% efficiency, these cells lower the overall efficiency of the power train significantly.

The battery selection is performed in this section. And it is determined that three ThunderPower lithium polymer batteries are to be installed with a total capacity of 432.9 Wh. Considering the final drag values and the proposed configuration changes, the battery selection should have a recalculation, which will then result in a fully optimized power system.

In order to control the motors an ESC is required for every motor, the Cobra 80A ESC with a 6 A, 5 V BEC is selected. This was mainly based on control and sensor power requirements. In order to optimise the solar power output, two MPPT's are used of the type GENASUN GV-10.

The overall power train containing all the efficiencies of the power systems is shown in Figure 15.13. Note that the largest efficiency loss comes from the solar panels. The design choice to apply crystalline silicon cells was made to reduce the cost of the PV modules. Applying triple junction Gallium Arsenide cells would have resulted in efficiencies of ±30%, but would increase the cost significantly, as can be seen in Figure 15.7. Furthermore, the power train loses overall efficiency at the motors and propellers, as they are overpowered for cruise flight.

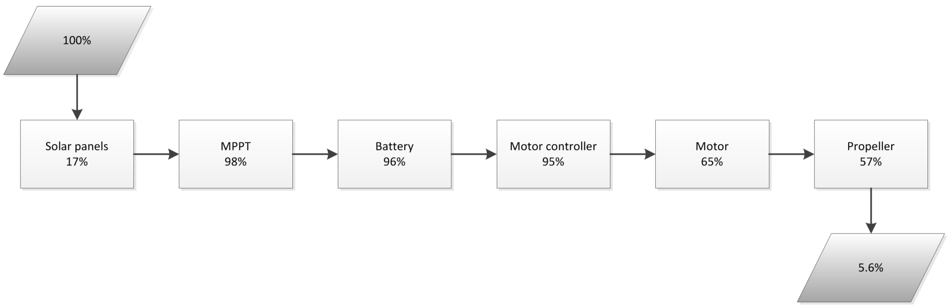

Figure 15.13: UAV power train efficiencies

Chapter 16

Structures, materials and maintenance

This section will elaborate on the structural, material and maintenance decisions in the UAV design. In designing the UAV, one should always be aware of the inherent correlation between structure, material selection and manufacturing.

This section starts off by describing design load cases in Subsection 16.1. Subsection 16.2 briefly explains the methods and tools used in the analysis needed to end up with a feasible design. In subsequent subsections the subjects of structures, materials and maintenance are treated successively. The resulting lay-up map of the UAV is depicted in Figure 16.1. Production of the UAV is treated in Section 17.5. Chapter 17.6 lists materials used respective structures.

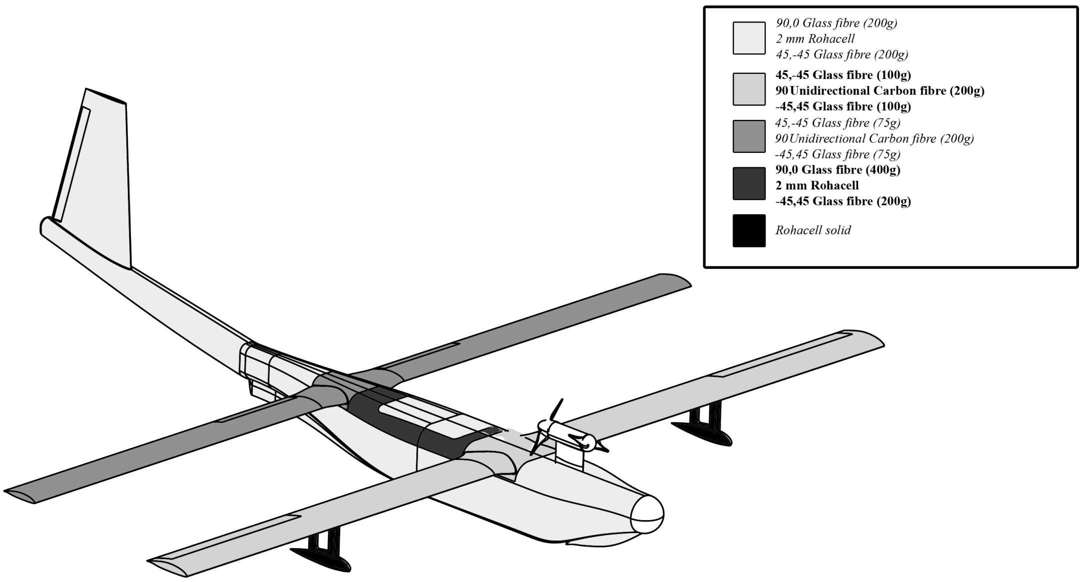

Figure 16.1: A map of the composite lay-ups used in the UAV.

16.1 Load cases

In this section, the characteristic extreme load cases during the surveillance mission are determined. The load cases considered are cruise, maximum wing loading and approach failure, vibration loads are separately discussed. The extreme cases of maximum wing loading and both approach failure cases are used as structural design criteria. A safety factor of 1.3 is applied to external loads, with the exception of impact loads; they are scaled with a safety factor of 1.5.

Cruise: Cruising flight is the simplest equilibrium flight mode for any aircraft. In this load case the total lift equals the weight of the plane and the thrust equals the drag. The load factor on the wings is 1, in this case the wing loading is 160 N/m^2.

Maximum wing loading: Maximum wing loading occurs at the highest load factor in the flight envelope. A maximum load factor of 2.5 is established from aerodynamics. For this loading case, the loading on the vertical tail plane is also assumed to be at maximum. Maximum vertical tail plane loading is 30N total when the UAV is sideslipping 15° at V_{max}.

Approach failure - body impact: In a successful landing, the UAV lands on the step of the fuselage (see Chapter 13). At the instant of touchdown this introduces a landing impact force acting at the step. In a worst case scenario this impact occurs at approach speed, which constitutes a vertical speed of 0.64m/s. In this case wing loading is assumed at $n = 1.5$, vertical tail is at maximum load. Fuselage impact force follows from maritime Chapters (Section 13.3) to be 320N.

Approach failure - floater impact: During approach, the glide path should ideally be oriented with the translational direction of the waves, such that a landing may be performed on a relatively stable stretch of water. However, if proper orientation of the glide path should fail, or in other semi-rare failure cases, a floater may collide with a wave before a flare manoeuvre is even initiated. Loading in this case is the same as the body impact case, except that there is not a body impact load of 320N, but a floater impact of 14.0N and a floater drag of 16.7N due to floater submersion (see Section 13.3).

Vibrations and aero-elastic effects: Vibration analysis is, regrettably, beyond the scope of the current state of the design process. Vibrations are mainly introduced by airflow over the wings and motor action. Aero-elastic stability will also need to be investigated in further analysis; particularly since the slender wing design of the amphibious UAV may be very sensitive to these effects. If divergent excitation should occur, this can usually be fixed by (locally) increasing structure stiffness[95]. One analysis that can quickly be performed is the aero-elastic case of two-dimensional wing torsional divergence. The currently used airfoil is found to be torsionally stable for all speeds, since the flexural centre is found to be forward of the aerodynamic centre [95]. The flexural centre is found using the MATLAB structural model.

16.2 Structural analysis methodology

This section describes the methodology used in structural analysis of the UAV design. This covers methods and tools used in sizing and weight estimation, stress- and deflection analysis.

Design methodology of the wing is driven by aerodynamic and hydrodynamic requirements, as described in Chapters 12 and 13 respectively. Structure design and material selection is then based on the loads from these analyses, described in the foregoing section. Wing sizing and stress analysis is first performed via a home cooked 3D numerical model in MATLAB. Implementation, as well as limitations of this model are discussed in 16.2.2. Due to these limitations, this numerical model usually produces relatively rough estimates. So when the MATLAB model produces feasible results, a 3D model is analysed in Abaqus is used to produce a more accurate evaluation. For analysis of more complex parts, like the hull, deflection and stress are only analysed in Abaqus. In this way, analyses in Abaqus also serve as a means to verify results obtained with the home cooked code.

The next sections, 16.2.1 and 16.2.2, explain used Abaqus and MATLAB models respectively.

16.2.1 Abaqus analysis

Due to the complexity of the shapes in the design, together with the use of composites, it is decided that FEA(Finite Element Analysis) methods are the best solution to evaluate the structure. For the FEA itself it was chosen to use Abaqus, the compatibility with CATIA was the main reason to do this.

The structure of the wing and the hull are analyzed using this method. These parts are made from composites and have complex shapes.

Wing: The wing is evaluated for the different load cases, the main load is during manoeuvres with a load factor of 2.5. Wing structure weight is also taken into account. The mounting surfaces are the boundary conditions, which are encastre. The load is introduced at the top surfaces of the wing. The model is constrained by tying the surfaces of the foam and shell of the lay-up. The lay-up consists of 6 layers, with a thickness of 0.1 mm, which coincides with a 200 g plain weave[96]. The directions are based on the coordinate system with respect to the lay-up, this implies that the main direction is the longitudinal direction. The layers are in the directions 45, −45, 90, 90, −45, 45 degrees with respect to the main direction, respectively.

With the results of the FEA, an iterative process begins. The two main considerations of the results are the deformation of the structure and the stress in the material. According to these results layers can be removed or added at certain areas to increase the strength of the structure. To increase the stiffness of the structure a foam core is added to increase the moment of inertia.

Hull: The Hull is analysed for the different load cases. The important parts are the wedge for impact, the tail boom and the connection to the wing. To analyse the different parts several boundary conditions are applied. In the case of the wedge impact, the wing mounting is set to be encastre. The tail boom uses the same boundary conditions. To analyse the connection of to wing the wedge is set to be encastre. For the hull a standard lay-up of 5 layers is used. The layers are orientated 0, 45, 0, −45, 90, respectively, the middle layer is made of foam to increase the rigidity of the hull the orientation of this foam is not important due to the isotropic properties of foam. The foam reinforcements to connect the wing to the fuselage also add to the stiffness of the structure. Again here the structure is optimised for the loads and stiffness and strength is added where needed or removed where possible to give the most lightweight structure.

The materials used are HMCF UD, E Glass UD and Rohacell 110 A. The properties of the materials used in this analysis can be found in Section 16.4.

16.2.2 MATLAB numerical model

The numerical model of the wing is basically a conventional finite-element model. The wing is divided into segments in the spanwise direction, with the axis system's origin at the leading edge, outboard of the port wing. Each spanwise segment is then comprised of airfoil skin segments. Figure 16.2 shows the axis definitions.

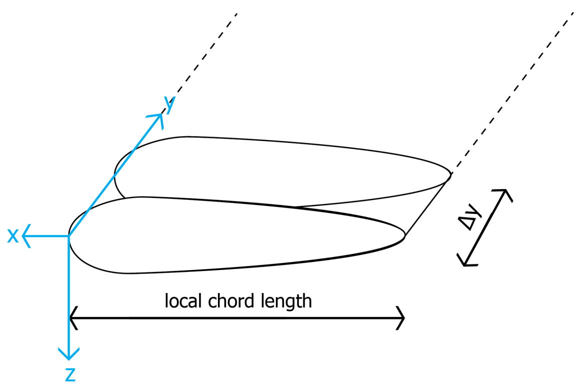

Figure 16.2: Axis and wing segment definitions in the MATLAB-based structural wing model. The origin is at the wing tip leading edge.

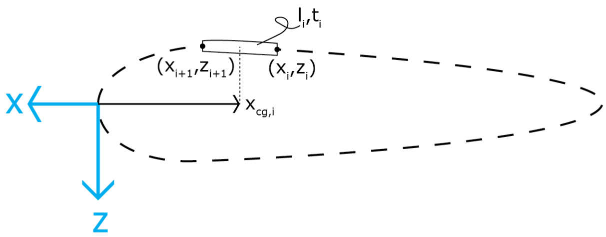

Figure 16.3: Discretisation of the airfoil geometry into elements with thickness t_i and length l_i.

External loads are simplified as discrete loads for floater weight and impact, and weights per meter of span for structural weight, PV weight and lift. Lift is assumed to act at the quarter-chord point; weights are assumed to act through the airfoil c.g. The wing skin is assumed to carry all loads; the wing structure is assumed to consist of a skin thickness concentrated around the airfoil geometry, defined by the Eppler 582 airfoil selected in Section 12.1. Figure 16.3 shows the discrete approximation of the airfoil geometry, consisting of elements of thickness t and length l between the Eppler 582 airfoil coordinates.

The internal stresses per segment are then computed using the formulas for internal stresses[95]. Normal stress distribution due to bending in the yz- and yx-plane is represented by Equation 16.1; shear flow due to torsion in the xy-plane is represented by Equation 16.2; and shear flow due to shear loading is represented by Equations 16.3 through 16.5.

$$\sigma_{y,bending} = \frac{I_{xx}M_z - I_{xz}M_x}{I_{xx}I_{zz} - I_{xz}^2}x + \frac{I_{zz}M_x - I_{xz}M_z}{I_{xx}I_{zz} - I_{xz}^2}z \tag{16.1}$$

with x and z coordinates in the cross-section, I_{xx} the moment of inertia about the x-axis, M_z the local moment about the z-axis.

$$q_{torsion} = \frac{T_y}{2A_{enclosed}} \tag{16.2}$$

with T_y torsion about y-axis and $A_{enclosed}$ the area enclosed by the segment cross-section.

$$q_s = q_b + q_{s,0} \tag{16.3}$$

wherein

$$q_b = \frac{I_{xx}V_x - I_{xz}V_z}{I_{xx}I_{zz} - I_{xz}^2}\int_0^s txds + \frac{I_{zz}V_z - I_{xz}V_x}{I_{xx}I_{zz} - I_{xz}^2}\int_0^s tzds \tag{16.4}$$

where V_x the local segment shear, t the local thickness of an airfoil element and s the circumferential coordinate following the cross-section outline, and:

$$q_{s,0} = -\frac{\oint \frac{q_b}{t}ds}{\oint \frac{1}{t}ds} \tag{16.5}$$

Note that the airfoil is unsymmetrical, I_{xz} is not zero, and the shear centre cannot readily be defined. The x-location of the shear centre is computed via relation 16.6[95], wherein V_z can be eliminated from both sides, as they are also included in both shear flow terms.

$$V_z x_{sc} = \oint pq_b ds + 2A_{enclosed}q_{s0,x} \tag{16.6}$$

Where x_{sc} is the location of the shear centre, p is the Pythagorean distance from the reference point to the c.g. of every skin element and $q_{s0,x}$ the shear flow (due to V_x) that needs to be added because of the virtual cut applied to the cross-section. A similar relation can be established to find z_{sc}.

These equations, together with simplifications made in the model, imply a set of assumptions. These are listed below:

- idealised clamping at the wing root.

- wing is a simplified beam: i.e. no control surfaces, floaters, hatches or other openings in the skin.
- stress evaluation excludes body forces.
- external loads are point loads
- homogeneous and isotropic material properties, which are be linearly extrapolated by thickness, from the glass-carbon-glass fibre skin lay-up, excluding foam, introduced in Section 16.2.1.
- deflections are small and obey Hooke's law.
- plane sections of a bending beam remain in-plane and perpendicular to the beam axis after deformation.
- torsion is not carried by direct stresses or τ_{xz}.
- $q = t\tau$: shear stress constant throughout skin thickness.
- deflections do not introduce extra stresses.
- open-ended wing cross-section.
- no airplane fuselage.

The internal stresses are combined to evaluate von Mises stress for each cross-sectional segment. This numerical model generally diverges from results obtained using Abaqus for loading cases causing high deflections. Given the assumptions, this is to be expected and moreover, not a large issue, since large deflections are generally undesired anyway.

16.3 Structures and parts

In this section the structural parts of the UAV are presented. Table 16.1 shows results of the structural analysis of main UAV structures. In addition to components mentioned in Table 16.1, the hatch, floaters, wing mounting, motor mount and the camera dome are discussed in the sections below.

Table 16.1: Summary of results from the FEA analysis. Highest stress and deflection are given for the critical load case, as well as the effective safety factor.

Parts	Critical load case	Stress [MPa]	Deflection [mm]	Safety factor
Hull	hull-water impact	98	40	6.66
Front wing	manoeuvre	68	35	14.7
Back wing	manoeuvre	77	40	13.0

16.3.1 Wing structure

Several options for the structure of the wing are considered. This depends on the material used in combination with the structure. For the wing a wing box, a sandwich structure or a laminate can be used.

Using a numerical model for the wing box, as described in Subsection 16.2, it is found that both stiffness and strength of the structure easily exceed required values if minimum sheet thickness is set to a handling thickness of 0.5 mm. Since laminate structures do not impose this minimum thickness, they provide a way to potentially reduce structural weight greatly without sacrificing required strength or stiffness. Since manufacturing and maintenance are a major focus of the UAV design, a load-bearing sandwich structure is not considered a viable option because of its complex manufacturing process and inefficient maintenance. A hybrid glass fibre / carbon fibre laminate is chosen, where stresses are mainly carried by the skins and a foam core provides the skin structure with extra moment of inertia, adding stiffness.

16.3.1.1 Preliminary analysis

A preliminary analysis is performed using the MATLAB numerical model as described in Section 16.2. Rough results are produced, for which the shear- and moment diagrams are shown in Figures 16.4a and 16.4b for the example of the float impact case for the front wing. In this case the maximum shear in at the root is found to be 104 N, and the maximum moment at the root is 69 Nm (bending upwards). The MATLAB model was generally found to be inaccurate for deflection analysis, compared to the Abaqus methods. This is to be expected due to the extra assumptions implied by the home-cooked model. Though real world testing will determine the actual accuracy of both methods.

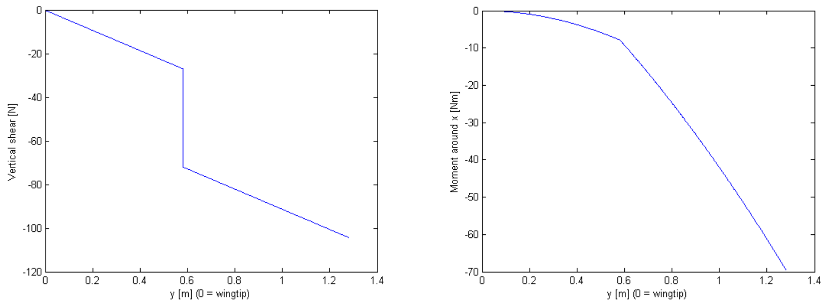

(a) (b)

Figure 16.4: Diagrams for vertical shear (a) and moment around the flight axis (b) of the front half-wing in the floater impact load case. Data obtained through MATLAB numerical analysis.

16.3.1.2 Analysis of the front wing

In this subsection the front wing is analysed for the manoeuvre- and floater impact load case. The following lay-up is used: a plain weave E-glass fibre layer of 100 grams under an inclination of 45°; a unidirectional layer of high modulus carbon fibres in the transverse direction of the wing of 200 grams, and a layer of plain weave E-glass fibres under an inclination of −45°. The foam core is made of Rohacell 110A.

Manoeuvre: For the structure of the wing several load cases are considered,: first the manoeuvre case is used in the FEA analysis. The wing is clamped at the wing mount and a pressure load corresponding to a wing load factor of 2.5, with a safety factor of 1.3 is applied at the top surfaces of the wing. A maximum stress of 68 MPa is found for this load case. With a material ultimate tensile strength of 1000 MPa, this constitutes an effective safety factor of 14.7[97].

Wing tip deformation due to this load is 3.5 cm; the deformation can be found in Figure 16.5. This will not result in failure of the PV cells due to the spacing of 1 mm: the current spanwise deformation in the wing top surface is 0.06 mm (compression). With a total of 33 PV cells in spanwise direction, the safety factor for deflection becomes 533. So in this load case the structure is strong enough.

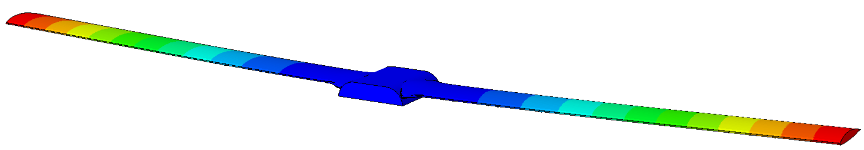

Figure 16.5: The deformation distribution of the front wing during manoeuvres

Floater impact: For the floater impact the mounting surfaces are constrained as being clamped. The loading is a point load at 700 mm from the centre of the wing of 21 N vertically upwards and 82.5 N horizontally aft. Also a wing loading of 1.5 was introduced at the top surface of the wing. A maximum stress of 76 MPa is found at the root and a wing tip deflection of 29 mm, which is presented in Figure 16.6.

A scale factor of 8 is applied to show deformation. For this load case, an effective safety factor of 14.2 is present.

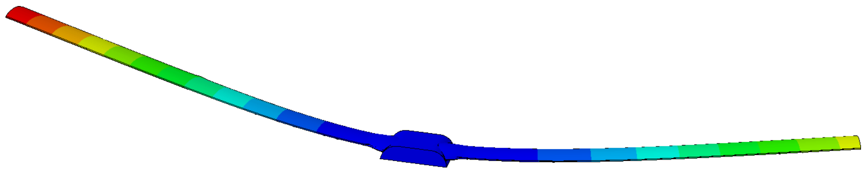

Figure 16.6: The deformation distribution of the front wing during floater impact. Range: 0(blue) to 29 mm (red)

16.3.1.3 Analysis of the back wing

In subsection 16.3.1.2 the front wing has been analysed. The back wing produces less lift and smaller shape; with this knowledge it is important to evaluate the back wing structure separately. The back wing does not have any floaters, so there is only the manoeuvre load case to consider. The final lay-up for the back wing is a plain weave of 75 g E-glass fibres at 45°, a unidirectional layer of high modulus carbon fibres in the spanwise direction of 200 grams and a layer of plain weave E-glass fibres of 75 grams at −45°. The foam core is made of Rohacell 110A. A maximum stress of 77 MPa and a maximum wingtip deflection of 40 mm are found for this load case. This constitutes an effective safety factor of 13.

16.3.2 Wing mounting

For the mounting of the wing to the hull, bolts have been chosen. The bolts have been chosen to be used in the UAV longitudinal direction. In this configuration the wing load is passed from the bolts to the hull inserts, which will amount to a more efficient mounting than if the bolts were to be mounted vertically from the top.

To determine the required bolt size, Equation 16.7 is used.

$$d_{bolt} = \sqrt{\frac{4F}{n\tau\pi}} \tag{16.7}$$

Where d_{bolt} is the minimal bolt diameter, F is the shear force at the wing mount, n is the number of bolts used to carry the wing and τ is the shear strength of the material used.

The force that is applied is 130 N, which is a worst case shear in the wing. A fail-safe number of bolts of 4 is chosen, to counteract the rotation of the wing. The shear strength τ is 170 MPa, which is the shear strength of steel[98]. With this data d_{bolt} should at least be 0.5 mm, however for maintainability and handling M4 bolts are chosen, which have a diameter of 3.838 mm. For this configuration the bolts have an effective safety factor of 7.6.

The next part is the connection of the bolts to the hull. Due to the use of composites the connection between bolts and the hull is not trivial. Steel inserts are bonded inside a foam reinforcement to accommodate the bolt connection. The point of failure will be the foam, since is has the lowest shear strength. The inserts are subjected to two loads: the axial shear load and the shear load due to the lift. Sizing based on the shear force is done with Equation 16.8.

$$r_{insert} = \frac{FN}{h_2 n\tau} - \frac{r_{bolt}h_1}{h_2} \tag{16.8}$$

In this equation τ is the shear strength of the foam, which is 2.4 MPa and N is a safety factor of 3. The wing load is not just carried by the insert: the foam at the bolt side also carries the load. It is assumed that the force is distributed evenly per unit of area.

The axial shear load is determined from bolt tightening. The relation between the bolt torque and axial force is given in Equation 16.9 [99].

$$T = F_t\left\{\frac{d_2}{2}\left(\frac{\mu}{cos\alpha} + tan\beta\right) + \mu_n\frac{d_n}{2}\right\} \tag{16.9}$$

Where T is the torque applied to the bolt, F_t is the axial force exerted on the bolt, d_2 is the bolt pitch diameter of 3.17 mm; μ is the friction coefficient of the threaded portion which is 0.2, α is the half angle of screw thread which is 30 °for ISO screws. β is the lead angle which is 3 °, μ_n is the friction coefficient of bearing portion which is also 0.2. d_n is the pitch diameter of bearing surface, which is 5 mm.

The axial force is found to be 682 N for a torque of 0.5 Nm. This analysis shows that the axial load is the design load for the bolts. The sizing of the insert is now done using Equation 16.10.

$$r_{insert} = \frac{FN}{2\pi h_2 \tau} \tag{16.10}$$

The radius and depth of the insert needed are found to be 9 mm and 15 mm, respectively.

These inserts are bonded with an adhesive to the holes in the foam. Figure 16.7 shows the insert, Figure 16.7a shows a section view with the dimensions; and Figure 16.7b shows the isometric view.

(a) Section view. Dimensions in mm.

(b) Isometric view

Figure 16.7: The bolt inserts for the wing mount.

Due to the smaller width of the hull at the back wing, the lateral spacing at the rear end of the back wing is not enough to mount 4 bolts. For this case 3 bolts are used to carry the loads. The safety factor of 7.6 will consequently decrease to 5.7. This is however still good enough to carry the loads of the wing, the safety factor is large enough to ensure that it will not fail.

16.3.3 Hatch

The inside of the UAV needs to be accessible for inspection and maintenance. For this purpose a hatch is designed on the top of the fuselage, allowing access to the wing mounting bolts and maintenance of internal components. The hatch is shown in Figure 16.8. The hatch is a thin plate under a compressive load, so thin plate buckling is analysed. This is done with inter-rivet buckling. The hatch is connected to the hull by 24 M3 screws to counteract inter-rivet buckling; the spacing is 40 mm, which follows from Equation 16.11 [100].

$$\sigma_{ir} = 0.9 c_r E_t \left(\frac{t_s}{s}\right)^2 \tag{16.11}$$

Where σ_{ir} is the compressive stress acting on the hatch, c_r is a constant dependent of the screw that is used - in this case 1 for counter-sunk screws -, t_s, s and E_t are the skin thickness, spacing and Young's modulus respectively.

With a stress of 10 MPa, the screw spacing is found to be be 95 mm. Due to the uncertainty of working with composites a safety factor of 2.4 is applied. The hatch geometry can be found in Figure 16.8.

16.3.4 Motor mount

Considering the fact that vibration analysis is not yet taken into account, the accuracy of the motor mount design is limited and a definitive design is not established. Some important design aspects are highlighted in this section.

The motor mount comprises of a load-bearing lightweight Al-2024 frame encapsulated in an aerodynamically shaped glass fibre shell. Usage of aluminium alloys for the load-bearing structure and connection to the hull is possible in this case, since the motor is mounted on the hull forward of the front wing. Since the

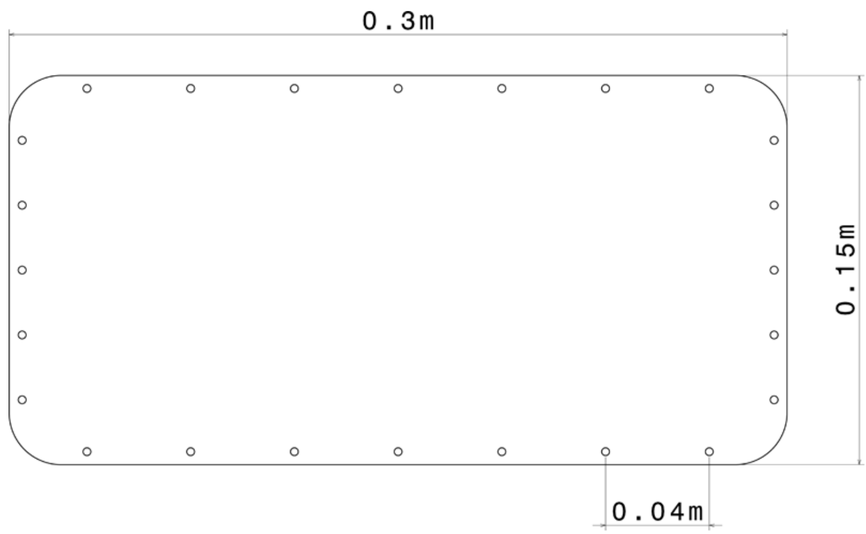

Figure 16.8: Technical sketch (top view) of the hatch with dimensions.

hull does not contain carbon fibre, galvanic corrosion issues as highlighted in Section 16.4 do not arise. The glass fibre shell only bears aerodynamic loads, and as such can be kept lightweight. From a maintenance and structural efficiency point of view, it is mounted with one set of bolts to fix both the frame and the shell to the fuselage.

16.3.5 Analysis of the hull

In this subsection the hull is analysed with FEA methods, under the load cases of landing impact and maximum manoeuvre load. First the lay-up will be discussed, after which the FEA results are presented.

As can be seen in Figure 16.1, an extra layer of glass fibres is added to the top structure to decrease the stresses in the top panel. The stresses are 98 MPa lower due to this extra layer, also decreasing the fatigue limit with a factor of 10 (see Section 16.4.2).

From the load cases of landing and manoeuvres, a maximum stress of 152 MPa and a maximum deflection of 3.98 cm are found. In Figure 16.9 and Figure 16.10 the deflection and stress distributions are shown respectively. With these stresses an effective safety factor of 6.66 present on the structure. The fatigue cycle for this stress is 10000 cycles for a glass fibre composite. [101].

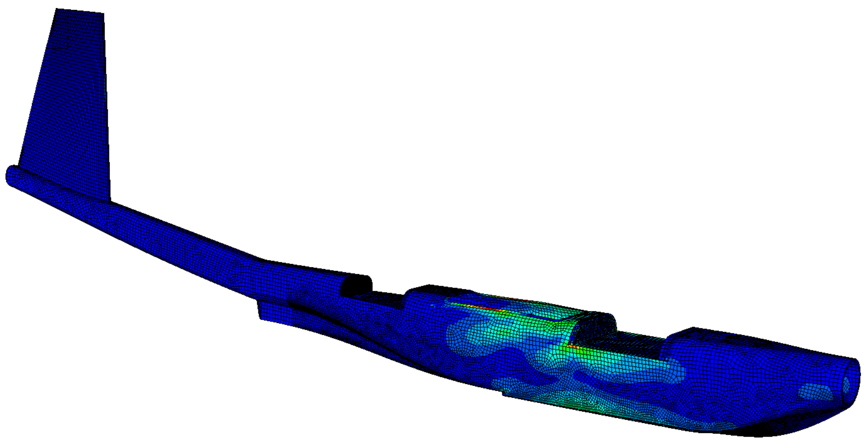

Figure 16.9: The stresses distribution of the hull

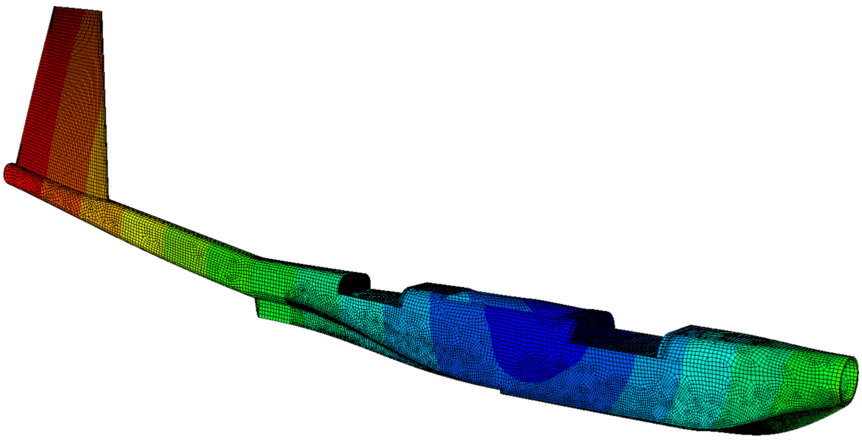

Figure 16.10: The deformation distribution of the hull

16.3.6 Floaters

Floater structural design is based on a worst case load induced by failed approach. The impact load on the floater is comprised of a vertical impact force of 14 N and a horizontal drag force of 16.7 N, which are calculated in Chapter 13. A safety factor of 1.5 is applied to these forces. The floaters are made from Rohacell foam, which is also used in the skin laminates. Using an Abaqus static load simulation, it is found that a foam structure easily suffices in this respect: maximum deflection is found to be 3 µm and maximum stress in the floater reaches 0.022 MPa, while the tensile strength of Rohacell foam is at 3.5 MPa.

16.3.7 Camera mount and dome

The BTC-88 camera, selected in Section 14.3, is mounted in the front of the UAV, under a polycarbonate dome. Polycarbonate is chosen for its transparency to visible and infra-red light and resistance to degradation in saline water, while also possessing impact resistance and medium specific strength and specific stiffness [102]. Acrylics (Poly(methyl methacrylate)) may also be considered for their transparency and weathering resistance, while being aware of their meagre mechanical properties [102]. Particularly impact hazards should be considered, since the camera dome constitutes the front of the plane.

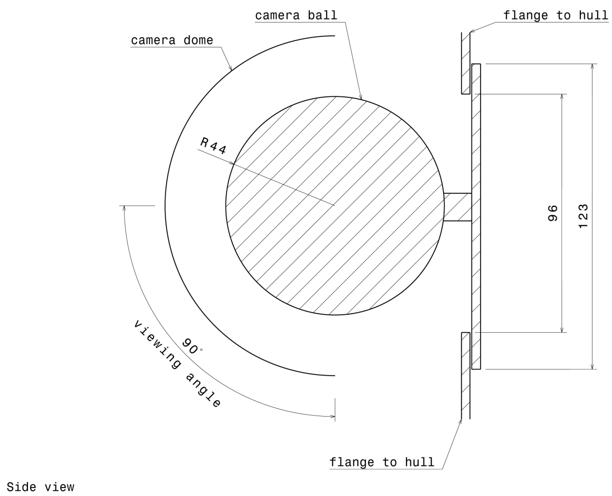

Figure 16.11: Simplified diagram of the camera mount in side cross-section. Flight direction to the left, dimensions in mm.

The camera itself will have to be mounted from the inside, through the hatch. An advantage of this is that it is easier to create a water tight connection between the camera dome and the hull, an disadvantage is the accessibility of the camera. The camera mount is anticipated to consist of a screw connection to flanges on the inside of the hull, illustrated by Figure 16.11. Note that not all dimensions and no precise position of mounting points are publicly published by MicroUAV [103].

16.4 Materials

Material selection in aerospace applications is mainly driven by lightweight properties. For the amphibious UAV the focus of material selection is on strength-to-weight ratio and stiffness, with some brief considerations to other relevant material properties. Because of this focus on strength- and stiffness-to-weight, the main focus is on composite structures. As discussed in Section 16.3, the wing and body skin will comprise of a laminate with a foam core to increase structural stiffness. After explaining why an aluminium-based body structure is disregarded, section 16.4.1 will elaborate on composite structures, besides that foam core material is also discussed. Sections 16.4.2 and 16.4.3 go on to consider fatigue- and corrosion behaviour respectively.

16.4.1 Material selection

In Table 16.2 some typical properties of applicable materials are listed. For a list of materials used in the final UAV design, refer to Section 17.6. As discussed in Section 16.3, it is decided to disregard aluminium alloys as efficient materials for wing and hull parts. The reason for this can be related to the information in Table 16.2: aluminium typically possesses lower specific strength than Fibre Composites (FC) do. Furthermore, minimum sheet thickness of aluminium-based structures is typically defined by a minimum handling thickness of no less than about 0.5 mm. For small-scale structures as used in the amphibious UAV, this would limit structural efficiency significantly. However, aluminium alloys are effective in other structural parts, such as the motor mount, where sheet thickness is not applicable and their advantage of isotropy and relatively cheap material and manufacturing cost come into play [102].

Table 16.2: Typical properties of selected engineering materials [102]. Fibre volume for all composites is 60%.

Material	**Modulus of elasticity [GPa]**	**Specific Yield strength [kNm/kg]**	**Specific tensile strength [kNm/kg]**	**Elongation [%]**
aramid fibre epoxy matrix				
longitudinal	76	-	990	1.8
transverse	5.5	-	21	0.5
high-modulus carbon fibre epoxy matrix				
longitudinal	220	-	450	0.3
transverse	6.9	-	17	0.4
glass fibre epoxy matrix				
longitudinal	45	-	490	2.3
transverse	12	-	19	0.4
Aluminium T2024-T3	72.4	125	175	18

Carbon fibre composites: Table 16.2 shows the stiffness advantage of carbon FC with respect to other materials. However, carbon fibres do have a relatively low elongation-to-failure compared to the other materials in the table, this implies less favourable impact properties. Care must be taken when implementing carbon FC in the UAV structure as they are electrically conductive should not come into contact with aluminium parts [102]. Carbon fibre structures also block out RF signals, so they cannot be used around antennae [104, 101].

Glass fibre composites: Glass FC are cheaper than both carbon- and aramid fibres, while still possessing a favourable specific tensile strength [102]. They also possess good impact resistant properties [101, 102]. Glass FC are not as stiff as other materials in table 16.2, but it should also be noted that the selected glass fibre type in the table is a relatively low-performance type: using S-2 or R-type glass fibres stiffness may be increased up to 20% and strength up to 38% [101].

Aramid fibre composites: Aramid-FC seem an attractive candidate due to their high strength-to-weight ratio and high impact- and creep resistance. A main disadvantage of aramids is their cost: aramid fibre composites are roughly 1.2 times more expensive than carbon fibre composites, and about 2.5 times as expensive as glass fibres[102].

Hybrid glass-carbon fibre composites: A common hybrid composite is attained by stacking carbon fibre layers for high strength and stiffness with glass fibre layers for impact resistance and cheaper material cost. Hybrid glass-carbon composites generally have higher impact resistance, are stronger, tougher and cheaper in production than either comparable all-carbon or all-glass reinforced plastics [102].

Conclusively it is anticipated that glass-FC are a preferred material to use in structural parts, as long as high stiffness is not imperative. Hybrid glass-carbon FC will be used in the wing to reduce tip deflection. Aluminium alloys are also still considered a viable option for some parts like the motor mount, although care must be taken so no electrically conductive connection between carbon- and aluminium structures exist [102]. Additionally, to reduce complexity in manufacturing and maintenance, the number of materials used should be limited where possible. Since manufacturing and maintenance are an important requirement of the UAV design, the structural implications of particular material choices should be considered. These structural implications are covered in Section 16.3.

In conjunction with structural analysis, presented in Section 16.3, it is decided that glass-FC are used in the UAV hull for impact resistance, to keep material costs low and because it does not interfere with RF signals. Hybrid carbon-glass FC are used in the wings for stiffness. Epoxy is used as a resin in all composite structures. The rationale for this decision is based on corrosion, presented in Section 16.4.3. To increase skin moment of inertia, adding structural stiffness, a foam core is used. For the propellers no material has been selected yet, but they are generally made from plastics or based on glass- or carbon fibres [105]. This will depend on the strength, weight and stiffness required. Section 17.6 provides a list of material configurations used in their respective parts. Figure 16.1 shows a map of of the composite lay-ups in the UAV.

16.4.2 Fatigue properties

Fatigue properties of glass- and carbon fibre composites are reviewed in this section. Since no extensive research is performed, data in this section can only serve as an indication.

Generally carbon FC possess superior fatigue properties to both metals and other composites. In any of the lay-ups $0°$, $+/-45°$, quasi-isotropic or $90°$, stressed at an amplitude of at most 58% of short term ultimate, each still have a fatigue life of 10 million tension-tension cycles [101].
Figure 16.12 illustrates the fatigue performance of E-glass FC in epoxy, which is generally much worse than carbon FC [101]. Fatigue life for the amphibious UAV is hence largely defined the fatigue life of the glass fibre components. For example, if a reasonably regular event like landing should be regarded as fatigue criterion with a minimum fatigue life of five years, the limiting number of cycles is about 5500 (assuming three landings per day). This amounts to a maximum longitudinal stress of about $0.6 \cdot 1000$ MPa $= 600$ MPa.

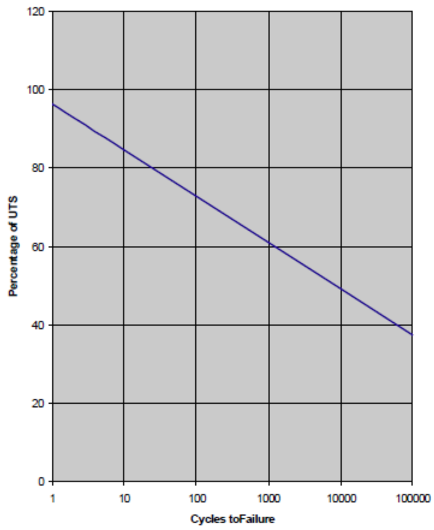

Figure 16.12: E-glass fine weave fabric-epoxy, modeled tension-tension fatigue (R=0.1) related as a fraction of ultimate strength [101]. Note that ultimate longitudinal strength of glass FC used is 1000MPa which can be seen in Table 17.4

16.4.3 Corrosion properties

Corrosion effects of materials to be used are reviewed in this section.

E-glass is highly resistant to most chemicals but is attacked by both mild acids and mild alkalis [101]. Since sea water has a pH roughly between 7.5 and 8.5 [106], it is important to design the composite laminate such that contact between sea water and the glass fibres themselves is limited as much as possible; particularly for the UAV hull. This goal can be attained by the resin, as well as with coatings. Glass (and aramid) fibres do not suffer from galvanic corrosion[101].

A polymer resin can be selected based on their resistance to corrosion in the salty and mildly alkaline environment of the sea. For aerospace applications, epoxy resins are widely used because of their high mechanical performance [101]. Epoxy resins are also highly resistant to degradation[101]. This is why epoxy resin is selected for all composite structures in the amphibious UAV.

However, epoxy resins are expensive both in material cost and manufacturing [101]. If costs need to be reduced, epoxy vinyl ester resins should be considered. In sea water, epoxy vinyl ester resins generally degrade less than polyester resins while being relatively cheap in material cost and manufacturing [107, 102]. This option is validated by the fact that epoxy vinyl ester resins are widely used in boats [107].

16.5 Maintenance

As specified by the design requirements (see Appendix A), up to 200 UAVs will return once per week for scheduled inspection and maintenance. Consequently, design of the amphibious UAV must also focus on efficient and effective maintenance. Maintenance and inspection considerations, which are taken into account are discussed in this chapter.

16.5.1 Modularity and parts replacement

The first aspect to improve maintenance characteristics is modularity. The UAV design integration is based on the idea that the failure of one part should not cause large parts of the UAV to be unnecessarily discarded. This is brought into practice by designing parts, such as the wings, to be replaceable as one piece:

Both wings can be removed, as they are attached to the hull by bolts horizontally penetrating the wing centre. This connection is shown in Figure 16.13. Internal parts like electronics can be accessed via the body hatch (see Section 16.3.3). The motor mount and the motor itself can be accessed from the outside, without needing to open the body hatch.

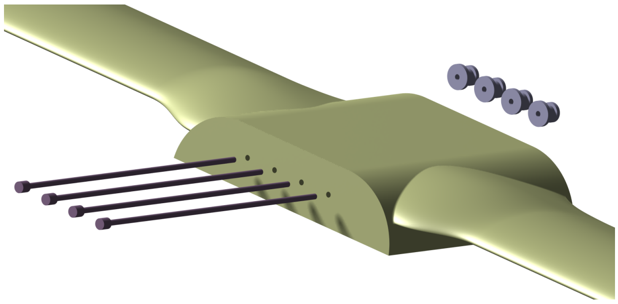

Figure 16.13: Wings are bolted to the fuselage in the UAV longitudinal direction. In the top right the inserts can be seen, which are bonded to the foam structure.

Control surface servos should be made accessible via respective tail- and wing hatches, regretfully these are not designed yet. An easy to remove tail section is anticipated to aid in both long-term maintenance cost and storage- and transport efficiency. A tail-hull connection as depicted in Figure 16.14 is suggested, though structural implications of this solution have not yet been asserted. Aluminium or stainless steel male-female shape-fitting parts would be bonded into the respective tail- and hull parts, locked into place by a locking pin. A channel is left for the rudder control wiring, which can be locally reconnected using plugs.

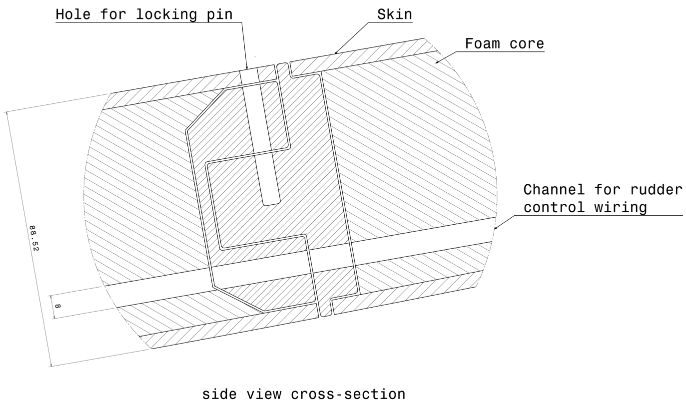

Figure 16.14: Cross-sectional diagram of a suggested tail connection concept. Local tail diameter is given in mm for reference.

Although no extensive research has been done on the attainable operational life of UAV parts, qualitative estimates can be made for the targeted replacement frequency of respective parts. Anticipated UAV component replacement frequencies and their assembly types are listed in Table 16.3. The rationale for assembly type should follow the anticipated replacement frequency. Bonding is not preferred for parts requiring frequent removal.

16.5.2 Inspection

For weekly inspection of the UAV, a set of guidelines will be needed. Currently, the design of the amphibious UAV is not sufficiently complete, or tested, to produce a definite maintenance manual. As a first effort towards a maintenance manual, an indicative list of inspection foci is listed below, as well as a preliminary guide for maintenance disassembly.

A preliminary list of inspection priorities

Table 16.3: Anticipated qualitative replacement frequency of UAV components. Replacement frequency is expressed in qualitative terms of frequent-occasional-rare.

Component	**Replacement frequency**	**Assembly type**
Structure		
tail boom & tailplane	occasional	shape-fit to fuselage with locking pin
front wing	occasional	bolted to fuselage
rear wing	occasional	bolted to fuselage
body	rare	N/A
camera dome	rare	bonded & bolted to fuselage
body coating	occasional	N/A
floaters	occasional	bolted to front wing
control surfaces	occasional to frequent	TBD
electronics support structure (ESS)	rare	bolted inside fuselage
Control		
Autopilot	rare	bolted to ESS
Sensors & camera assembly	rare	bolted inside fuselage
Control servos	occasional to frequent	TBD
Comms equipment	rare	bolted to ESS
Power		
PV cells	rare	hopefully not bonded to wings (& fuselage)
batteries	rare to occasional	TBD
Power control electronics	rare	bolted to ESS

- Inspection for leaks and water tight seals
- Inspection of structural connections
- Inspection of control surfaces structural health
- Evaluation of servo performance
- Evaluation of PV performance and battery health
- Camera and electronics diagnostics
- Inspection of camera dome health and transparency

A preliminary guideline for maintenance disassembly

1. Place UAV on soft surface to avoid damaging the hull
2. Detach the tail section:
   (a) remove locking pin
   (b) disconnect tail section, disconnecting the rudder control wiring

   Rudder and rudder servo, as well as the tail structural connection can now be inspected.
3. Open body hatch by unscrewing hatch screws
4. Detach the wings:
   (a) unscrew wing bolts inside the body

   (b) remove wings, disconnecting respective aileron- and elevator control wiring

   Ailerons, elevators, respective servos and wing structural connections can now be inspected, as well as UAV internals. PV surfaces can be cleaned.

5. Unscrew the camera from its mount inside the UAV body

   The inside of the camera dome can now be inspected for leaks.

   After reassembly:

6. Run standard electronics- and control diagnostics
7. Perform short test flight

Chapter 17

Final design

From the analyses and considerations presented in Chapters 11 to 16, a final design is established. This chapter discusses final design characteristics, such as layout, costs, production plan and performance analysis.

17.1 Layout

In this section, the internal layout of components is presented. The internals basically consist of the surveillance and communications payload and power supply components, as well as control components. For more information on these components, please refer to Chapters 14 and 15. The external layout is extensively covered in Chapter 16.

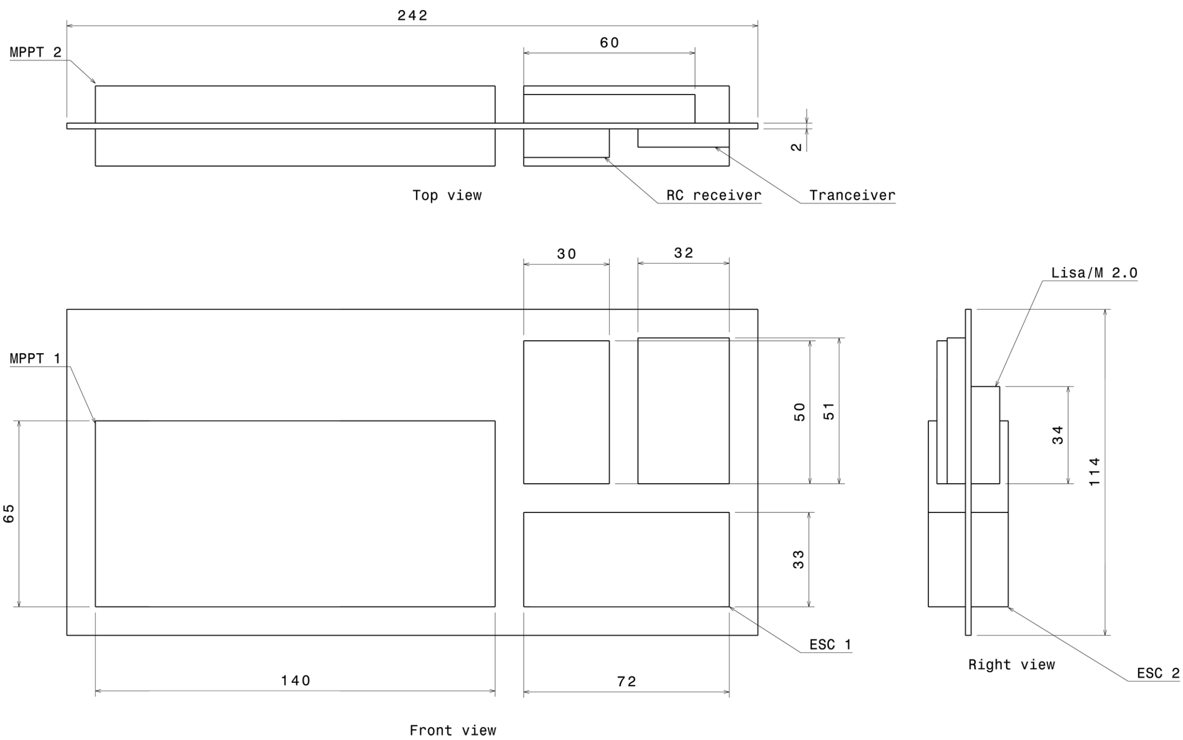

Figure 17.1: Electronics assembly structure concept. Units in mm; all minimum part spacing is 10 mm. This board can be taken out through the hatch as one part.

For maintenance purposes it is decided to fix electronic components to a dedicated Electronics Support Structure (ESS), which should be removable through the body hatch, with dimensions 300x150 mm. The electronics support structure itself has dimensions 242x114mm, as illustrated in Figure 17.1. The board fits both Maximum Power Point Trackers, both Electric Speed Controllers, the RC receiver, comms transceiver and the Lisa/M board. It should be noted that the current ESS design easily fits through the body hatch, leaving enough spatial headroom if the UAV design requires more electronics equipment in later design stages.

The ESS is located directly under the body hatch for easy access; this leaves the three (136x43x70 mm) batteries to be positioned to the front and the antenna (400x33 mm) in the rear of the hull. The camera is positioned in the front of the UAV under the camera dome, as illustrated in Section 14.3. In general, there is ample room for internal components due to the large hull volume imposed by the water buoyancy requirement: the volume available in the hull is 34 L, excluding the tail.

Control surface servos are located in the wings themselves, so that only wiring is needed to bridge the distance between control surfaces and the Lisa/M autopilot. Cut-outs in the wing foam will be made to accommodate wiring from the control servos and PV cells. Wiring that bridges detachable structural connections, such as the wing-fuselage mount, is locally reconnected using plugs.

17.2 Costs

This section will show the cost breakdown and the return on investment for the UAV.

17.2.1 Cost breakdown

In Table 17.1 the cost breakdown for the UAV is shown, with the price of each individual component and the total cost. The stated costs are for a production run of 200 units.

A distinction can be made between two different cases; commercial off-the-shelf (COTS) products and newly manufactured products. The COTS parts include the photovoltaic (PV) cells, the maximum power point tracker (MPPT), the electrical speed controller (ESC), the motors, the batteries, the control system, autopilots, sensors, communication, the ground control system and the wiring (partly). Thus the costs stated in Table 17.1 are the prices of each of these parts.

The wings, fuselage, floaters, propellers will be manufactured specially for this UAV. The costs stated here are the approximated manufacturing and material cost. They are calculated as following: The wings will use negative moulds, which have to be milled, the cost of milling the three mould with this precision and size will cost around 15000 euros, which is the cost for all units. To create the lay-up the wings the materials are needed, which come to a cost of 144 euros per squared meter. The labour consists of three days, one for the preparing of the moulds, one for the lay-up and one for the product removal of the mould. This is done by three people with a salary of 20 euros per hour. The hull has the same conditions as the wings the only difference is the surface area increases and there there is an increase in costs.

The floater will cut be from foam, these costs are relatively low, being done with hot wire cutting. This costs 50 euros per hour and the cutting is done for both floaters within 3 hours. With a foam cost of €40 for both the floaters, the total cost will become €190.

The propeller is made with injection moulding and this will come to cost of 40 euros per propeller.

Taking a 20 percent contingency for unforseen costs, the cost price of the UAV will become €32717.

17.2.2 Return on investments

Now that the cost of the UAV is know, this subsection will deal with the return on investment.

The UAV can either be used to replace current operations of the DCCG or to expand on the operations of the DCCG. They will never be able to replace the entire fleet of naval and aerial vehicles of the DCCG. When a potential threat is spotted, a boat is still required to investigate. But the UAVs will be able to replace the (some) of the current surveillance done by the helicopters and airplanes.

In 2011 the DCCG spent €12177000 on 1923 Dash-8 and 700 AS-355 helicopter flight hours [1]. No hard data can be found on what kind of mission these hours were exactly spent on. So it can not be determined how much money was spent on aerial surveillance, thus a direct comparison is hard to do. Also some surveillance which is currently done by boats can be replaced by an UAV, but no data on this is

Table 17.1: Cost breakdown

Part	Cost [€]
Wings	2 422
Fuselage	2 391
Floaters	190
PV Cells	16 835
MPPT	233
ESC	150
Motors	165
Propellers	40
Batteries	675
Control system	273
Autopilot	187
Sensors	3 150
Communication	450
GCS	94
Wiring	9
Total	**27 264**

known either. Assuming the UAVs cost €32717 per UAV, this leads to purchase costs of €6543400 for 200 units. Also maintenance costs of €6000 per unit per year are assumed. This figures comes from 4 man hours of maintenance per UAV per week and an additional 92 hours of additional maintenance per UAV per year, with labour costs of €20/hour. Depending on the amount in reduction of cost for the normal operation they provide they will repay them in several years. If, for example, they reduce the cost of regular aerial operation by 20% they would repay themselves within 5.3 years.

With these stated costs and an assumed lifetime of 6 years and a uptime of 80% of the days, this would lead to a cost per UAV, per km^2 of 0.05 €/km^2.

17.3 Requirement compliance

When finishing a design, it is important to look back at where the project started and what was initially the desired outcome of the project. The goal of any project is to fulfill the requirements that are pre-set, so an analysis of these requirements can be used to see how succesfull the project turned out to be. First of all, the top level requirements will be analysed in Table 17.2.

Table 17.2: Requirement compliance matrix

Requirement	Met?	Actual value
Maximum mass of 35 kg	✓	8.8 kg
Maximum air speed of 15 m/s	✓	31 m/s
Minimum rate of climb of 10 m/s	×	7.5 m/s
Minimum flight endurance of 1 hour	✓	1.1 hour
Endurance at maximum thrust larger than 10 minutes	✓	12 minutes
Propulsion must be electric	✓	-
Minimum production series of 200 units	✓	-
Take off and landing from water with waves no greater than 2.5 meters (WMO 4)	✓	-

As can be seen in Table 17.2, all of the requirements are met except one. Very early in the design process, it was already observed that the rate of climb requirement was very high. During the design, this requirement was still taken into account and was designed for. However, mainly concerning the design of the motors, the rate of climb requirement seemed largely out of line compared to the other requirements.

The motors needed for this climb rate would mean that the motors are heavily over-designed for all other flight phases. This is why in the end, in agreement with the client, this requirement was dropped.

Next, the requirement discovery tree will be analysed. This tree has been put together in the beginning of the project, and goes into more detail of what the UAV will have to be able to do, to make sure the mission can be fulfilled. The requirement discovery tree can be found in Appendix A.

All of the requirements in the requirement discovery tree, except requirements 1.4a, 1.5d and 2.3b. These are the following requirements:

- **1.4a: 1.6 mbit bandwidth for HD video transfer**. After analysis and careful consideration of the effects that having a 1.6 mbit bandwidth will have on the design, it was concluded that a bandwidth of 1.6 mbit would demand too much power. It was decided that for surveillance, sending pictures to the ground station, would suffice. However, if HD video data needs to be sent anyway, this can still happen. With the installed bandwidth of 1 mbit, this will just take longer than it would have with a 1.6 mbit bandwidth.
- **1.5d Low charge time**. The goal was to have a low charge time, to be able to increase the uptime of the UAVs. However, the currently designed UAV has a charge time of 4 to 5 hours. The UAV has a large solar cell area, converting a lot of solar power to energy. However, the take-off is very demanding, using a lot of power. This means that a big battery is needed to provide for both taking off and an hour of endurance.
- **2.3b Minimum rate of climb of 10 m/s**. As mentioned before, this requirement is also net met.

The following requirement needs more explanation:

- **1.2b: Infrared imaging**. The designed UAV will be able to be equipped with an infrared camera. However, this camera is very expensive. Thus, it is not included in for example the cost estimation, and is treated as an optional feature.

17.4 RAMS characteristics

In this section an overview of the reliability, availability, maintainability and safety characteristics is provided. The reliability of the final design is mostly determined by components used and the reliability of those components. The components have a failure rate which is constant during most of its operating life [108].

Furthermore, the number of components increase the probability of failure. E.g. if two components with a failure rate of 90% are combined the rate of total failure changes to 81% [108]. From this observation follows that it is important to keep the design simple, with as few components as possible. For the mission the direct critical components are the sensors and communication, but also the energy supply, like the batteries and solar cells. Of course the UAV itself also needs to take-off in order for the data to have any value. Thus all these systems need to work in order the UAV to perform its mission. This means that the total UAV reliability is a cumulative sum of all the parts. Only the batteries and the floaters are redundant to a certain extent. Without the floaters the UAV will most likely still be able to perform its mission, but the wings would be in the water during the idle phase. For the batteries, if one battery breaks down the other batteries can still provide power (since they are in parallel), but the total energy would be less. Thus the endurance requirements will not be met. All the other components need to be designed or selected to be of a safe-life standard.

It is important to design a UAV with a focus on safety. Even if the vehicle is unmanned, safety to its operating environment is not to be neglected. With the use of COTS components, designing a safe and reliable system becomes increasingly challenging. This is due to the fact that component safety specifications are not provided by manufacturers [109].

To increase the safety and reliability of the UAV several options are possible. To ensure the reliability of the propulsion system, a second motor is used. With this second motor, it is possible to maintain flight and return to base in the event of a single motor failure. This is an example of a fail-safe design. For the mission the direct critical components are the sensors and communication, but also the energy supply, like the batteries and solar cells. Of course the UAV itself also needs to take-off in order for the data to have any value. Thus all these systems need to work in order the UAV to perform its mission. This means that the total UAV reliability is a cumulative sum of all the parts. Only the batteries and the floaters are redundant to a certain extent. Without the floaters the UAV will most likely still be able to perform its mission, but the wings would be in the water during the idle phase. For the batteries, if one battery breaks down the other batteries can still provide power (since they are in parallel), but the total energy would be less. Thus the endurance requirements will not be met. But all the other components need to be designed or selected to be of a safe-life standard.

An advantage of COTS components is a relatively high availability. For the custom components no production infrastructure exists. This means that until this infrastructure is fully operational the availability of these (spare) parts will be low.

Maintenance on COTS components may consist of swapping the entire unit for a new one, or maintaining the unit, which can be performed using COTS-subcomponents. The UAV is designed with modularity of components in mind. The aim is to have most of the components easily replaceable. This includes the wings, sensors, communication systems and power systems. This will save on the maintenance costs, since instead of replacing an entire UAV, only a part can be replaced. This also increases the availability, since it takes less time to replace just one part of a UAV than to replace an entire UAV. COTS components have maintenance procedures imposed by the manufacturer; these procedures are to be followed. Using COTS components also gives the advantage of always having replacement parts available for the maintenance of these components.

17.5 Production plan

The production is done in different ways for different parts, in this section the production of the different parts are discussed. First the wings and the hull will be discussed, after that the floaters and motor mount are discussed, finally the assembly is discussed in more detail. In Figure 17.2 the overview of the complete production is shown.

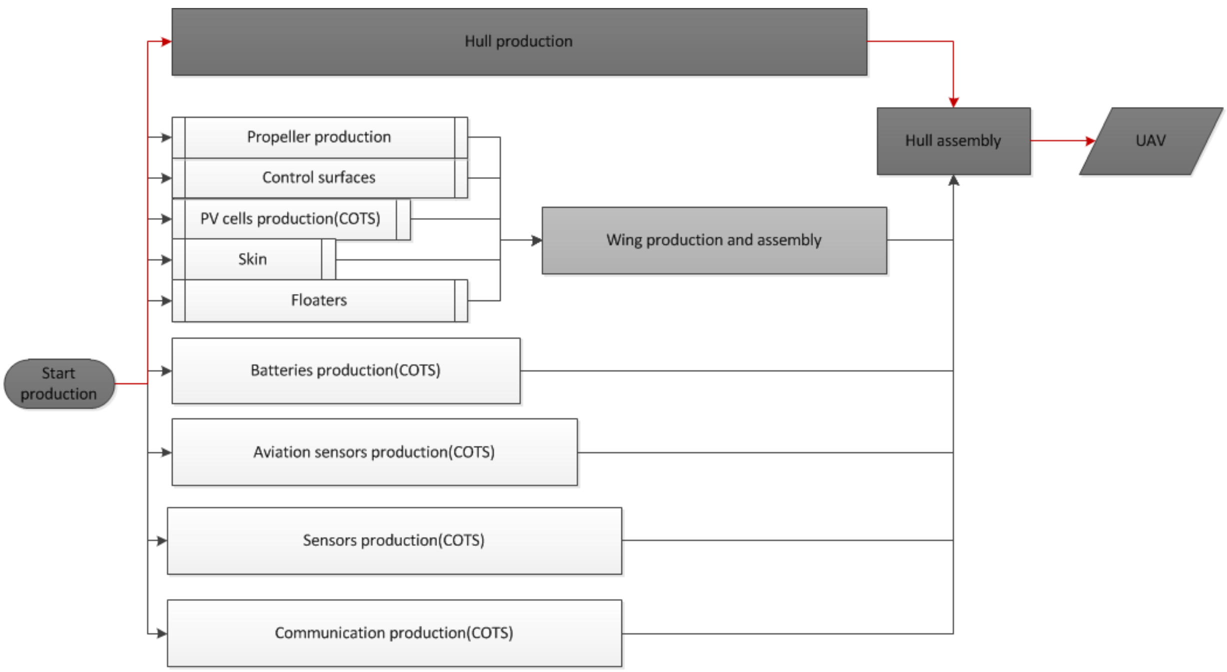

Figure 17.2: Production plan of the UAV

17.5.1 Hull

The hull is made from a laminate and therefor will need negative mould to properly define the top surface. Therefor the hull is split into two parts, it is cut through the xz-plane. In this way both parts of the hull can be made with releasing moulds, this is necessary to reuse the moulds for the production line of 200 units. At this cut a flange of 5 mm is added for assembly purposes. This flange is designed by hand-ability, with a shear strength of 35 MPa the bonding can withstand a shear force of 896 kN [110]. The lay-up is done with vacuum infusion, this gives the best surface finish and makes the hull more watertight. The foam parts are bonded to the half section of hull, in Figure 17.3 the design of the hull is shown.

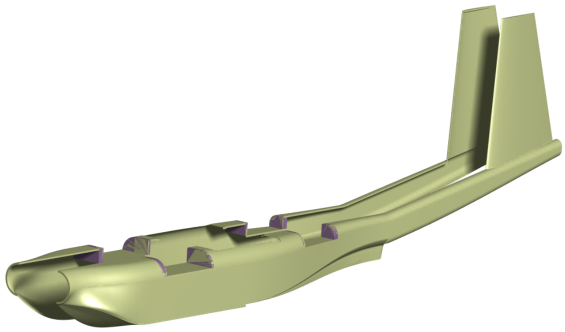

Figure 17.3: Production of the hull

17.5.2 Wings

For the wings the top surface is critical, again negative moulds are made. the wings are produced in three parts, this is again due to the need of releasing moulds. In this case no flanges are needed, the complete foam core which is also cut in three parts, and these are the surfaces which are bonded to each other. In Figure 17.4 the configuration is shown of the assembly of the different parts. As can be seen the cut is not planar with the axis system but with the camber-line of the airfoil.

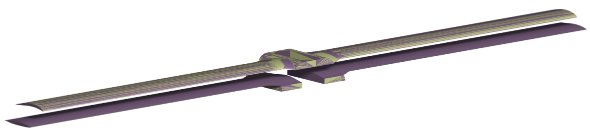

Figure 17.4: Production of the wing

17.5.3 Floaters

The floaters are made from foam due to the easy manufacturing and the weight decrease is not significant enough. If it is made from glass fibres the weight is 0.3 grams and the weight of the foam floater is 15 grams. To mount the floater to the wing it is bonded to a stiffener which is in turn bonded to the front wing. The foam is cut with hot wire cutting and is given a water resistant coating.

17.5.4 Motor mount

The motor mount consists of four parts, the mounting of the motors are done by a beam to connect them to the body. To reduce the aerodynamic drag a body is made around this beam, this exists of three parts, two parts are bonded together and the top part is removable. This is necessary to access the motors and remove the engine mount. In Figure 17.5 the separate parts are shown.

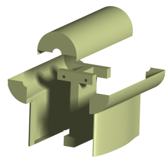

Figure 17.5: Production of the motor mount

17.5.5 Assembly

With all of the seperate parts assembled, the total assembly can begin. The floaters are bonded with the wing, the wings are mounted to the hull and the motor mount is mounted to the hull. This can be seen in Figure 17.6.

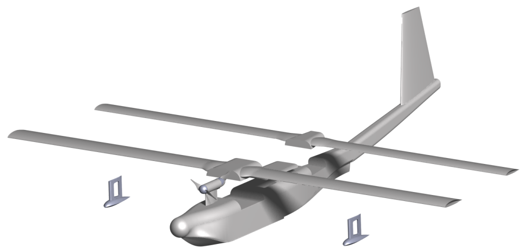

Figure 17.6: Assembly of the Dragonfly

17.6 Material characteristics

This section lists materials used in the respective structures. Table 17.3 lists which materials are used in which structures and Table 17.4 lists properties of used materials. It should be noted that most materials choices are specified in terms of a material type. As such, many material properties are still indicative, as they are subject to change when specific material products are selected.

Table 17.3: Material usage map

Part	**Material(s) used**
Wing	E-glass FC; HM carbon FC; PMI foam
Floater & floater-wing connection	E-glass FC; PMI foam
Hull	E-glass FC; PMI foam
Tail boom	E-glass FC; PMI foam
Vertical tail plane	E-glass FC; PMI foam
Motor mount	E-glass FC; PMI foam; Al 2024-T3
Propeller	TBD
Camera dome	Polycarbonate
Structural connections	Stainless steel; Al2024-T3

Table 17.4: Material characteristics[101, 97, 102, 98]. All composite fibres are UD in epoxy resin with 60% fibre content, cured at 120°

Material name	**Density** [g/cc]	**Modulus** [GPa]	**Tens. strength** [MPa]	**Compr. strength** [MPa]	**Ult. tensile strain** [%]	**Ult. compressive strain** [%]
E-glass composite	1.90					
- longitudinal		40	1000	600	2.50	1.50
- transverse		8	30	110	0.35	1.35
High-modulus CF composite	1.60					
- longitudinal		175	1000	850	0.55	0.45
- transverse		8	40	200	0.50	2.50
Rohacell® 110A PMI foam	0.110	0.160	3.50	3.00	4.5	–
Al 2023-T3	2.77	69	345	-	18	-
Stainless steel 405	7.8	200	170 (Yield)	-	20	-
Polycarbonate	1.2	2.38	62.1 (Yield)	-	6 (Yield)	-

Chapter 18

Sustainable development strategy

In a world where the human population can grow to 10 billion before the end of the century [111] and with a limited amount of natural resources, a serious study must be performed concerning the placement of the product in a sustainable, responsible environment. This has to be taken into account in both the design process and the product life-cycle, since sustainability is of growing importance in these processes and life-cycles. In order to contribute to a social, environmental, economic and organizational sustainability, design teams need to apply an overarching strategy detailing key goals and aspirations.

A focus on sustainability will imply minimisation of the carbon dioxide (CO_2) footprint of the UAV's life-cycle as well as minimisation of waste. During operations, the CO_2 footprint of the UAV is reduced through the use of solar power. The UAVs are complementing the present aerial surveillance vehicles, which may result in a net reduction of air pollution due to maritime surveillance. CO_2 and waste can further be reduced in the production cycle, the materials used, the power and the propulsion of the UAV. The attainable sustainability in these categories is discussed in the paragraphs below.

Materials: Material selection plays an important role in the sustainability of the UAV. For the UAV to be sustainable from manufacturing to end-of-life, the ecological impact of the used materials must be taken into account. This should not only include consideration of structural materials, but also materials used in batteries, electric circuits, etc. The UAV will be able to operate on water, therefore special attention will be given to the toxicity of used materials, even when immersed in water. In the event of structural damage to the vehicle, no toxic materials, such as harmful battery components, should permanently find their way into the sea. An other design philosophy could be to focus on minimising the use of toxic materials, rather than avoiding that the materials pollute the environment. This can be achieved by using biocomposite materials that consist of natural fibres and vegetable or animal resins. One limiting factor is the lack of material data [112]. Concerning the fact that the UAV is designed to be exposed to seawater for long periods, the design choice was made to rather use materials that do not degrade and react with the environment, in contrary to natural materials. However, if in the near future the research and development of the natural fibres grows substantially, biocomposites could be better applicable. In conclusion, the applied materials should be selected with recyclability and environmental production costs in mind. Any non-recyclable materials used will require a suitable end-of-life solution.

Production and maintenance: In a design process, the sustainability of the production methods are easily overlooked. When producing the UAV, a lean and efficient process should be applied in order to be sustainable. An efficient process should be based on reducing waste material and energy usage. Furthermore the use of toxic materials during production should be considered, including emissions of production plants and the recyclability of production waste. Parts and sub-assemblies should be interchangeable between UAVs where possible and as simple as possible, to aid in efficient maintenance and reduction of operational waste. COTS components are used to attain this goal, provided they are integrated in a way that allows easy access for maintenance.

Furthermore, production and assembly of the UAV should be done in close proximity to the area of operations, if possible. In this way transportation costs and waste are reduced.

Power and Propulsion: Due to the requirements set by the client, the power production itself is carbon-neutral: the propulsion system is required to be electric and the energy for all the systems on board comes from solar panels. This way, the UAV will operate emission free. However, the production of the solar panels produces greenhouse gasses and pollution. Studies show that the use of solar panels can be carbon-neutral, provided they are used for a period of 30 years [113]. While completely carbon-neutral propulsion for the amphibious UAV is unfeasible, it is more sustainable than current fossil fuel-powered UAVs on the market. The batteries and other electric circuits which are non-recyclable have to be disposed in a sustainable manner at the end-of-life in order to prevent pollution.

Integration: A good way to make the design of the UAV more sustainable is to allow for easy component integration. The different components of the UAV have to be implemented in such a way that they are 'plug and play'. This allows for easy maintenance, if one part is broken, the entire UAV does not has to be discarded. Easy upgrades are possible this way, extending the life of the UAV.

Emission reduction: In Chapter 17 it was stated that in 2011 the DCCG has logged 1923 flight hours with the Dash-8 and 700 with the AS-355. A rough estimate indicates that the total CO_2 emissions for 2011 is 8800 metric tonnes [114]. This concerns aerial surveillance operations as well as SAR operations. The designed UAV is not required to perform SAR operations, but mainly will replace the aerial surveillance operations of the DCCG. Next to that, territorial waters are monitored by means of boats and ships. The UAV can replace surveillance by ships as well. By doing so, it will reduce the CO_2 emissions during operation.

Chapter 19

Technical risk assessment

Every aspect of an engineering process comes with a certain amount of risk. An occurring event contains a risk if the event may prevent the product from reaching one or multiple requirements. The risk of an event depends on the probability of occurring and consequences for the mission requirements. The first step in being able to account for risks, is to produce an overview of the risks in the form of a risk analysis. A complete risk map provides information on where problems may arise and shows which problems introduce the highest risks. In this way more resources can be assigned to the parts of the design with the highest risk in order to be able to minimize these risks.

Preliminary risk assessments where presented in the baseline and mid term report. The risk map presented in this chapter is an expansion of these earlier versions, as more knowledge about potential risks and their consequences is obtained throughout the project. First a list of risks is presented in Section 19.1 which states the risks which are left with the final design completed. Then, the risks are arranged by severity and probability in Section 19.2.

19.1 List of risks

Now that the final design is finished, the risk analysis can be narrowed down to more detailed subjects. This section identifies all the risks, these are stated in table 19.1 and 19.2, section 19.2 uses the numbers assigned to the risks in order identify the severity of the risks.

Table 19.1: List of risks

risk number	risk	Comments
1	Approximated impact loads are inaccurate	Not very big chance as a safety factor is applied. This category is both for hull & floaters
2	Lands against the waves, being bounced back & stalling	Probability of crash due to this behaviour
3	Land perpendicular to the waves	Large side forces, probability of tipping over
4	Bouncing up from waves during take-off	Crash due to unexpected dynamic behaviour
5	Skipping during take-off	Enough hydrodynamic lift generated to take-off before adequate aerodynamic lift is generated: stall
6	Damage due to wildlife	For instance attacked by sharks
7	Theft	The UAV is a valuable product
8	Collision when idle	Possible collision with boats
9	Hit by lightning	Possible electronic failure
10	Thrust cannot overcome drag	Drag and or power determination are wrong
11	Structural analysis models are inaccurate	Risks mitigated by safety factors and validation via existing designs
12	Delaminations, vibrations, aeroelasticty,..	High risk as analyses are not yet performed
13	Material properties not as expected	Safety factors mitigate risk
14	Structural connections failure	High-risk area due to inherent complexity of interfaces
15	Layup quality introduces defects	Low probability for 200 units. learning effects reduce impact for complete UAV fleet
16	UAV exceeds design weight	Risk mitigated by mass budget contingency
17	Parts do not fit	Risk mitigated as long as tolerances are properly taken into account. Payload: plenty of volume inside UAV due to volume needed for buoyancy
18	Wings turn out to be less efficient	Increase in drag, worst case: not able to take-off
19	Due to our configuration; approximations may be invalid	Can result in an unstable or unflyable UAV
20	Wing is lost	Will result in a crash
21	Vertical tail is lost	Will result in a crash
22	Large imperfections on wing	Would give a big drop in lift and an increase in drag
23	Large imperfections on fuselage	Would only give a increase in drag, which is not wanted but not horrible
24	Battery failure due to overheating	If the ambient temperature or the current drawn is too high, the battery can fail to produce the required power

Table 19.2: List of risks continued

risk number	risk	Comments
25	Battery leakage	Due to degradation and ageing, the battery can leak and malfunction
26	Solar cell failure	Due to thermal stresses
27	Solar cell failure	Due to moisture damage
28	Solar cell failure	Due to mechanical loading
29	Solar cell shading by structure	Cells can be shaded by the structure of the UAV
30	Solar cell shading by environment	Cells can be shaded by environmental deposits
31	Mppt failure	half of the solar panels will not provide power
32	Wiring&connectors failure	Due to oxidation, disconnection due to mechanical loads
33	Short-circuit	Wiring insulation failure, moisture
34	Control board failure	Due to overheating or peak currents, the control board can fail
35	Motor controller failure	Due to overheating, the motor controller can fail
36	Motor failure	Due to overloading/ overheating
37	Motor failure	Due to lack of sufficient lubricant
38	Motor failure	Due to water ingestion
39	Propeller failure	Physical damage due to impact
40	Propeller failure	Due to overloading
41	Aileron servo failure	Results in an uncontrollable aircraft
42	Aileron structural failure	Results in an uncontrollable aircraft
43	Elevator servo failure	Results in an uncontrollable aircraft
44	Elevator structure failure	Results in an uncontrollable aircraft
45	Rudder servo failure	Results in an uncontrollable aircraft
46	Rudder structural failure	Results in an uncontrollable aircraft
47	Lisa/M fail	Wrong flight plan/non-water- poof
48	Ground control station fail	Power out/System crash
49	Camera electronic failure	Camera breaks
50	Camera mechanical failure	Gimbal breaks

19.2 Risk mapping

Every risk is rated on probability of occurrence and consequence on the mission.

The probability levels, arranged by increasing probability, are:

- Low probability
- Medium probability
- High probability
- Very high probability

The consequence subgroups, arranged by increasing severity, are:

- Negligible
- Marginal
- Critical
- Catastrophic

The probability of occurrence of a risk is determined using the calculated parameters of the UAV. When a requirement is easily met, the risk is rated lower than when a requirement is barely met. The POS, MNS and top-level requirements are used as a guideline to determine the severity of the requirement risks, since they define the main objectives. When the POS and/or the MNS can not be achieved the risk is considered to have catastrophic consequences. When only a top-level requirement is not met, the risk is considered to have critical or marginal consequences, depending on the importance of the affected top-level requirement(s). A short explanation of the risks is given in the last column of table 19.1 and 19.2 The results of the risk map are given in table 19.3.

Table 19.3: Risk Map

Probability\consequence	negligible	marginal	critical	catastrophic
very high				
high		29	4; 36	2; 3; 12
medium	49; 50	9; 45; 46	16; 26; 27; 28; 31; 35; 37; 38; 43; 44	1; 7; 8; 10; 14; 24; 39; 40; 41; 42
low		30	15; 17;47	5; 6; 11; 13; 25; 32; 33; 34; 48

Chapter 20

Post Project Development

Now that the UAV is designed, the post project development can be evaluated. This post project development contains the activities to perform after the DSE is finished. Firstly a Project Design & Development (PD&D) logic is created and finally a project Gantt chart is developed.

20.1 Project design and development logic

The PD&D logic shows the logical order of the activities to be executed in the post-DSE phases of the project. These activities must be specified for the project and reflect the technical characteristics of the project.

The logical order of activities to perform after the DSE starts with doing finite element analyses (FEA) and Computational Fluid Dynamics (CFD) analyses. With this information the design can be validated and optimised. After this step, all the subsections of the UAV can be tested to check the design with experimental data. Then, testing a scale model can be done to validate the complete design. With this scale model, wind tunnel tests and towing tank tests can be performed. The last activity to perform after this verification and verification process is to build a prototype, which can be put to full scale prototype tests, giving the last opportunity to optimise the design.

The overview and logical order of these activities and processes can be found in Figure 20.1.

20.2 Project Gantt chart

The activities and the activities' logical order defined in Section 20.1 can be presented in a Gantt chart. The Gantt chart allocates start and end dates to each activity and places them in a time order. This post-DSE schedule can be found in Figure 20.2.

In order to perform all these tasks in parallel, multiple persons are needed to perform these tasks. The numerical analysis can be performed simultaneously by one person for each task, so for this task two persons are needed. For the second stage of the post DSE activities, the sub-assembly testing, two persons are allocated to designing the moulds and every other task can be performed by one person. Building the scale model requires three persons and two weeks.

Then one of the most important phases in the post project development is the scale model testing. This activity needs a lot of time, since it includes towing tank testing, wind tunnel testing and propeller wind tunnel testing. Five persons where assigned to each of these subtasks for six months.

When the scale model tests have been performed and an optimal design is produced, materials and products can be ordered to build a prototype. This ordering would probably require one week and the prototype building requires a team of 10 persons for four months.

Finally, when a full prototype is produced a full scale testing program can be performed by 10 persons for the time span of one year. After all of these activities, the design is finished an ready to be introduced into the market.

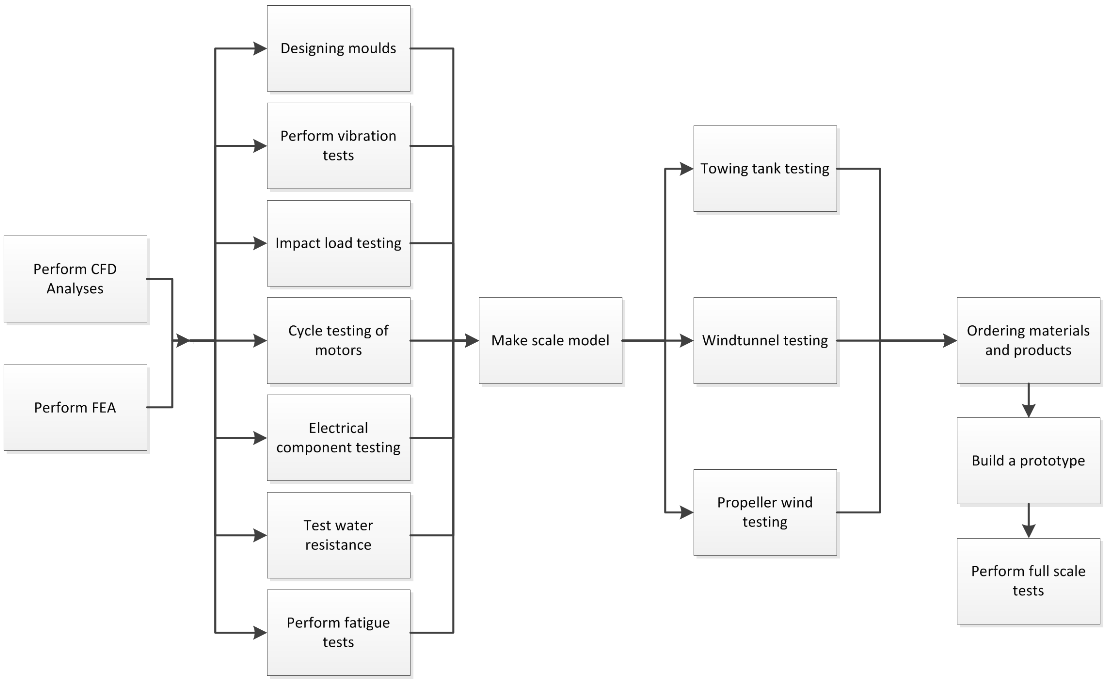

Figure 20.1: The project design and development logic

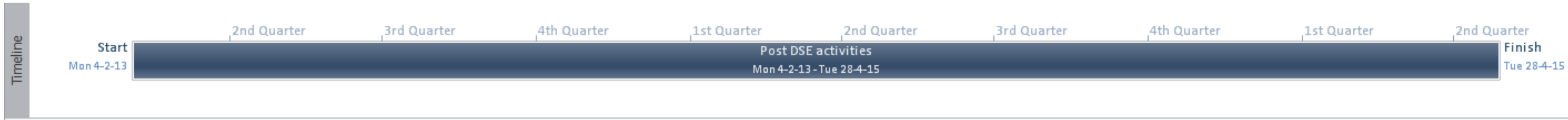

Gantt Chart

	Task Name	Work	Start	Finish	Predecessors
1	**1 Post DSE activities**	**43.640 hrs**	**Mon 4-2-13**	**Tue 28-4-15**	
2	**1.1 Numerical analysis**	**960 hrs**	**Mon 4-2-13**	**Tue 11-6-13**	
3	1.1.1 Perform CFD Analyses	480 hrs	Mon 4-2-13	Tue 11-6-13	
4	1.1.2 Perform FEA	480 hrs	Mon 4-2-13	Tue 11-6-13	
5	**1.2 Sub-assembly tests**	**800 hrs**	**Wed 12-6-13**	**Tue 9-7-13**	**2**
6	1.2.1 Designing moulds	80 hrs	Wed 12-6-13	Tue 18-6-13	2
7	1.2.2 Perform vibration tests	120 hrs	Wed 12-6-13	Tue 2-7-13	2
8	1.2.3 Impact load testing	120 hrs	Wed 12-6-13	Tue 2-7-13	2
9	1.2.4 Cycle testing of motors	120 hrs	Wed 12-6-13	Tue 2-7-13	2
10	1.2.5 Electric component testing	80 hrs	Wed 12-6-13	Tue 25-6-13	2
11	1.2.6 Test water resistance	120 hrs	Wed 12-6-13	Tue 2-7-13	2
12	1.2.7 Performing fatigue tests	160 hrs	Wed 12-6-13	Tue 9-7-13	2
13	**1.3 Make scale model**	**240 hrs**	**Wed 10-7-13**	**Tue 23-7-13**	**5**
14	**1.4 Scale model testing**	**14.400 hrs**	**Wed 24-7-13**	**Tue 7-1-14**	**13**
15	1.4.1 Towing tack testing	4.800 hrs	Wed 24-7-13	Tue 7-1-14	13
16	1.4.2 Windtunnel testing	4.800 hrs	Wed 24-7-13	Tue 7-1-14	13
17	1.4.3 Propeller wind testing	4.800 hrs	Wed 24-7-13	Tue 7-1-14	13
18	**1.5 Ordering materials and products**	**40 hrs**	**Wed 1-1-14**	**Tue 7-1-14**	**13**
19	**1.6 Build a prototype**	**6.400 hrs**	**Wed 8-1-14**	**Tue 29-4-14**	**18**
20	**1.7 Full scale testing**	**20.800 hrs**	**Wed 30-4-14**	**Tue 28-4-15**	**19**

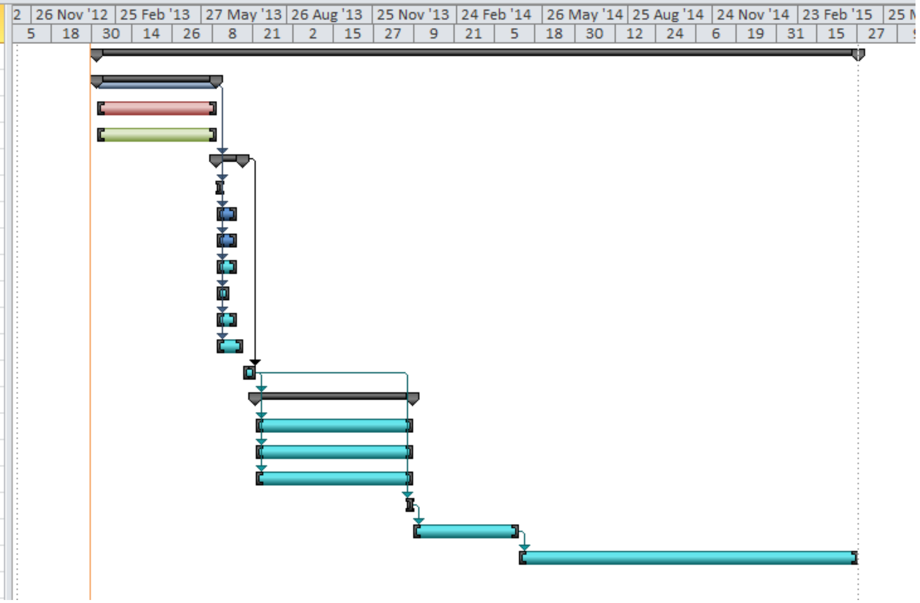

Figure 20.2: The project Gantt chart

Chapter 21

Conclusion

This final report is the concluding document of the design of an Unmanned Aerial Vehicle (UAV) with the mission need statement:

To conduct an economically and ecologically competitive autonomous maritime surveillance operation in the coastal area of Curaçao.

The UAV is designed to accomplish this mission and meet the top-level requirements and has a total mass of 9.9kg.

The wings have a span of 2.6 and 2.3 m for the front and aft wing respectively. Their aspect ratios are 17.3 for the front wing and 20 for the aft wing and they are designed for optimal efficiency during cruise. With the tandem wing the UAV has a total surface area of 0.64 m^2, the wing span is minimized which improves the ability to withstand loads during flight and landing and optimizes handleability. The control surfaces are placed conventionally, with the ailerons placed on the front wing, elevators on the aft wing and the rudder is placed on the vertical tail. The cruise velocity is 22 m/s. The top-level climb requirement was not met in accordance with the client.

The hull is designed for optimal hydrodynamic stability, aerodynamic efficiency and buoyancy. The floaters ensure static stability and are placed to avoid the wings getting damaged by hitting the water.

The UAV is equipped with a commercial off-the-shelf (COTS) autopilot system named 'Lisa/M 2.0' to execute the desired missions and in combination with a 'ublox' GPS chip it provides full attitude and altitude control. The autopilot is based on the open source Paparazzi system. It is connected to a communication system to allow the transfer of positioning data, mission programs and visual data over a distance of 80 km and thus provide full area coverage. Imaging is done with a COTS camera placed on a pan-tilt system to maximize the viewing area. The ground control system, which consists of a computer positioned on the main land of Curaçao, provides direct communication to the UAV

The UAV uses an electric motor system with a custom designed propeller. The surface area of the wing is optimised to be able to fit a maximum amount of solar cells on the given surface. A check has been done that an integer amount of cells fit on the wings. Where possible, the topside of the fuselage is also fitted with solar cells. Batteries are able to provide energy for flights of up to 1 hour of cruise time when the solar cells are not used. During daytime the endurance is increased to 1.8 hours. The batteries weigh 2.7kg and deliver 433Wh of energy. The two engines are sized to take-off power and the two engine lay-out provides an extra factor of redundancy.

The wings will be made out of a glass-carbon-glass composite, the front and back wing use different layer thicknesses for the lay-up. This leads to a lower overall weight. The fuselage consists of a glass-foam-glass composite, an additional layer is placed on the top part of the hull, in between the wing mounts. For the production, releasing moulds are used to facilitate mass production.

The total cost per UAV is €32400, including production, components and excluding maintenance.

Chapter 22

Recommendations

22.1 Aerodynamics

CFD and Windtunnel testing: A good initial way to verify the design is to do a computational flow dynamics (CFD) analysis, this was currently beyond the scope of this report. An advantage of a CFD analysis is that it can be done without any building. Thus the design can easily be tweaked and checked. After this CFD analysis a windtunnel test would be the next step, first a scaled model (to keep the cost down) and then a full scale model. For the scale model, however, care must be taken that the windspeed does increase to compensate for the lower Reynolds number, due to the smaller dimensions. Focus points of these analyses must on the interaction between the front wing and rear wing, the vertical tail sizing, wing fuselage interaction and the horizontal distance between the wings. These are parameters that have large influences on stability and efficiency.

After the windtunnel tests have been done, tweaking to the design will probably be needed after real flight tests. The real world conditions will always differ from the windtunnel.

Further sensitivity analysis: Further research also has to be done into a sensitivity analysis of the eigenmodes. Thus how do all the aerodynamic coefficients affect the stability of these eigenmodes. This will help during the tweaking of the design; what parameters can be changed without too much problems and what parameters are critical. Some intial analysis has been done, the contribution of each individual part has been determined.

Wingtip devices and flaps: Another area of research could be wingtip devices and flaps. No research has been done into wingtip devices for this report due to time constraints and the initial assumption that the increased weight would not compensate for the reduced drag. Flaps have also not been investigated, since it was assumed that the reduced take-off speed that flaps would provide, do not give any improvements for the overall mission.

22.2 Maritime

Towing tank testing: From the maritime part of the design, some recommendations can be stated. First of all, it is very important to perform towing tank tests to validate the drag and impact loads calculated in Chapter 13.

For the take-off drag calculation a constant width is used. However, at the end of the hull the width decreases into a point. If a way to incorporate this into the take-off drag formula would be found, the actual equilibrium trim angles would be determined in a more precise fashion, they would decrease with respect to the current values. In together with practical test data these calculations will be more detailed and precise.

Wave swell detection: Further, a system needs to be designed to detect the direction of the wave swell and change the attitude of the UAV in the same direction of the wave swell. This is important since the attitude of the UAV for take-off, idling and landing behaviour is dependent on the wave swell direction.

22.3 Structures and maintenance

Structures: Current analysis of most structures currently is limited. Particularly aeroelastic effects, vibrations and fatigue need to be included in future analysis. Fatigue has shown to be an important design criterion, following Section 16.4. When structural analysis of the wings and hull has been expanded, structures can be further optimised. In the long term, it is important to validate structural design by real-life testing. This is especially true for body-water impact load cases. Structural analysis of motor mount, propeller, camera dome & -mount and control surfaces have not yet been performed and are an important subject for future study.

A problem that has not been treated in this report is the likely issue of overheating of internals, particularly due to the thermal insulating properties of skin foam. Future design efforts are recommended to evaluate internal heat balance and find solutions. A solution may, for example, apply an open air cooling system or a closed loop liquid system with a heat sink around the rear bottom end of the UAV.

Materials: Material selection should be further investigated in future design. For structural components like the body and wings this is an optimisation problem; for most other parts material selection needs to be (re-)evaluated to include structural criteria as mentioned in the structural recommendations above:

Composite material selection for the body, wings and floaters, as well as material selection for structural connections can be narrowed down and re-evaluated based on specific material products. The currently selected foam used in skin structures is based on the experience of the authors, and selection of this foam should be optimized to the specific requirements of the UAV structure. Material selection for propeller, motor mount, control surfaces and body-tail structural connection has not yet been performed; camera dome material selection is recommended to be reconsidered based on impact loading and flexure of both the fuselage and the dome itself.

Maintenance: Maintenance efficiency philosophy is currently mostly based on the authors' engineering knowledge; since maintenance is an important aspect of the surveillance mission, future study is recommended include maintenance trade-offs grounded in maintenance experience. Reliability figures should be estimated. Most importantly, any future design studies should aim to keep maintenance as a design focus.

The camera is currently mounted from the inside of the fuselage. While this may allow for a better seal of the camera dome, from a maintenance point of view it would be preferred to mount the camera from the front by designing the camera dome to be detachable. Structural implications of this should be looked into. In current structural analysis, the body, tail and vertical tailplane are assumed to be one single part. For maintenance purposes, the tail is recommended to be removable at the tail boom, by way of a shape fit, secured with a locking pin (see Section 16.5). Structural implications of this solution need to be evaluated. Control surface attachment is yet to be designed such that they can be easily removed from the wing for replacement, maintenance and inspection. But the most urgent replaceability issue is that of the PV cells. They comprise 55% of the cost of the UAV (see Section 17.2), strongly suggesting the importance of designing the PV cell assembly such that they can be removed from the wing.

22.4 Propulsion and power

Motors and propellers: As explained in Chapter 15, the current motor configuration is based on take-off redundancy, i.e. each single engine is designed to perform full flight including take-off. As it turned out during the last design iteration of the hull, the take-off drag increased substantially. Due to this, a single motor is no longer able to perform take-off. This raises the question whether the take-off redundancy should be attained by resizing motors and propellers, or if the redundancy should be discarded. In the latter case, the motor efficiency can be increased significantly, by using one motor for cruise flight and one motor for take-off and climb, therefore it is adviced to research this possibility.

Propeller performance requires wind tunnel testing for design validation and to investigate propeller interference, besides this the selected propeller can be made more efficient by performing another design iteration with use of the last update on the drag values.

Photovoltaics: The current PV module consists of cells with an efficiency of 17%. The overall efficiency could be increased by a factor two using high efficiency PV cells, although this would increase the module costs by a factor four. The performance of the PV cells requires physical testing and simulation.

The battery charging depends on the current produced by the PV module. The UAV should have a optimised charging strategy, that determines the peaks in irradiance and forces the UAV to benefit from these peaks. The surveillance activities of the UAV swarm should incorporate an alternating charge-surveillance schedule in order to optimise the simultaneous area coverage.

22.5 Operation

Antenna: The directional antenna is preferred over the omni-directional antenna because of the higher gain and better anti-jamming property. It is recommended to design a compact and light weight mechanism for the direction antenna which can be suited in the UAV.

Paparazzi software and Autopilot: Without a pre-programmed autopilot with Paparazzi software, the UAV can not take off. However, since the configuration differs a lot from existing Paparazzi models, more time is needed to study this software and program the Autopilot. Also, detailed communication between the selected components should be investigated.

Imaging system: Research is required to implement the collection of infra-red images for operation during flight. IR sensors are very expensive (in the range of $10000) so a careful assessment should be done, considering the specific requirements and possible products.

Bibliography

[1] DCCG, "Dutch caribbean coastguard yearly report," 2011. http://www.rijksoverheid.nl/bestanden/documenten-en-publicaties/jaarverslagen/2012/05/16/jaarverslag-2011-kustwacht-koninkrijk-der-nederlanden-in-caribisch-gebied/jaarverslag-2011-kustwacht-koninkrijk-der-nederlanden-in-caribisch-gebied.pdf.

[2] DCCG, "Dccg organization overview." http://www.kustwacht.an/organizatie.html.

[3] DCCG, "Dccg operation area." DCCG, May 2012. http://www.kustwacht.an/organizatie-operatigebied.html.

[4] Warrior (Aero-Marine) Ltd., "Gull uav," November 2012. http://www.warrioraero.com/GULL/.

[5] QinetiQ, "Qinetiq zephyr solar uas the world leader in truly persistent," November 2012. http://www.qinetiq.com/news/PressReleases/Pages/QinetiQ-Zephyr-Solar-UAS-The-world-leader-in-truly-persistent,-cost-effective-airborne-surveillance-and-communications.aspx.

[6] Rotomotion LLC, "Sr100 helicopter uav specifications," January 2011. http://www.rotomotion.com/datasheets/sr100_uav_sheet.pdf.

[7] airforce technology.com, "Fury 1500 unmanned aerial vehicle," November 2012. http://www.airforce-technology.com/projects/fury-1500-uav/.

[8] naval technology.com, "Scaneagle," November 2012. http://www.naval-technology.com/projects/scaneagle-uav/.

[9] DRS and Technologies, "Rq-15 neptune data sheet," November 2012. http://www.drs.com/Products/UAS/PDF/neptune.pdf.

[10] N. Piercy and W. Giles, "Making swot analysis work," *Marketing Intelligence & Planning*, vol. 7, no. 5/6, pp. 5 – 7, 1989.

[11] C. C. Haddal and J. Gertler, "Homeland security: Unmanned aerial vehicles and border surveillance," July 2010. http://www.fas.org/sgp/crs/homesec/RS21698.pdf.

[12] S. Cambone, K. Krieg, P. Pace, and L. Wells, "Uav roadmap 2005-2030," tech. rep., United States of America Department of Defense, 2005.

[13] Lucintel, "Growth opportunity in global uav market," tech. rep., Lucintel, 2011.

[14] Homeland Security News Wire, "Mini-uav helps in monitoring natural disasters," October 2008. http://www.homelandsecuritynewswire.com/mini-uav-helps-monitoring-natural-disasters.

[15] DCCG, "Vijf nieuwe boten voor de kustwacht," November 2012. http://www.kustwacht.an/newsitem.php?id=190.

[16] G. Khoury, *Airship technology.* Cambridge University Press, 2012.

[17] Augustinus, R. et al., "Mid-term report dse group 4," tech. rep., TU Delft, 2012.

[18] Gilbert A. McCoy, Todd Litman, John G. Douglass, *Energy-Efficient Electric Motor Selection Handbook.* Washington State Energy Office, 1993.

[19] World Meteorological Organisation, "Wmo in brief," November 2012. http://www.wmo.int/pages/about/index_en.html.

[20] World Meteorological Organisation, *Manual on Codes - International Codes Volume I.1 Part A - Alphanumeric Codes*, 2012.

[21] Meteorological Department Curacao, "Times of sunrise and sunset for curacao at sealevel in 2012," November 2012. http://www.meteo.an/include/Pub/documents/SunrisesunsetCuracao2012.pdf.

[22] Meteo, "Climatological summaries," tech. rep., Meteorological Department Curacao, 1961-2008.

[23] S. Hsu, E. Meindl, and D. Gilhousen, "Determining the power-law wind-profile exponent under near-neutral," *Journal of Applied Meteorology*, 1994.

[24] Seakayak, "Beaufort wind force scale and sea state," January 2013. http://www.seakayak.ws/kayak/kayak.nsf/0/E4E2C690916A3A24852570DA0057E036.

[25] Sherwin Williams Protective & Marine Coatings, "MIL-E-1115D," January 2013. http://protective.sherwin-williams.com/detail.jsp?A=sku-26474%3Aproduct-6932.

[26] Sherwin Williams Protective & Marine Coatings, "TT-P-645," January 2013. http://protective.sherwin-williams.com/detail.jsp?A=sku-26534%3Aproduct-6948.

[27] Sheldahl, "G430300," January 2013. http://www.sheldahl.com.

[28] Anti-Seize Technology, "Battery protector and sealer," January 2013. http://catalog.antiseize.com/item/protectants-coatings/battery-protector-and-sealer/17211?

[29] Anti-Seize Technology, "Battery coating with indicator," January 2013. http://catalog.antiseize.com/item/protectants-coatings/battery-protector-and-sealer/17210?

[30] Scientific American, "What happens when lightning strikes an airplane?," January 2013. http://www.scientificamerican.com/article.cfm?id=what-happens-when-lightni.

[31] J. Roskam, *Airplane Design.* Roskam Aviation and Engineering Corporation, 1985.

[32] J. Roskam, *Methods for estimating drag polars of subsonic airplanes.* The University of Kansas, 1973.

[33] A. G. Smith, "The full-scale air drag of some flying-boat seaplanes," *Aeronautical research council reports and memoranda 3082*, 1959.

[34] United Nations, Department of Economic and Social Affairs, "Population division, population estimates and projects section," November 2012. http://aviationearth.com/aircraftdata/rutanvoyager.html.

[35] J. A. Mulder, et al., "Flight dynamics lecture notes," tech. rep., TU Delft, 2011.

[36] M. Sadraey, *Aircraft Design: A Systems Engineering Approach.* Wiley Publications, 2012.

[37] NASA, "Beginner's guide to aeronautics," January 2013. http://www.grc.nasa.gov/WWW/k-12/VirtualAero/BottleRocket/airplane/.

[38] E. A. S. Agency, "Certification specifications for very light aeroplanes," 2003.

[39] G. Tenney, "Servo torque calculator," 2013. http://www.geistware.com/rcmodeling/calculators.htm.

[40] Horizon Hobby, "Spektrum a7020 digital wing servo specifications," January 2013. http://www.horizonhobby.com/products/a7020-digital-wing-servo-SPMSA7020#t4.

[41] Horizon Hobby, "Spektrum a2020 nanolite servo specifications," January 2013. `http://www.horizonhobby.com/products/a2020-nanolite-servo-SPMSA2020#t2`.

[42] L. Larsson and R. Eliasson, *Principles of Yacht Design.* Adlard Coles Nautical, 2011.

[43] F. Fossati, *Aero-Hydrodynamics and the Performance of Sailing Yachts.* McGraw-Hill, 2007.

[44] N. Willford, "Seaplane design considerations," *EAA - Sport Aviation*, 2006.

[45] J. Parkinson, "Notes on the skipping of seaplanes," tech. rep., Langley Memorial Aeronautical Laboratory, 1943.

[46] W. Diehl, "The application of basic data on planing surfaces to the design of flying-boat hulls," tech. rep., National Advisory Committee for Aeronautics, 1940.

[47] T. v. Karman, "The impact on seaplane floats during landing," tech. rep., National Advisory Committee for Aeronautics, 1929.

[48] "Flight Standards Service", *Seaplane, Skiplane, and Float/Ski Equipped Helicopter Operations Handbook.* U.S. Department of Transportation - Federal Aviation Administration, 2004.

[49] S. Hoerner, *Fluid-Dynamic Drag.* Hoerner Publishing Company, 1965.

[50] D. Savitsky, "Hydrodynamic design of planing hulls," tech. rep., Marine Technology, 1964.

[51] *International Towing Tank Conference*, 2008.

[52] L. Peng and Z. Jun, "Water-impact force calculation and analysis for aircraft over sea contacted by waves," in *2010 3rd International Conference on Advanced Computer Theory and Engineering*, 2010.

[53] W. Diehl, "Static stability of seaplane floats and hulls," tech. rep., National Advisory Committee for Aeronautics, 1924.

[54] M. L. Neal Lineback, "Curacao: World's newest country," *Geography In The News*, 2010.

[55] I. Leon W.Couch, *Digital and Analog Communication Systems.* Pearson Education, 2007. p41–44.

[56] Defense Technical Information Center, "Development and operation of uavs for military and civil applications," tech. rep., North Atlantic Treaty Organization, 2000.

[57] L. W. II, *Digital and Analog Communication Systems.* Pearson Education, 2007. p46.

[58] The Paparazzi Project, "Comparison table of paparazzi autopilots," 12 2012. `http://paparazzi.enac.fr/wiki/Autopilots`.

[59] Team ATMOS, "Description of team atmos." `www.teamatmos.nl`.

[60] lr.tudelft.nl, "Facilities and institutes: Mav lab." `http://www.lr.tudelft.nl/organisatie/afdelingen-en-leerstoelen/department-of-control-and-operations/section-control-and-simulation/facilities-and-institutes/mav-lab/`.

[61] D. Schucker, "Autopilot integration on micro aerial vehicles," tech. rep., The university of arizona, 2012.

[62] Microhard system, January 2013. `http://www.microhardcorp.com/n920.php`.

[63] Aironet Wireless Commnication Inc, *Antenna Guide for 900 MHz and 2.4 GHz.* Aironet Wireless Commnication Inc.

[64] R. market, January 2013. `http://www.ercmarket.com/r6008sp-2.4-ghz-rasst-f0993.html`.

[65] e. Rafi, F., "Autonomous target following by unmanned aerial vehicles," tech. rep., University of Central Florida, Orlando FL, USA, 2005.

[66] e. J. Asmat, “Uas safety: Unmanned aerial collision avoidance system,” tech. rep., George Mason University, 2006.

[67] *UAV 2007 conference in Paris*, 2007.

[68] UAVFactory, “Portable ground control station,” January 2013. `http://www.uavfactory.com/product/16`.

[69] Lockheed Martin, *BTC-88 Gimbal*. Lockheed Martin Procerus Technologies.

[70] N. Kopeika, *A system engineering approach to imaging*. SPIE Press, 1998.

[71] ENAC university and TUD mavlab, January 2013. `http://paparazzi.enac.fr`.

[72] L. Couch II, *Digital and Analog Communication Systems*. Pearson Education, 2007. p584–586.

[73] Vince Stueve, Micrel, Inc, “Making choices in wireless networks,” January 2013. `http://www.digikey.com/us/en/techzone/wireless/resources/articles/making-choices-in-wireless-networks.html`.

[74] A. J.Clot, “Communications command and control,” tech. rep., Remote services limited, 2009.

[75] M. Hepperle, “Javaprop,” January 2013. `http://www.mh-aerotools.de/airfoils/javaprop.htm`.

[76] Scorpion power system, “Scorpion power system catalogue.” `http://www.scorpionsystem.com`.

[77] Hyperion, January 2013. `http://www.hyperion-eu.com/`.

[78] Plettenberg, January 2013. `http://www.plettenberg-motoren.com/`.

[79] Plettenberg, “Datenblaeter, orbit 15/14,” tech. rep., Plettenberg, 2005.

[80] P. Swatton, *Principals of flight for pilots*. Wiley, 2010.

[81] J. Lewis, “Theoretical max propeller efficiency,” month year. `http://www.jefflewis.net/aviation_theory-theo_prop_eff.html`.

[82] Georgia Institute of Technology, “Introduction to performance,” tech. rep., Georgia Institute of Technology, 2006.

[83] I. designs, “Cobra 80a esc with 6a switching bec,” January 2013. `http://www.innov8tivedesigns.com/product_info.php?products_id=903&osCsid=f6ce5b6750bebfeaeeb8a899ae171cf0`.

[84] Z. M. Salameh, “Advanced lithium polymer batteries,” *IEEE Xplore database*, 2009.

[85] A. Noth, *Design of Solar Powered Airplanes for Continous Flight*. PhD thesis, ETH Zurich, 2008.

[86] T. P. RC, “G6 pro lite 25c series,” tech. rep., Thunder Power RC, 2013.

[87] W. Ockels and J. Melkert, “Ae1105 lecture slides,” tech. rep., TU Delft, 2009.

[88] A. Luque and S. Hegedus, *Handbook of photovoltaic science and engineering*. John Wiley & Sons Ltd., 2003.

[89] A. Smets, “Et3034 lecture slides,” tech. rep., TU Delft, 2012.

[90] AZUR SPACE Solar Power GmbH, “Data sheet silicon solar space cell s32,” tech. rep., AZUR SPACE, 2006.

[91] R. Lanzafame, S. Nachtmann, M. Rosa-Clot, P. Rosa-Clot, P. Scandura, S. Taddei, and G. Tina, “Field experience with performances evaluation of a single-crystalline photovoltaic panel in an underwater environment,” *Industrial Electronics, IEEE Transactions on*, vol. 57, pp. 2492 –2498, july 2010.

[92] G. Rizzoni, *Principles and Applications of Electrical Engineering*. McGraw-Hill Education, 2006.

[93] “Automax solar mppt,” January 2013. http://www.solarmppt.com/index.php?main_page=product_info&cPath=1&products_id=1.

[94] Genasun, *GV-10 MPPT*. Genasun, January 2013.

[95] T. Megson, *Aircraft structures for engineering students*. Elsevier Ltd., 2007.

[96] JPS Industries, “Composite materials,” tech. rep., JPS Industries, 2013.

[97] P. C. Ltd., “Mechanical properties of composites,” 01 2013. http://www.performance-composites.com/carbonfibre/mechanicalproperties_2.asp.

[98] Matweb, “Material property data,” January 2013. http://matweb.com/index.aspx.

[99] Tohnichi, “Handbook vol.7 tohnichi torque,” tech. rep., Tohnichi, 2007.

[100] S. Chintapalli, “Prelimenary structural design optimization of an aircraft wing-box,” tech. rep., Concordia University, 2006.

[101] J. Quinn, *Composites - design manual*. James Quinn Associates Ltd, 1998.

[102] W. J. Callister, *Fundamentals of materials science and engineering*. John Wiley & Sons Ltd, 2001.

[103] Micro UAV, “Btc-88 micro pan/tilt unit specifications,” 2011.

[104] D. Chung, “Electromagnetic interference shielding effectiveness of carbon materials,” *Carbon*, 2001.

[105] J. Gundlach, *Designing Unmanned Aircraft Systems:A Comprehensive Approach*. AIAA, 2012.

[106] G. M. et al., “ph of seawater,” *Marine Chemistry*, 2011.

[107] V. Visco, AM; Brancato and N. Campo, “Degradation effects in polyester and vinyl ester resins induced by accelerated aging in seawater,” *Journal of composite materials*, 2011.

[108] D. Keccecioglu, *Reliability Engineering Handbook, Volume 1*. DEStech Publications, 2002.

[109] D. Uhlig, K. Bhamidipati, and N. Neogi, “Safety and reliability within uav construction,” *25th Digital Avionics Systems Conference*, 2006.

[110] 3M Scotch-weld, “3m scotch-weld 9323 b/a,” tech. rep., 3M, 2010.

[111] United Nations, Department of Economic and Social Affairs, “Population division, population estimates and projects section,” November 2012. http://esa.un.org/wpp/unpp/panel_population.htm.

[112] M. B. et al., “Dse final report: Low cost high performance uav,” tech. rep., TU Delft, 2012.

[113] V. Fthenakis, H. Kim, and E. Alsema, “Emissions from photovoltaic life cycles,” *Environmental Science & Technology*, vol. 42, 2008.

[114] Conklin and de Decker Associations, “Co2 emissions and offset calculator,” January 2013. https://www.conklindd.com/CO2Calc.aspx.

Appendix A

UAV requirements

1. On-board systems

   1.1 General

      a) Open source technology
      b) COTS components are used whenever possible

   1.2 Sensors

      a) HD video surveillance system
      b) Infrared imaging

   1.3 Avionics

      a) Autonomous take-off and landing
      b) Autonomous flight
      c) Programmable flight routines
      d) Waypoint navigation
      e) Patrol mission flight patterns
      f) Search mission flight patterns

   1.4 Communication

      a) 1.6 mbit bandwidth available for HD video transfer
      b) Continuous availability
      c) Operation beyond line of sight

   1.5 Power

      a) Power is electric
      b) Solar power generation
      c) Power storage sufficient for required endurance
      d) Low charge time

2. Vehicle

   2.1 Structural integrity

      a) Protected from saline water
      b) Protected from wildlife
      c) Design robust against enviromental degradation
      d) Withstands wave loads
      e) Light weight
      f) Structural strength sufficient for withstanding multiple deployment cycles

   2.2 Propulsion

a) Electric propulsion
b) Thrust sufficient for take-off, flight and landing

2.3 Performance
a) Maximum speed larger than 15 m/s
b) Rate of climb 10 m/s maintained for at least 5 seconds
c) Minimum flight endurance 1 hour
d) Maximum flight endurance at least 10 minutes
e) Takeoff & land from water with waves no greater than 2.5 meters

2.4 Mass constraints
a) Upper limit of 35 kg

2.5 Aerodynamics
a) Sustained flight
b) High lift over drag ratio

2.6 Stability & Control
a) Stable flight
b) Controllable flight

3. Infrastructure requirements

3.1 GCS Functionality
a) Mission planning capability
b) Control and monitoring of multiple vehicles
c) Real time telemetry tracking
d) Real time data transmission
e) Dynamic mission adjustments
f) Easy deployment and transportation
g) High degree of automation

3.2 Maintenance sector
a) Weekly checkups and repairs

4. Design requirements

4.1 General
a) Development time 10 weeks
b) Team of 10 people

4.2 Production
a) Minimum production series of 200 units
b) Economic competitiveness
c) Low cost manufacturing costs are prioritised

4.3 Sustainability
a) As sustainable as possible in production & operation
b) The least amount of toxic materials as possible is used

4.4 Mission
a) Required to conduct survellance
b) Operates in Caribbean sea

4.5 Safety
a) Emergency recovery capability
b) Command & control link failure back-up
c) Safe autonomous flight
d) Safe human machine interface
e) Safe control station environment

Appendix B

Deliverable item list

Table B.1: Deliverable item list

Item number	Deliverable	Part of report
1	Functional flow diagram	4.2
2	Functional breakdown	4.3
3	Resource allocation/ Budget breakdown	2
4	Technical risk assessment/ risk map	19 and 8
5	Market analysis	3
6	Operations and logistic concept description	14.9
7	Project design and development logic	20.1
8	Project Gantt chart	20.2
9	Cost break-down structure	17.2
10	H/W, S/W block diagrams	14.1
11	Electrical block diagram	15.6
12	Data Handling block diagram	14.1
13	Sustainable development strategy	18
14	Compliance Matrix	17.3
15	Sensitivity Analysis	Implemented in design chapters
16	Communication flow diagram	14.1
17	Verification & Validation Procedures	Implemented in design chapters
18	Manufacturing, Assembly, Integration plan	17.5
19	Return on investment, operational profit	17.2
20	RAMS characteristics	17.4
21	Performance analysis	12
22	Configuration/ layout	17.1
23	Communication (spacecraft) system characteristics	14.4
24	Aircraft system characteristics	12.3
25	Aerodynamic characteristics	12, 14.1 and 12.3
26	Structural characteristics	16
27	Material characteristics	17.6